INSTITUT
DE RADIOPROTECTION
ET DE SÛRETÉ NUCLÉAIRE

EURATOM RESEARCH FRAMEWORK
PROGRAMME 1998-2002

"NUCLEAR FISSION "
Operational safety of existing installations

Core Loss During a Severe Accident (COLOSS Project)

Contract FIKS-CT-1999-00002
(Cost-shared action)

IRSN/DPAM/Dir/04-0008, SAM-COLOSS-P078

COLOSS Final Synthesis Report

B. Adroguer, F. Bertrand, P. Chatelard, J.P. Van Dorsselaere,
N. Cocuaud, C. Duriez, (IRSN-DPAM), L. Bellenfant (IRSN-DSR),
A. Miassoedov, M. Steinbrück, J. Stuckert,
G. Schanz, W. Krauss, W. Hering, C. Homann (FZK),
D. Bottomley, D. Knoche (JRC/ITU),
V. Vrtilkova (ÚJP-PRAHA),
L. Belovsky (ALIAS CZ),
K. Müller (JRC/IE),
Z. Hózer, L. Matus, I. Nagy, Gy. Gyenes, A. Pintér, P. Windberg (AEKI),
G. Bandini, S. Ederli, (ENEA),
J. Birchley (PSI),
T. v. Berlepsch, I. Kleinhietpass (RUB),
M. Buck (IKE),
J. A. Fernandez Benitez, F. Martin-Fuertes (UPM),
E. Virtanen (LTKK),
S. Marguet (EDF),
G. Azarian, A. Caillaux (Framatome ANP SAS), H. Plank (Framatome ANP GmbH),
M. Veshchunov, A. Berdyshev, A. Boldyrev (IBRAE),
V. Kobzar, A. Volchek, Y. Zvonarev, (NSI/RRC-KI),
A. Goryachev, V. Smirnov (RIAR)

COLOSS distribution list

B. Adroguer	IRSN/DPAM/Dir/Cadarache	(5ex)
J.P. Van Dorsselaere	IRSN/DPAM/Dir/Cadarache	
C. Duriez	IRSN/DPAM/SEREA/Cadarache	
N. Cocuaud	IRSN/DPAM/SEREA/Cadarache	
P. Chatelard	IRSN/DPAM/SEMCA/Cadarache	
F. Bertrand	IRSN/DPAM/SEMCA/Cadarache	
B. Chaumont	IRSN/DSR/SAGR/Far	
L. Bellenfant	IRSN/DSR/SAGR/Far	
H. Plitz	FZK/Karlsruhe	
G. Schanz	FZK/Karlsruhe	
W. Krauss	FZK/Karlsruhe	
A. Miassoedov	FZK/Karlsruhe	
M. Steinbrück	FZK/Karlsruhe	
J. Stuckert	FZK/Karlsruhe	
W. Hering	FZK/Karlsruhe	
C. Homann	FZK/Karlsruhe	
D. Knoche	JRC/Karlsruhe	
D. Bottomley	JRC/Karlsruhe	
J. P. Glatz	JRC/Karlsruhe	
J. Kubant	ÚJP-PRAHA, Prague	
V. Vrtilkova	ÚJP-PRAHA, Prague	
L. Belovsky	ALIAS CZ, ÚJP consultant/Prague	
K. Müller	JRC/Petten	
Z. Hózer	AEKI/Budapest	
I. Nagy	AEKI/Budapest	
Gy. Gyenes	AEKI/Budapest	
P. Winberg	AEKI/Budapest	
A. Pinter	AEKI/Budapest	
M. Pezzilli	ENEA/Roma	
G. Bandini	ENEA/Bologna	
S. Ederli	ENEA/Roma	
S. Guentay	PSI/Villigen	
J. Birchley	PSI/Villigen	
M. K. Koch	RUB/Bochum	
I. Kleinhietpass	RUB/Bochum	
M. Buck	IKE/Stuttgart	
S.A. Alonso	UPM/Madrid	
E. Gallego	UPM/Madrid	
F. Martin-Fuertes	UPM/Madrid	
J. Fernandez Benitez	UPM/Madrid	
E. Virtanen	LTKK/Lappeenrenta	
S. Marguet	EDF/Clamart	
Y. Dutheillet	EDF/Clamart	
G. Azarian	Framatome ANP/Paris	
A. Caillaux	Framatome ANP/Paris	
H. Plank	Framatome ANP/Erlangen	
M. Veshchunov	IBRAE/Moscow	
A. Berdyshev	IBRAE/Moscow	
A. Boldyrev	IBRAE/Moscow	
Y. Zvonarev	KI/Moscow	
V. Kobzar	KI/Moscow	
V. Smirnov	RIAR/Dimitrovgrad	
A. Goryachev	RIAR/Dimitrovgrad	

ENTHALPY and EVITA projects

A. De Bremaecker	IRSN/PDAM/SEMIC/Cadarache
H.J. Allelein	GRS/Cologne
K. Traumbauer	GRS/Munich

THENPHEBISP project

B. Clément	IRSN/DPAM/SEMIC/ Cadarache
T. Haste	PSI/Villigen

EC distribution

M. Hugon	DG Research J.4 /Bruxelles
A. Zurita	DG Research J.4 /Bruxelles

IRSN distribution list

De Franco	IRSN/Pg/Clamart
J. Bardelay	IRSN/Pg/Clamart
R. Dallendre	IRSN/RI/Clamart
M. Durin	IRSN/DSR/Clamart
S. Roche	IRSN/DSR/Clamart
J. Lewi	IRSN/DESTQ/Clamart
M. Schwarz	IRSN/DPAM/Dir/Cad
G. Hache	IRSN/DPAM/Dir/Cad
J.C. Micaelli	IRSN/DPAM/Dir/Cad
M. Faury	IRSN/DPAM/SEREA/Cad
R. Gonzalez	IRSN/DPAM/SEMIC/Cad
P. Giordano	IRSN/DPAM/SEMIC/Cad
N. Alpy	IRSN/DPAM/SEMIC/Cad
M. Barrachin	IRSN/DPAM/SEMIC/Cad
F. Barré	IRSN/DPAM/SEMCA/Cad
F. Camous	IRSN/DPAM/SEMCA /Cad
S. Pignet	IRSN/DPAM/SEMCA/Cad
G. Repetto	IRSN/DPAM/SEMCA/Cad
S. Bourdon	IRSN/DPAM/SEMCA/Cad

Institut de Radioprotection et de Sûreté Nucléaire Direction de Prévention des Accidents Majeurs		
Nat. Document	Rapport Technique DPAM/Dir 04-0008 SAM-COLOSS-P078	
TITRE	**COLOSS Final Synthesis Report**	
Auteur(s)	***B. Adroguer et al.,***	
Type de Diffusion :	"Mots clés" : COLOSS project, Severe Accidents, core degradation, synthesis	Nbre de pages : 90 Nbre annexes: 0

Résumé :

Le projet COLOSS (Core Loss of integrity) du 5ème PCRD , d'une durée de 3 ans a été initié en février 2000. Ce rapport final est une synthèse des activités du projet. Les principaux résultats expérimentaux ainsi que les activités de modélisation, de validation de codes de calcul Accident Grave ainsi que les calculs réacteurs y sont résumés. Les principales recommandations et conclusions du projet sont données.

Abstract :

The COLOSS project was a 3-year shared-cost action, which started in February 2000. This report gives a synthesis of the experimental and modelling-validation work-packages as well as of the plant calculation activity. Main conclusions from the project are drawn along with recommendations for further activities.

B. ADROGUER	*B. CLEMENT*	*J.-C. MICAELLI*
Rédaction : Nom/Visa/Date Signed	Vérification : Nom/Visa/Date Signed	Approbation DPAM : Nom/Visa/Date Signed

Content

LIST OF ABBREVIATIONS AND SYMBOLS

AECL	Atomic Energy of Canada Limited
AEKI	Atomic Energy Research Institute from the Hungarian Academy of Sciences
ANL	Argonne National Laboratory, US
ASTEC	Accident Source Term Evaluation Code
B_4C-CR	B_4C Control Rod
BWR	Boiling Water Reactor
CEA	Commissariat à l'Energie Atomique
CEC	Commission of the European Communities
CIT	Corium Interactions and Thermochemistry project (4^{th} FP)
COBE	Core Behaviour project (4^{th} FP)
COLOSS	Core Loss project (5^{th} FP)
ECCS	Emergency Core Coolant System
EC	European Commission
EDF	Electricité de France
EDX	Energy Dispersive Micro-Analysis
ENEA	Ente per le Nuovo Tecnologie, l'Energia e l'Ambiente
EU	European Union
EPMA	Electron Probe Micro-Analysis
EPR	European Pressurized Reactor
EVITA	European Validation of the Integral Code ASTEC (5^{th} FP)
Ex-V.	Ex-Vessel
FLHT	Full Length High Temperature
FP	Fission Product
5^{th} FP	5^{th} Framework Programme of the EC
FZK	Forschungszentrum Karlsruhe (formerly Kernforschungszentrum Karlsruhe (KfK))
GRS	Gesellschaft für Anlagen und Reaktorsicherheit, Germany
HFI	High Frequency Induction
IBRAE	Nuclear Safety Institute of Russian Academy of Sciences
IKE	Institut für Kernenergetik und Energiesysteme, Universität Stuttgart, Germany
In-V.	In-vessel
IRSN	Institut de Radioprotection et de Sureté Nucléaire (formerly IPSN)
ISTC	International Science and Technology Center (Moscow)
ITU	Institut des Trans-Uraniens
JRC	Joint Research Centre
KfK	see FZK
KI	Russian Research Centre " Kurchatov Institute "
LOCA	Loss of Coolant Accident
LTKK	Lappeenranta University of Technology, Finland
LSK	Saint Petersburg Electrotechnical University, Russia
LWR	Light Water Reactor
MP	Melting Point
MOX	Mixte Oxides
NAS	New Associated States
NED	Nuclear Engineerind and Design
NPP	Nuclear Power Plant
NoE	Network of Exellence

NSI	Nuclear Safety Institute (IBRAE) from the Russia Academy of Sciences
OPSA	Oxidation Phenomena in Severe Accidents project (4^{th} FP)
OECD	Organisation for Economic Cooperation and Development
PAG	Plant Analysis Group in COLOSS
PBF	Power Burst Facility, United States
PTE	Post-Test Examination
PIRT	Parameter Identification and Ranking Table
PNL	Pacific Nord-Est Laboratory
PORV	Power Operated Relief Valve
PSI	Paul Scherrer Institute, Swiss
PWR	Pressurised Water Reactor
RCS	Reactor Coolant System
RIAR	Institute for engineering and scientific research for Nuclear Power Plants Dimitrovgrad (Russia)
RUB	Ruhr Universität Bochum, Germany
SARNET	Severe Accident Research Network (6th FP)
SBO	Station Blackout sequence
SCDAP/R5	SCDAP/RELAP5 code (S/R5)
SET	Separate Effects Tests
RPV	Reactor Pressure Vessel
SA	Severe Accident
SAM	Severe Accident Management
SEM/EDX	Scanning Electron Microscopy/Energy-Dispersive X-ray analysis
SNL	Sandia National Laboratory, US
SOAR	State of the Art Report
TMI-2	Three Mile Island Unit 2
UJP-PRAHA	formerly SKODA-UJP, Zbraslav, Czech Republic
UPM	Universidad Politecnica De Madrid
U-Zr-O	Mixtures involving core materials resulting from the liquefaction of fuel rods (UO_2, Zr, ZrO_2)
VVER	Pressurized Water Reactor of Russian type

Executive Summary

The COLOSS project was a 3-year shared-cost action, which started in February 2000. The work-programme performed by 19 partners involved complementary activities aimed at improving the core degradation phase during of severe accident. Risk-relevant issues of particular interest regarding H_2 production, melt generation and the source term were studied in a large number of experiments devoted to a) dissolution of fresh and high burn-up UO_2 and MOX by molten Zircaloy, b) simultaneous dissolution of UO_2 and ZrO_2, c) oxidation of U-O-Zr mixtures, d) oxidation of pure B_4C material and degradation-oxidation of B_4C control rods.

Corresponding models were developed and implemented in severe accident computer codes. Upgraded codes were finally used to calculate key severe accident sequences occurring in different plants such as PWR-900, PWR-1300, BWR, VVER-1000, EPR and in the TMI-2 accident. Main experimental and analytical results are:

A large experimental database was produced involving key results:

- Main B_4C oxidation issues have been largely resolved. The large database produced from SETs and CODEX and QUENCH bundle tests showed that B_4C oxidation is strongly dependent on thermal-hydraulic conditions. Productions of limited H_2, CO, CO_2, very low CH_4 and large amounts of aerosol were found. The CO and CO_2 production is sufficient to affect the FP chemistry in the circuit, in particular the iodine and caesium speciation.
- Data obtained on oxidation of U-O-Zr mixtures showed faster kinetics than for pure Zr. These data confirm that mixtures are a significant source of H_2 production during core degradation and, mainly, during core reflooding. This is a key insight for the modelling the H_2-peak production during reflooding, which is presently inadequate in SA codes.
- Results on simultaneous UO_2 and ZrO_2 dissolution improved understanding of core liquefaction. More data are needed on the induced clad failure and rod collapse.
- Data were produced on the burn-up effect on UO_2 dissolution and, for the first time, on MOX fuel dissolution, showing enhanced kinetics and greater apparent dissolution than for fresh fuel. Burn-up is a key factor suspected to favour the early fuel rod collapse.

Mechanistic and parametric models were produced on B_4C oxidation, fuel dissolution and oxidation of U-O-Zr mixtures enabling SA codes under development in the EU to be upgraded. This effort was continued after the project to take full account of the findings and improve the coupling between phenomena. Improvements were launched on the Zry oxidation which was deeply revised and investigated during the project.

A large series of plant calculations was done, final ones run with codes improved by the project. Sensitivity studies and code-benchmarks enabled code uncertainties to be evaluated on the H_2 production, B_4C-reaction gases and corium behaviour. This activity enabled a) the assessment of codes to calculate core degradation, b) the identification of main uncertainties and needs for short-term code developments and c) the evaluation of the safety challenges of the results produced by the project.

Perspectives: Remaining uncertainties and SA code weaknesses in safety-relevant phenomena of core degradation have been transmitted to the PIRT review on SA carried out in the EURSAFE thematic network (5^{th} FP) to be addressed in the SARNET network of excellence (6^{th} FP). In particular results on dissolution of irradiated fuel and oxidation of metal-rich mixtures during core degradation and reflooding should be consolidated. The follow-up of the COLOSS activity on plant calculations with sensitivity studies and benchmarking exercises has also been recommended. SA code weaknesses identified in the project will be addressed, the priority being put on the improvement of the European ASTEC code.

A. OBJECTIVE AND SCOPE

From the beginning of nuclear power plant developments, it has been realized that a severe accident (SA) in which the core cooling is lost could lead to fuel elements melting and FP release beyond the plant limits. Nuclear power plants are designed with engineering systems and associated operational procedures which provide a defense-in-depth against such accidents. Even if the probability to have a severe accident is very low, in view of the potential large radiological consequences of such severe accidents, it is now a common practice to assess the risks associated with SA conditions using computer codes to model the accident progression, and potential source term to the environment. The reliability of the assessment strongly depends on the predictive capability of the computer codes. Ensuring such a capability requires to collect the scientific information needed to better understand and describe the physical phenomena playing a role during the progression of the accident. This approach is usually done by the means of experimental programmes and modelling activities.

A severe accident, which can arise in a nuclear reactor in case of safety systems failure, could develop via core heat-up in steam, interaction phenomena between core components, loss of core integrity, melt relocation and corium melt pool formation if other counteracting measures are not successful. Core degradation and liquefaction are the source of risk from gas and fission products (FP) releases and corium formation and progression. This, in turn, raises the problem of corium retention in the reactor vessel. Consequently, the mechanisms of core degradation and the related core material interactions require detailed analysis and quantification. Powerful computer codes are used for safety studies to evaluate these effects and improve the accident management and hence reduce the overall risk of radioactive contamination.

In spite of significant progress in the last 20 years on the understanding of the core degradation, remaining areas have not advanced enough to resolve the following key issues:

a) What is the impact of UO_2 and ZrO_2 dissolution on the loss of core geometry and how can the burn-up effect affect the dissolution of UO_2 and MOX?

b) How does the oxidation of U-O-Zr mixtures contribute to the H_2 peak production during the reflood of degraded cores?

c) What is the B_4C effect (from the absorber elements) on core degradation and melt progression?

d) Can the oxidation of B_4C material affect the chemistry of volatile FPs, in particular the production of volatile organic iodine?

These issues were addressed by the COLOSS project, which involved 19 partners including experimentalists, analysts, code developers and code users. The main objective was to improve the knowledge on key core degradation phenomena affecting the corium formation, and thus the gas and FP release. Unresolved risk-relevant issues regarding H_2 production, melt generation and B_4C control rod degradation and oxidation were studied, through a large number of experiments. In parallel, corresponding models were developed for SA computer codes. These codes were also used to apply experimental results in plant calculations and evaluate their consequences on key SA sequences in different plants involving B_4C and in the TMI-2 accident.

Issues of fuel dissolution and quench effects relevant to questions a) and b) were previously addressed in the CIT (Ref. [1]) and COBE (Ref.[2]) projects of the previous EC Nuclear Fission Safety Programme which respectively dealt with core material interactions and quench effects during core degradation. At that time, experimental results on fuel dissolution and on quenching indicated strong effects on early core liquefaction and H_2 peak production but the database was not sufficient for understanding and modelling in SA codes. At the beginning of the project, the status of codes on fuel dissolution and quench effects was as follows:

- Existing fuel dissolution models in SA codes did not take into account the following aspects: a) the simultaneous dissolution of the external ZrO_2 layer of the cladding (Ref.[3]) which occurs, in the fuel rod geometry, during the UO_2 dissolution by molten Zr, b) the burn-up effect and c) the dissolution of MOX. The first two effects were suspected of being driving factors in fuel liquefaction, the clad failure, the loss of rod geometry and the kinetics of FP release.
- Models for the oxidation of Zr-rich compounds in degraded cores could not predict on a physical basis the risk-relevant H_2 peak during quench conditions. This was illustrated several years ago in the International Standard Problem ISP-31 on the CORA-13 test (Ref.[4]) and very recently in the ISP-45 on the QUENCH-06 test (Ref.[5]). The proposal of the project was to study the oxidation of Zr-rich mixtures suspected to be a key source of H_2 during quench.
- The project was also focused on B_4C oxidation and B_4C control rod degradation in order to answer questions c) and d). These topics were poorly understood and models in SA codes were either unsuitable or missing (Ref.[6]). The main concern here was to identify the impact of B_4C on core liquefaction, on H_2 production and on the formation of boron and carbon gaseous species (CO, CO_2, CH_4, B_2O_3 and boric acids), which could modify the chemistry and the transport of certain volatile FPs, in particular iodine (gaseous forms) and caesium. This is of prime importance for the evaluation of the source term from the containment.

In order to reduce uncertainties on the above-mentioned topics, well-targeted experimental programmes were carried out involving tests at different scales. The objective was to provide sufficient experimental databases enabling modelling improvements and validation activities of main SA codes used in the EU. The priority being put on the application of results in SA codes and on the implications of results for the safety viewpoint, the experimental and analytical activities were tightly linked with plant calculations of key SA sequences for different European LWRs, in particular those with B_4C-CR such as PWR-1300, VVER-1000, EPR and BWR.

Main achievements at the end of the project (January 2003) and recommendations for future R&D activities are summarized in this synthesis report.

B. WORK PROGRAMME

The work plan involved four work-packages (WP):

a) Small-scale experiments for the investigation of the following phenomena:

- The dissolution of fresh and irradiated UO_2 and MOX by molten Zircaloy (Zry),
- The simultaneous dissolution of UO_2 and ZrO_2 by molten Zry for PWR and VVER rods,
- The oxidation of pure B_4C material from different plant designs,
- The degradation and oxidation of single PWR and VVER B_4C control rods (B_4C-CR),
- The oxidation of U-O-Zr mixtures by steam and the related H_2 production.

Table 1: Revised COLOSS Work-Packages and Partners (as decided at the Mid-Term Assessment meeting).

Work-Packages	**Description of the tasks and partners involved**	
WP1 : SET. Dissolution of irradiated fuel	WP1.1 Irradiated UO_2 and MOX dissolution tests	(JRC/ITU)
	WP1.2 Analysis of tests	(IRSN)
WP2: SET. Simultaneous UO_2 and ZrO_2 dissolution	WP2.1 Simultaneous UO_2 and ZrO_2 dissolution tests	(RIAR, JRC/IE)
	WP2.2 PWR and VVER single rod degradation tests	(AEKI)
	WP2.3 Analysis of WP2 tests	(IRSN, IBRAE, KI, JRC/IE, ENEA)
WP3: SET. U-O-Zr oxidation	WP3.1 U-O-Zr oxidation tests	(ÚJP-PRAHA)
	WP3.2 Analysis of U-O-Zr oxidation tests	(JRC/IE, RUB, IRSN)
WP4: SET. B_4C oxidation & control rod degradation	WP4.1 B_4C oxidation tests	(FZK, IRSN)
	WP4.2 B_4C control rod degradation tests	(FZK)
	WP4.3 Analysis of B_4C oxidation/degradation tests	(IRSN, ENEA, EDF)
WP5: VVER bundle test	WP5.1 VVER bundle test with a central B_4C control rod	(AEKI)
	WP5.2 Analysis of the VVER bundle test	(AEKI, KI, IKE, ENEA, LTKK)
WP6: PWR bundle tests	WP6.1 PWR/BWR bundle tests with a central B_4C control rod	(FZK)
	WP6.2 Analysis of the PWR/BWR bundle tests	(FZK, PSI, IKE, UPM, IRSN)
WP7: Modelling	WP7.1 B_4C oxidation/degradation	(IRSN, ENEA, EDF, IKE)
	WP7.2 U-O-Zr oxidation	(JRC/IE, RUB, IRSN)
	WP7.3 Simultaneous UO_2 and ZrO_2 dissolution by Zry	(IBRAE, JRC/IE, IRSN)
WP8: Plant calculations of SA sequences	WP8.1 PWR-1300, VVER-1000, BWR, EPR: Impact of new B_4C models	(IRSN, FZK, PSI, NSI-KI, LTKK, EDF, IKE, Framatome-ANP/Fr & Ge)
	WP8.2 TMI-2: Impact of new fuel models	(ENEA, IRSN, EDF)
	WP8.3 Synthesis / Feedback on SA codes and safety	(All WP8 partners)

b) Large-scale experiments with one VVER and two PWR representative fuel rod bundles characterized by a central control B_4C rod. Each test was supported by pre- and post-test calculations in order to prepare the test, analyse the results and contribute to the validation of SA codes improved in the project.

c) Model developments and coupling in SA codes used by Utilities, Industry and Safety Authorities such as the detailed ICARE/CATHARE, ATHLET-CD and SVECHA codes, and the integral ASTEC and MAAP4 codes.

e) Plant calculations to assess the consequences of new experimental data and models on key SA sequences for different plant designs. In particular, main power plants with B_4C material such as PWR-1300, VVER-1000, BWR, EPR and also the TMI-2 reference accident were investigated. This large WP involved 11 partners using several SA codes such as ASTEC, MAAP4, MELCOR, ICARE/CATHARE, ATHLET-CD and SCDAP/RELAP5. Calculations of key SA sequences mainly focussed on core degradation.

This activity enabled

- the assessment of codes to calculate core degradation more particularly core oxidation and H_2 production (both the rate and the total production), B_4C effects, and corium formation including fuel dissolution and burn-up effects,
- the identification of main uncertainties and needs for short-term code developments and
- the identification of safety implications of new results. Table 1 gives a description of WP and partners.

C. WORK PERFORMED AND RESULTS

A large experimental database has been produced, enabling significant progress in modelling, SA code improvements and assessment. All these results have been presented in the two FISA-01 and FISA-03 conferences (Ref. [7], Ref. [8]), more information has been given in Special NED FISA issues (Ref. [9], Ref. [10]) and of course in the Final Extended Reports (Ref. [11], Ref. [12]).

C.1 Small-scale experiments

C.1.1 Fuel dissolution tests (AEKI, JRC/IE, RIAR, JRC/ITU)

Above the melting temperature of Zry, partially oxidized fuel rods are affected by the simultaneous UO_2 and ZrO_2 dissolution by molten Zry. These chemical interactions affect 1) the liquefaction of UO_2 and ZrO_2 at about 1000 K below their melting points, 2) the clad failure and the U-O-Zr melts formation and relocation, and 3) the H_2 generation and early FP release.

Three complementary experimental programmes were carried out on fuel rod dissolution: separate-effects tests (SET) to study the simultaneous dissolution of UO_2 and ZrO_2 using

crucibles, semi-global tests to study the same topic using representative fuel rods and SETs to compare UO_2 and MOX dissolution and study the burn-up effects.

C.1.1.1 Simultaneous dissolution of UO_2 and ZrO_2 by molten Zry (RIAR, JRC/IE)

These tests were characterised by a UO_2 crucible, a central ZrO_2 rod and Zry in-between. The UO_2 crucibles were similar to those used in the earlier tests carried out in the CIT project (Ref.[13], Ref.[14] which showed unexpected results with larger dissolution than expected that could affect the loss of rod geometry for temperatures greater than 2450K. The bottom of the crucible is insulated from the melt by an yttria disk. Tests are performed in an electric resistance furnace filled with argon at atmospheric pressure (Fig. 1). The test matrix involved two test series at 2100 and 2200 °C with different annealing time from 100 to 600s.

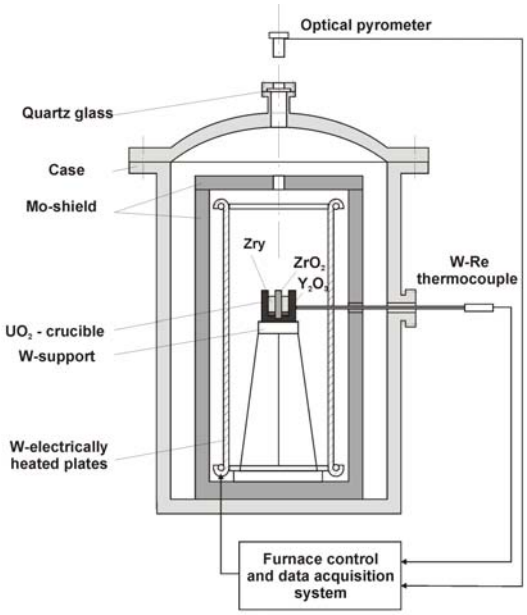

Fig. 1: Scheme of the RIAR facility

Figure 2 illustrates the configuration of the crucible with an upper Y_2O_3 disk in order to reduce upper heat losses, lateral holes for TC implementation and an axial cutting of the crucible at the end of the experiment.

The analysis of the initial tests showed that the temperature difference between the melt and the crucible could have been a driving parameter of the dissolution. For the final series of tests, an upper heat-insulating layer was added to reduce axial heat losses and crucible wall temperature gradients. The sample temperature is determined by a two-beam pyrometer focused on the Zry charge and two thermocouples installed into the recesses at the crucible sidewall. The location of these two thermocouples (TC) was changed for the final test series. The internal TC was implemented in a hole near the bottom of the crucible and near the inner crucible surface in order to have a better control of temperature differences in the wall (Fig. 1). The final set of tests

showed that the temperature gradient in the crucible wall was lower than initially expected when taking into account the pyrometer reading as the reference temperature. It was in fact quite negligible. Finally TC readings were confirmed as the right temperature reference in opposition to what was believed at the beginning of the programme and showed that initial experiments were carried out at temperatures ~100 K higher than measured by the pyrometer.

The post-test examinations included the determination of the ratio of the dissolved uranium mass to the mass of the created melt. The determination of the dissolved uranium amount was carried out by two methods:

- the quantitative image analysis using photos of longitudinal sections of the tested samples,
- the chemical analysis of the melt.

The melt was characterized by a homogeneous distribution of two main phases: U-Zr metallic and $(U,Zr)O_{2-x}$ phase. Figures 3 and 4 illustrate dissolution tests at 2100°C and 2200°C.The two methods showed similar results and indicated results consistent with previous AECL results of the CIT project (Fig. 3).

The experimental database produced was used for dissolution modelling and validation of the SVECHA code.

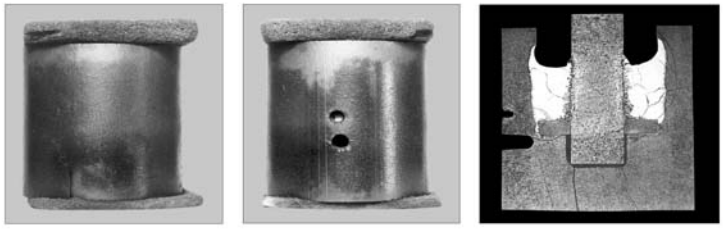

Fig. 2: RIAR Test 2 on simultaneous dissolution of UO_2 and ZrO_2 (2200 °C, 200 s).

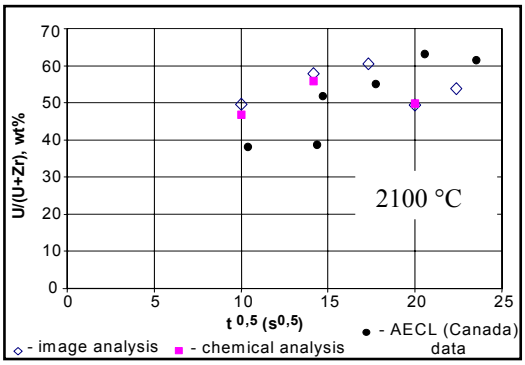

Fig. 3: Test at 2100°C; U/(U+Zr) ratio in the melt, results of chemical and image analysis

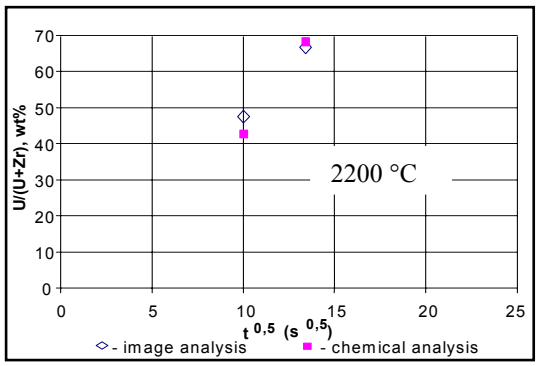

Fig. 4: Test at 2200°C; U/(U+Zr) ratio in the melt, results of chemical and image analysis

C.1.1.2 Simultaneous dissolution of UO_2 and ZrO_2 using short fuel rods (AEKI)

A new facility was build to carry out short VVER and PWR fuel rod dissolution tests. The test matrix involved 9 VVER and 11 PWR fuel rod tests (short rods with four or two fresh UO_2 pellets). The test protocol was based on a first oxidation phase at temperature (various oxidation

temperature and times) followed by a dissolution stage at a higher temperature in the range 2200-2500 K. The oxidation was carried out in steam, then the atmosphere was changed to argon and the temperature was increased up to the selected dissolution temperature without intermediate cooling down.

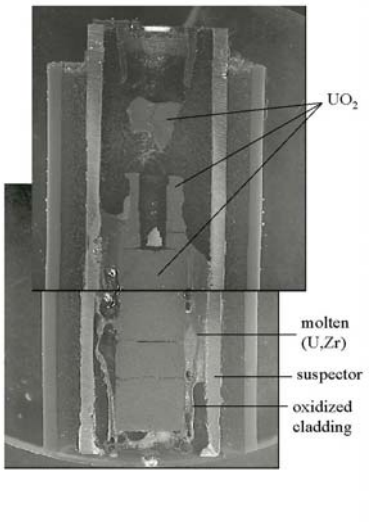

Fig. 5: Axial cross section of sample (test D23).

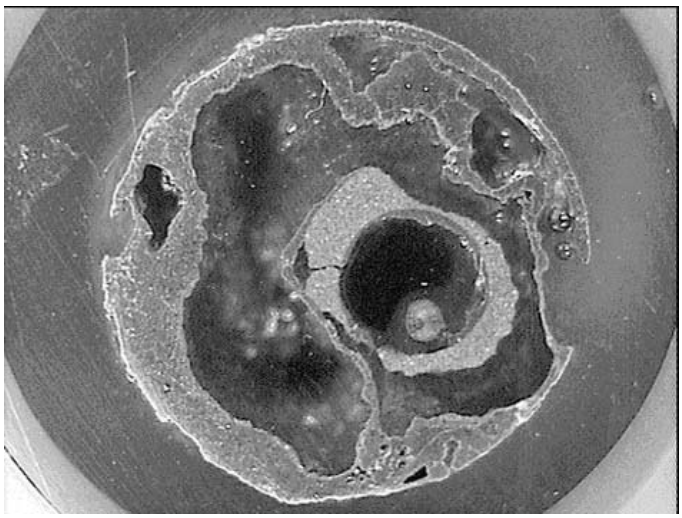

Fig. 6: Cross section of a fuel rod showing large part of pellet dissolved (test D20).

Post-test examination showed clear dissolution of both the external ZrO_2 cladding scale and the inner UO_2 pellets for tests carried out above the melting point of Zry and relocation of resulting U-O-Zr melts (Figures 5 and 6). A downward movement of the melts with penetration in-between fuel pellets and in the upper central pellet holes was observed. Main results were:

- differences on fuel dissolution phenomenology at the *rod scale* due to additional coupled phenomena compared with crucible tests, in particular concerning the UO_2-cladding gap effect and the inner U-O-Zr melt relocation to lower positions into the space between pellets,
- local effects with non-uniform axial and radial UO_2 and ZrO_2 dissolution due to stronger dissolution in zones with smaller UO_2-cladding gap width,
- complete dissolution of ZrO_2 in some tests with a thin initial oxide layer,
- cladding failures due to radial cracking or total dissolution of the outer ZrO_2 layer. They did not induce external relocation of the U-O-Zr melts,
- no significant difference between PWR and VVER rods regarding fuel rod dissolution and the resulting clad failure processes.

These data were analysed with the fuel rod dissolution models of ICARE/CATHARE and SVECHA codes, the latter having being improved based on RIAR results.

C.1.1.3 Calculations of the fuel rod dissolution tests (IBRAE, ENEA, KI)

Calculations were provided for the preparation of the tests and the analysis of results. The final objective was modelling improvements and code validation on early fuel liquefaction and

cladding failure. Three codes were involved in this task: SVECHA, ICARE/CATHARE and SCDAP/R5.

SVECHA: This single-rod code was specially designed for detailed modeling of fuel rod degradation phenomena such as clad oxidation and deformation, fuel-pellets mechanical and chemical interactions and clad failure. The AEKI tests were analysed using a version of the simultaneous UO_2 and ZrO_2 dissolution model developed in the CIT project and upgraded with new RIAR results.

Analysis of experimental data shows that observed oxide scale thickness is much thicker than predicted by pre-test calculations. Figure 7 illustrates for test D10 that the oxide scale of the cladding and uranium pellets are attacked by molten Zircaloy during the annealing stage. Before metal Zircaloy melting, the oxide thickness decreases during the heat-up stage under steam starved conditions owing to re-dissolution of the ZrO_2 scale in the under-laying α-Zr(O). To explain this disagreement, it was suspected that pure steam starved conditions were not completely realised in the tests and that some steam was also accessible in the final high temperature dissolution stage.

A post-test calculation of test D10 was done with the assumption of steam supply in the final stage of the tests (Fig. 8). It shows a noticeable pellet dissolution and does not show a complete dissolution of ZrO_2 as observed in the pre-test calculation. Nevertheless the ZrO_2 scale is overestimated compared with the test. The hypothesis of some oxygen access during the dissolution stage was not refuted by AEKI while oxidation conditions simulated in the post-test calculation seems overestimated.

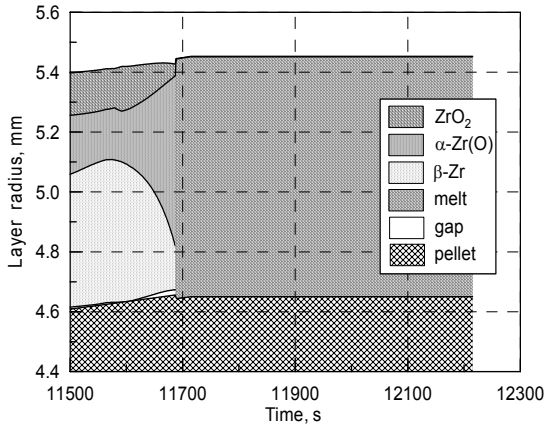

Fig. 7: Pre-test calculation; evolution of fuel rod layers in the AEKI test D10.

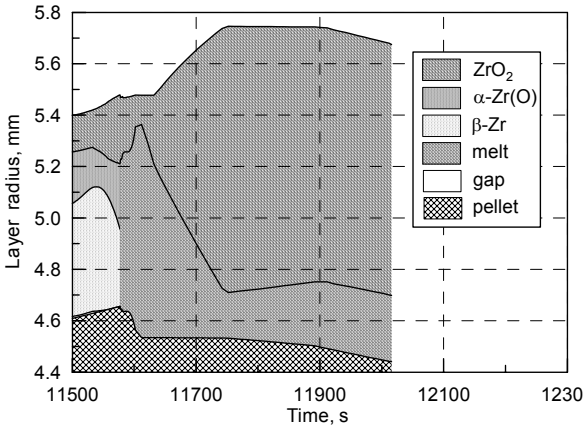

Fig. 8: Post-test calculation; evolution of fuel rod layers in the AEKI test D10.

ICARE/CATHARE and SCDAP/RELAP5 codes: Pre-test and post-test calculations as well as sensitivity studies were carried out by ENEA and KI to evaluate the effect of some parameters on the fuel rod dissolution. When the ZrO_2 dissolution model was used in ICARE/CATHARE, the limiting effect on UO_2 dissolution and the enhanced effect on clad failure were overestimated compared to experimental results. The prediction of UO_2 dissolution was found very dependent on three parameters: the initial extent of clad oxidation, the efficiency of the parallel ZrO_2 dissolution and the fuel solubility in the U-O-Zr melt. The code-to-data comparison was difficult,

the observed internal melt relocation being not taken into account in the dissolution models. In addition, uncertainties were found on the oxidation state reached just before the dissolution stage.

Main characteristics of analysed PWR fuel rod tests and ICARE/CATHARE and SCDAP/R5 code results are summarized in Table 2.

Table 2: Summary of results of post-test analysis

AEKI TEST	Test Conditions		RESULTS					
	Tox (°C) tox (s)	Tdis (°C) tdis (s)	CODE	ZrO2 layer thic. (µm)	Clad failure	ZrO2 layer dissol. (%)	UO2 dissol. (%)	% of UO2 in the mixture
D2	1150	2050	ICARE	317	no	55.2	17.4	32.6
	10600	272	SCDAP	270	no	0	26	51
D7	1050	2000	ICARE	223	no	38.1	6.4	15.6
	10800	--	SCDAP	168	no	0	0	0
D10	1050	2150	ICARE	222	yes / no	100 / 0	16.1 / 31.8	-- / 50.9
	10700	225	SCDAP	167	no	0	51.3	62
D16	1050	1900	ICARE	248	no	1.6	0.6	2.8
	13400	--	SCDAP	187	no	0	0	0
D17	1050	2050	ICARE	158	yes / no	100 / 0	11.4 / 31.8	-- / 49.2
	5400	--	SCDAP	119	no	0	26.5	44
D18	1050	1760	ICARE	159	no	1.9	0	0
	5400	--	SCDAP	120	no	0	0	0
D19	1050	2026	ICARE	186	no	19.9	0.4	1.3
	7200	--	SCDAP	140	no	0	22.3	41
D20	1050	1900	ICARE	223	no	8.1	1.2	4.1
	10800	50	SCDAP	168	no	0	18.3	39
D23	1050	1900	ICARE	130	no	1.5	0.8	3.2
	3600	129	SCDAP	98	no	0	0	0
D27	1150	2061	ICARE	199	yes / no	100 / 0	15.5 / 22.9	-- / 42.1
	4000	--	SCDAP	169	no	0	23.2	43
D28	1050	2084	ICARE	110	yes / no	100 / 0	7.9 / 32.9	-- / 48.7
	2550	58	SCDAP	83	no	0	25.4	42
D29	1050	2160	ICARE	89	yes / no	100 / 0	6.2 / 35.1	-- / 49.8
	1650	78	SCDAP	67	no	0	27.9	44

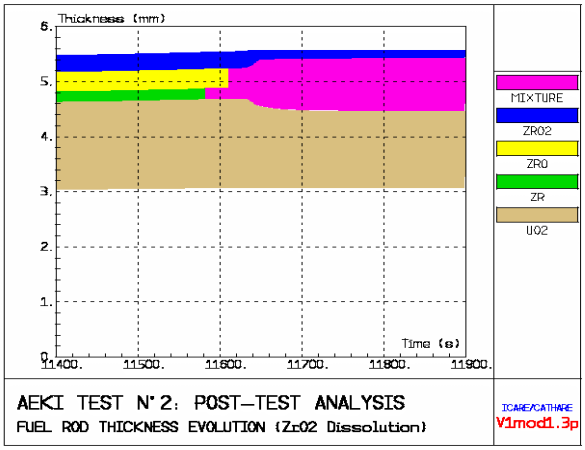

Fig. 9: Fuel rod thickness for D2 test

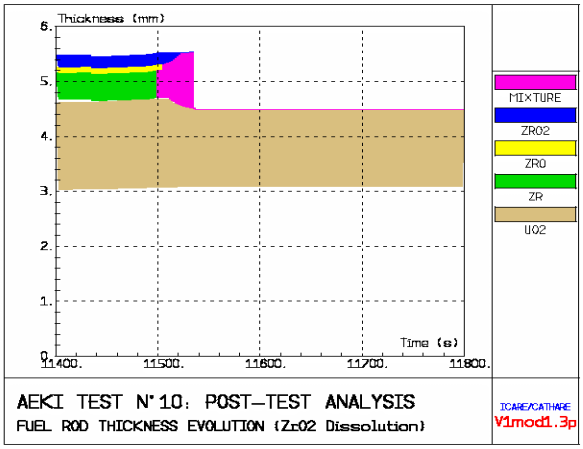

Fig. 10: Fuel rod thickness for D10 test

Discrepancies in the code results depend mainly on different code models as was found verified in the pre-test analysis. In general SCDAP/RELAP5 overpredicts UO_2 dissolution with respect to ICARE/CATHARE. No ZrO_2 dissolution is modelled by SCDAP/RELAP5. The fuel dissolution calculated by ICARE/CATHARE is illustrade in Figures 9 and 10 for tests D2 and D10. For the former, there is no clad failure and the dissolution is limited by the solubility limit. The fuel dissolution calculated by ICARE/CATHARE can be significantly limited by the oxide scale chemical dissolution responsible of the clad failure and molten mixture relocation, as observed in the calculation of test D10 (Fig. 10).

Comparison with Experimental Data

In many tests, the relocation of the melt to lower positions and the penetration of molten material into the space between pellets complicates the pictures of dissolution process. Furthermore, the interactions were non-uniform in axial and radial directions. Small cracks and local effects were able to accelerate the local dissolution and the movement of molten materials. Because of that, the comparison of code results with experimental data was somewhat difficult.

High dissolution of UO_2 by molten Zircaloy was observed in the tests, when the temperature of the cladding was high enough to promote the interaction between the UO_2 and the cladding. High UO_2 dissolution is calculated by the codes, for tests at higher temperature (over 2000 ºC), in reasonable agreement with experimental data. In general, SCDAP/RELAP5 code seems to overpredict fuel dissolution, while ICARE/CATHARE underpredicts it, owing to different dissolution limit. In general, both codes tend to underpredict fuel dissolution for tests conducted at temperature below 2000 ºC.

Complete dissolution of external oxide scale took place in some tests with thin initial oxide layer. This behaviour is quite well captured by ICARE/CATHARE which models chemical dissolution of ZrO_2.

The use in ICARE/CATHARE of the Kim-Olander convective model for fuel dissolution with a solubility limit between the liquidus and solidus lines of U-Zr-O phase diagram can be recommended to better reproduce tests at high temperature (T>2000 °C). The evaluation of fuel dissolution in the lower temperature range is much more uncertain. The need to model oxide scale dissolution has been confirmed while this effect seems overestimated in the current model. This process remains limited if the initial Zry charge is mainly α-Zr(O).

C.1.1.4 UO_2 and MOX dissolution tests using fresh and irradiated fuel (JRC/ITU)

In the previous CIT project, a considerable accelerating effect of irradiation on fuel dissolution behaviour was demonstrated and it was evident that the effect of burn-up needed to be further investigated. The main objective of the new dissolution tests was the examination of high burn-up UO_2 and MOX dissolution by Zry and comparison with fresh fuel. However the burn-ups were not comparable. For irradiated UO_2 the available fuel had mainly a very high burn-up of ~90 GWd/tU (few samples with a burn-up of ~65 GWd/tU were also available) and the irradiated MOX had a burn-up of only ~46 GWD/tU.

A new furnace was constructed to work in a hot cell. In spite of difficulties, tests were successfully done by heating simultaneously a fresh and an irradiated sample of either UO_2 or

MOX samples located in two Y_2O_3 crucibles, one placed top of the other inside an external tungsten crucible inside the furnace. Samples were slices of cladded fuel rods, few mm thick. Post-test analysis enabled the dissolution to be quantified. Tests at constant temperature between 1700 and 2200 °C were carried out in *pure He* ramping to temperature with two heat-up rates 0.5 K/s or 5 K/s. After testing, the crucibles were removed from the furnace and photographed using the periscope from above in their crucibles. After photography the fuel samples were embedded in resin and cut vertically for post-test analysis in order to quantify the fuel dissolution.

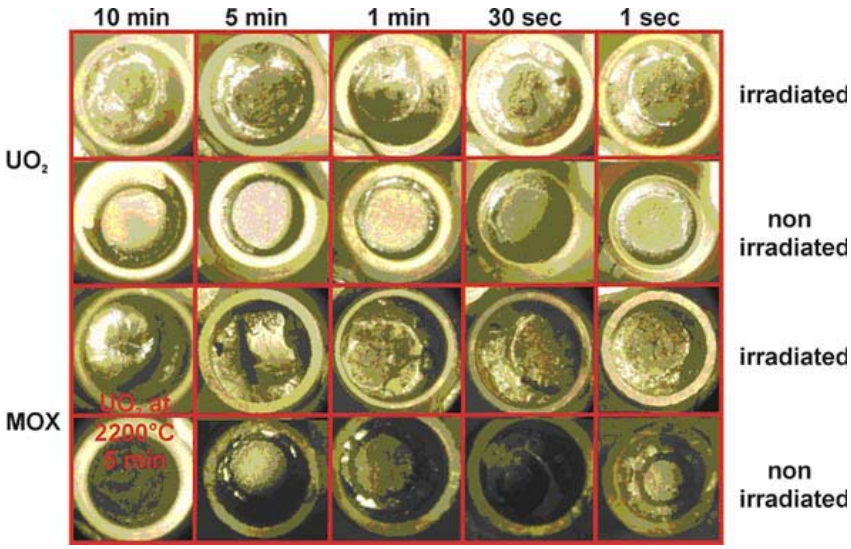

Figure 11: Upper views of the crucibles with irradiated and non-irradiated UO_2 and MOX fuel heated to 2000 °C for various times and to 2200 °C for two MOX tests at 10 min (lower part left).

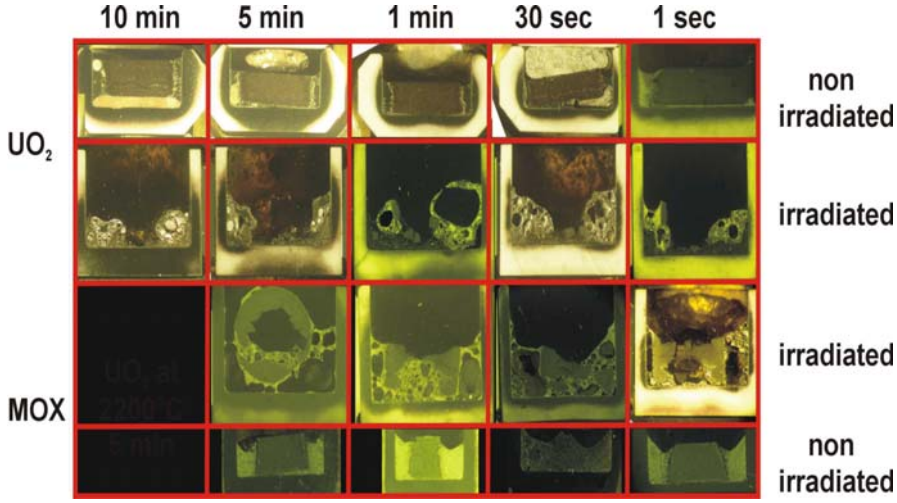

Figure 12: Axial views of the crucibles for irradiated and non-irradiated UO_2 and MOX heated to 2000 °C for various times.

Figure 11 shows periscope photos of tests at 2000 °C for different periods. Dissolution of irradiated UO_2 and MOX is compared to dissolution of fresh fuel in the same conditions. Figure

12 shows vertical cross-sectional examinations of the same series of UO_2 and MOX tests. These two figures show that the burn-up is an important parameter in the process of fuel dissolution during a severe accident. There is clearly a higher and heterogeneous dissolution of irradiated fuel and disintegration of the fuel into fragments compared to the uniform nature of the attack for fresh MOX and UO_2 fuel. This is for two main reasons:

- (i) the thermal cracking in the irradiated fuel allows melt penetration and assists the fuel break-up,
- (ii) the fission gas release can enlarge the grain boundaries as well as causing bubbling of the melt and generally improve the melt-fuel contact.

The high burn-up UO_2 fuel (~ 90 GWd/tU) from these tests appears to dissolve faster than the medium burn-up MOX fuel (~ 45 GWd/tU). Whether the UO_2 or the MOX fuel of similar burn-up dissolves faster could not be concluded from these experiments, since the burn-ups of the two fuels are too different. Final tests with irradiated MOX and UO_2 (90 GWd/tU) showed a wide scattering of results. Additional data are needed with improved quantification of the kinetics and more comparable burn-ups for MOX and UO_2.

C.1.2 Tests on U-O-Zr oxidation by steam (ÚJP-PRAHA)

The objective of these tests was to quantify the oxidation kinetics of selected U-O-Zr mixtures representative of those generated in the early phase of core degradation. The tests were performed in a new test facility equipped with a resistance furnace and continuous measurement of the generated H_2 from the oxidation based on gas thermal conductivity (Special NED issue on FISA-01). Various solid U-O-Zr alloys with different compositions were studied up to 1670 K.

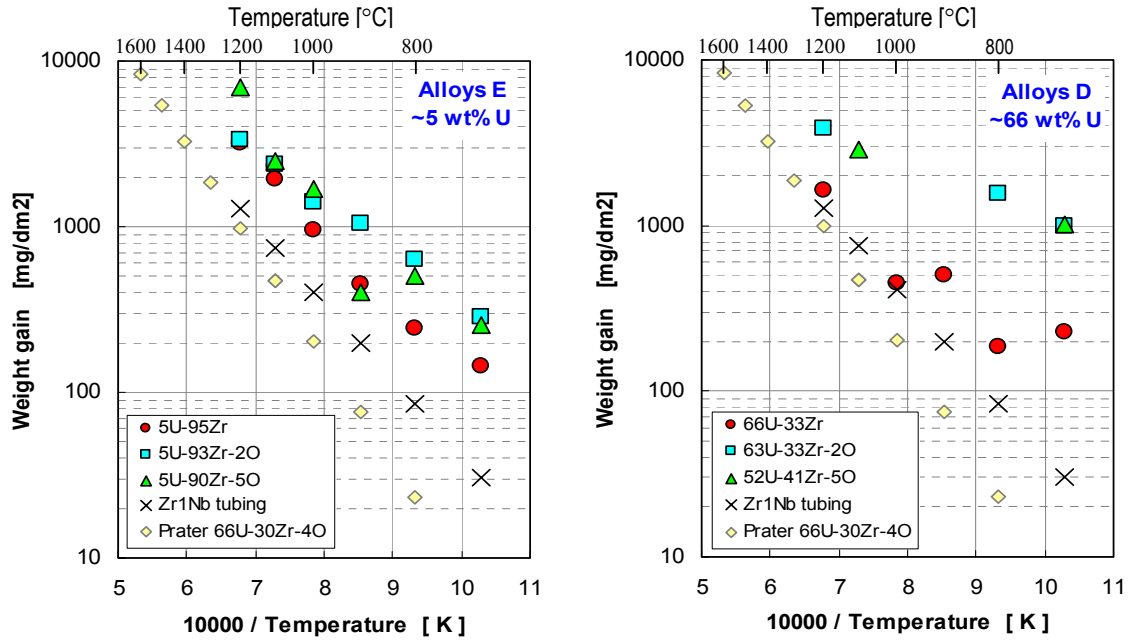

Fig. 13: Weight gain of two U-Zr-O specimens after 10min in steam in isothermal conditions at temperatures between 700-1200°C.

Figure 13 gives the weight gain of two series of low and high U content alloys. Results are compared with the oxidation of Zr1%Nb and with Prater results. The oxidation of the tested U-Zr-O alloys in the temperature range 700-1200 °C is faster than that of Zr1%Nb or the 66U-30Zr-4O wt% alloy of Prater. Alloys with higher U content show oxide spalling and cracking already at the test temperature and also during cooling. These effects were responsible for the non-parabolic behaviour of the oxidation resulting in enhanced H_2 release. The largest difference compared with oxidation of Zr1%Nb was found at low temperatures (~700°C) for alloys with both high U and O content. Alloys with ~60 wt% U oxidised ~33 times faster than Zr1%Nb alloy. At 1200 °C, the fastest oxidation was observed for alloys with 5 and 15 wt% U and 5 wt% O, the enhancement factor against Zr1%Nb being ~5.5.

Main efforts were focused on 30U-65Zr-5O and 5U-90Zr-5O wt.% alloys, respectively named C2* and E2*. Figure 14 illustrates the oxidation kinetics of these alloys. Main results are:

- All U-Zr-O alloys oxidise faster than pure Zry in the temperature range 400-1400 °C. This behaviour generates more hydrogen than expected using pure Zry oxidation kinetics,
- Oxide spalling and sample cracking are responsible for the enhanced oxidation,
- Larger oxidation rates were found for alloys with O content >2 wt.% and U content >15 wt.%. Some U-rich alloys are pyrophoric and disintegrate during oxidation at 970 K,
- While results are consistent with the Prater parabolic law at 1670 K, they show significantly higher kinetics than the extrapolation of this law to lower temperatures (Ref.[15].

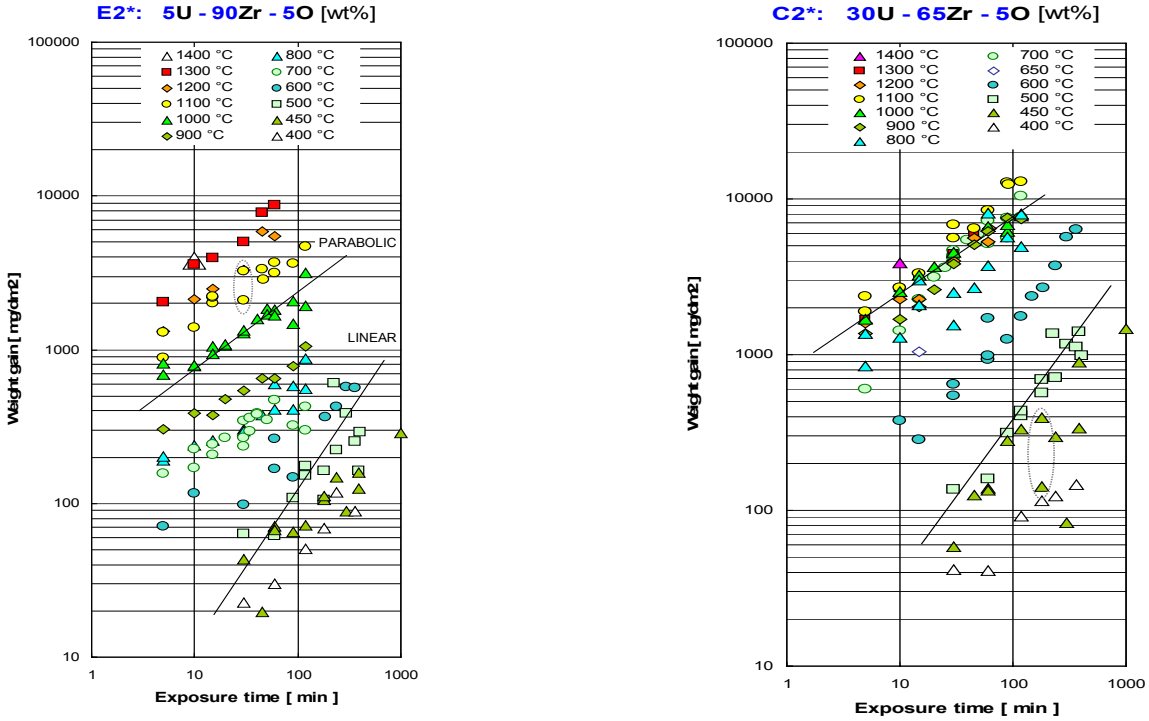

Fig. 13: Oxidation kinetics for E2* and C2* alloys in Ar/steam mixture.

These results support the hypothesis that the unexplained enhanced H_2 production observed during the reflood of degraded fuel could be caused for a large part by oxidation of relocated U-Zr-O alloys. This oxidation process is not considered in SA codes that cannot predict on any

physical basis the H_2 peak observed during reflood. A preliminary model has been proposed and introduced in the ICARE/CATHARE code (see § C.3.2).

C.1.3 ZrO_2 dissolution tests and oxidation of molten Zr-O mixtures (FZK)

For modelling purpose for the oxidation of Zr-O and U-Zr-O melts new FZK tests were carried out to study the dissolution of Y_2O_3-stabilised ZrO_2 crucibles by molten Zry. These single-effect tests were specially designed for the investigation of long-term behaviour of the melt-ZrO_2 interaction considered representative of a melt oxidation process. Isothermal heating experiments at 2100 °C and 2200 °C with annealing times up to 290 min were performed (Ref.[32]).

The specimens were inductively heated by means of a tungsten susceptor in the LAVA furnace used also in the previous CIT test series (Ref.[16]). The specimen was heated to the desired test temperature (2200-2400 °C) with a heating rate of about 15 K/s. After a pre-determined annealing time the specimen was rapidly cooled down. The crucible temperatures were continuously recorded by a monochrome pyrometer and a W/Re thermocouple. The majority of tests were characterized by the outer surface of the crucible sidewall hotter than the crucible bottom and by significant temperature gradient between the crucible wall and the inner melt due to heat losses by heat radiation from the melt surface.

The tests can be divided into three characteristic groups: tests at 2100 °C, tests at 2200 °C with S/V=770 m^{-1} and tests at 2200 °C with S/V=720 m^{-1}. Figures 15 and 16 shows the temperature behaviour and the cross-sections of some crucibles used with the measured values of the transition layer thickness. Figure 16, which also illustrates the final axial cross-section of the crucible found in a test with a shot interaction period (15 min.), shows three characteristic zones: the crucible wall with the α-Zr(O) precipitates on the grain boundaries, the corrosion transition layer ZrO_{2-x} and the inner refrozen melt.

The test series at 2200 °C with S/V=720 m^{-1} includes the tests with a long time of annealing. The test FA10 of this series has a maximum test duration in isothermal conditions of 290 min and is characterised by the complete dissolution of the corrosion layer (Fig. 16). Some cross-sections show the presence of relatively large voids in the melt. These voids can be interpreted as gas bubbles that formed at temperature with the tin vapour from Zr melt or with the oxygen not dissolved in the melt.

A quantitative image analysis of the melt was performed in order to determine the composition of the melt and its oxygen content. Melts compositions were found to be representative of the two-phase region of the Zr-O phase diagram (melt with ZrO_{2-x} precipitates). With the oxygen gradient between the wall and the melt, the oxygen content in the melt increases continuously and can reach the concentration that corresponds to a total melt oxidation (Ref.[17]). Main results were as follows:

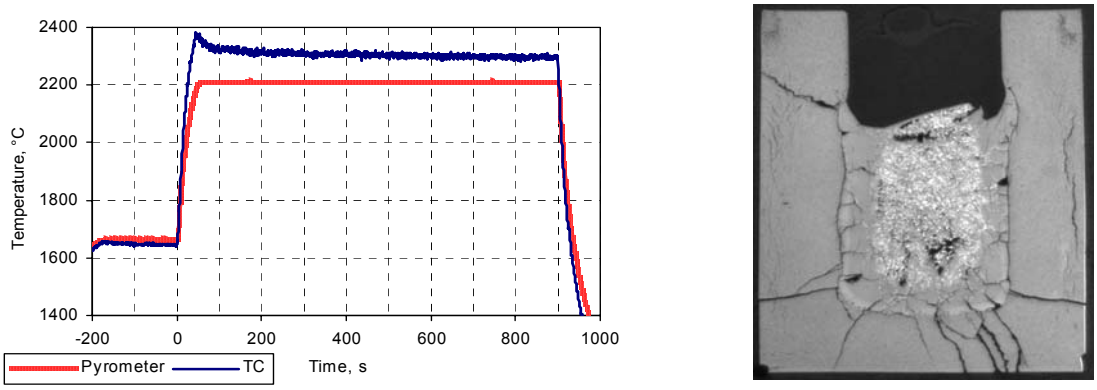

Fig. 15: Test FA9, S/V=770 m^{-1}, 15 min. Temperature behaviour during the test at 2200 °C at bottom of the crucible and cross sections of the ZrO_2 crucible after 15 min. of dissolution by molten Zry

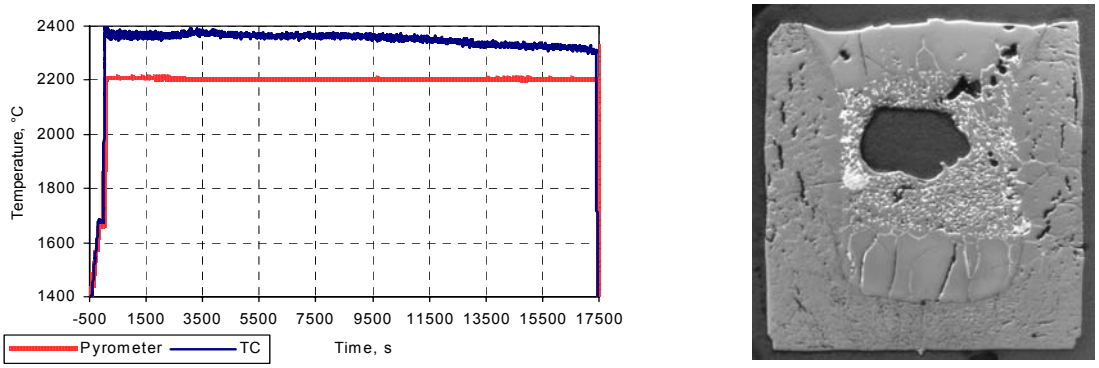

Fig. 16: Test FA10, S/V=720 m^{-1}, 290 min. Temperature behaviour during the test at 2200 °C at bottom of the crucible and cross sections of the ZrO_2 crucible after 290 min. of dissolution by molten Zry

- Three stages of interaction were observed, 1) a short-term phase of crucible wall dissolution named “early dissolution” or “erosion”, 2) a medium-term phase named “corrosion phase” with oxide layer formation at the crucible-melt interface and 3) a long-term phase of the repeated wall dissolution named “late dissolution”.

- Two oxygen sources for the melt oxidation can be distinguished: the oxygen from the dissolved part of the crucible in the early dissolution phase and the oxygen continuously transported to the melt by diffusion from the ZrO_2 crucible matrix.

- The kinetics of the process was controlled by the temperature distribution in the system, in particular by the temperature difference between the melt and the crucible wall.

- For all tests, the oxygen content in the melt (liquid and ZrO_{2-x} precipitates) was representative of the two-phase region of the Zr-O phase diagram.

- This database was used for modelling the oxidation of molten Zr-rich mixtures in steam.

C.1.4 Tests on B_4C oxidation and B_4C-CR degradation (FZK, IRSN)

B_4C oxidation and related effects on core degradation was a key topic of the COLOSS project. It was investigated through various SETs at IRSN using the VERDI furnace and at FZK using various set-ups 1) a thermo-balance suitable for on-line measuring of kinetics (TG-tests), 2) the new BOX rig with a mass spectrometer to measure the gases resulting from B_4C and B_4C-steel-Zr oxidation, 3) the QUENCH-SR rig to study the degradation of short B_4C-CR. Different temperatures, flow rate and steam partial pressure conditions were studied by the two experimental teams enabling the production of a significant database covering different aspects of the oxidation of various B_4C materials (BWR, VVER and PWR design).

The context of this topic has been given in the Special NED issue on FISA-01 (Ref.[7])). The main concern was to identify the impact of B_4C on core liquefaction, on H_2 production and on the formation of boron and carbon gaseous species (CO, CO_2, CH_4, B_2O_3 and boric acids), which could modify the chemistry and the transport in the primary circuit of certain volatile FPs, in particular iodine (gaseous forms) and caesium. This is of prime importance for the evaluation of the source term from the containment. These data were also of particular interest for the preparation of the PHEBUS FPT3 experiment planned with a central B_4C control rod.

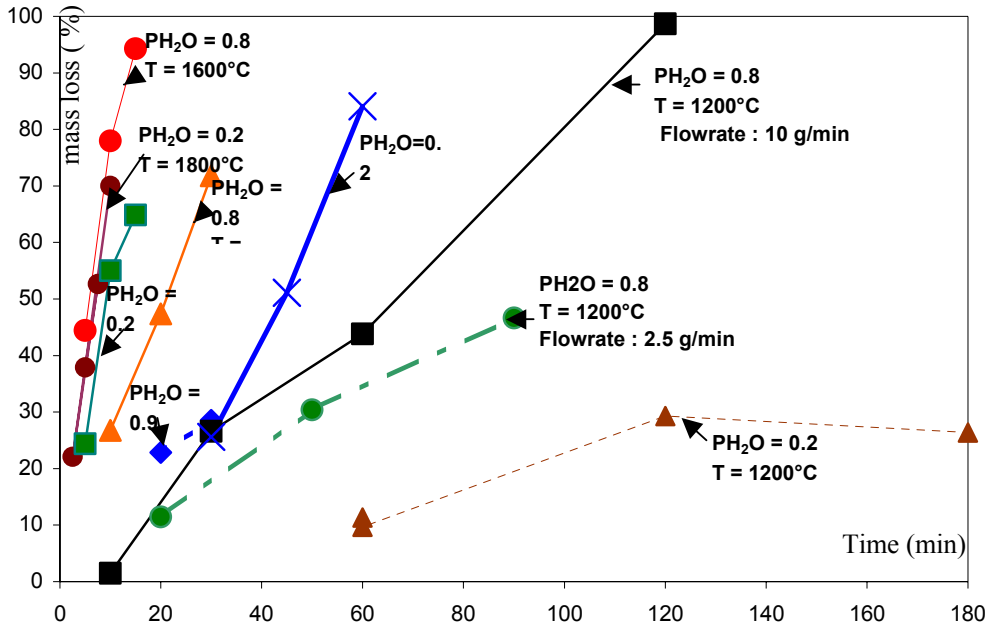

Fig. 17: B_4C mass loss versus time for different temperature and partial pressure conditions.

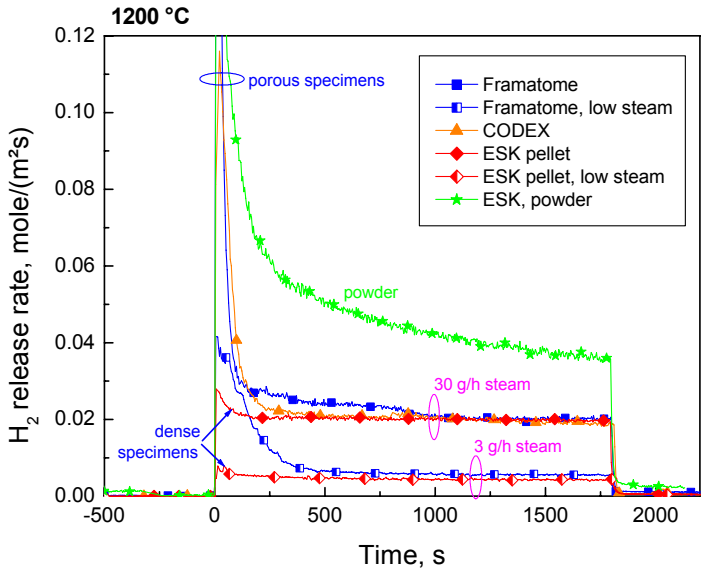

Fig.18 : Specific hydrogen release rates during isothermal oxidation of the various B_4C specimens. Influence of porosity and steam flow rate.

Several B_4C oxidation tests have been performed in the VERDI, TG and BOX rigs in different conditions with temperatures between 1200 °C and 1800 °C (isothermal and transient conditions), total flow rates between ~ 2 to 10 g/min and the steam partial pressure between 0.2 and 0.9 Pa. Figure 17 illustrates VERDI results on the mass loss of standard Framatome 1300/1450 PWR B_4C pellets versus time for different temperatures and thermal-hydraulic conditions (partial pressures, steam flow rate). In particular, this figure illustrates the effect of steam flow rate on two series of tests carried out at 1200°C and with steam partial pressure of 0.8 atm.

The BOX rig tests enabled the measurement of gases produced by the B_4C oxidation. Besides H_2 and boron species, CO and CO_2 are the main reaction products. Only negligible amounts of methane were released during high temperature oxidation and low amounts were only produced at the lowest experimental temperature studied (800 °C). The oxidation of different B_4C samples studied in the BOX rig is presented in Figure 18. The initial H_2 peak production is tightly correlated with the B_4C porosity. Large initial H_2 rates are only observed for the porous pellets and B_4C powder. They are followed by a quite constant oxidation rate dependent only on thermal-hydraulic boundary conditions (steam flow rate). At the onset of oxidation, the formed liquid B_2O_3 fills or clogs up pores during a 1st phase whose duration depends on B_4C porosity. Afterwards only the geometric surface is available for steam access during the constant rate reaction phase.

IRSN and FZK results indicated a large sensitivity of B_4C oxidation to the temperature and to the thermal-hydraulic conditions. In particular the steam partial pressure and, to a less extent, steam flowrate were found to be sensitive parameters whatever the temperature is (Figure 17 and 18).

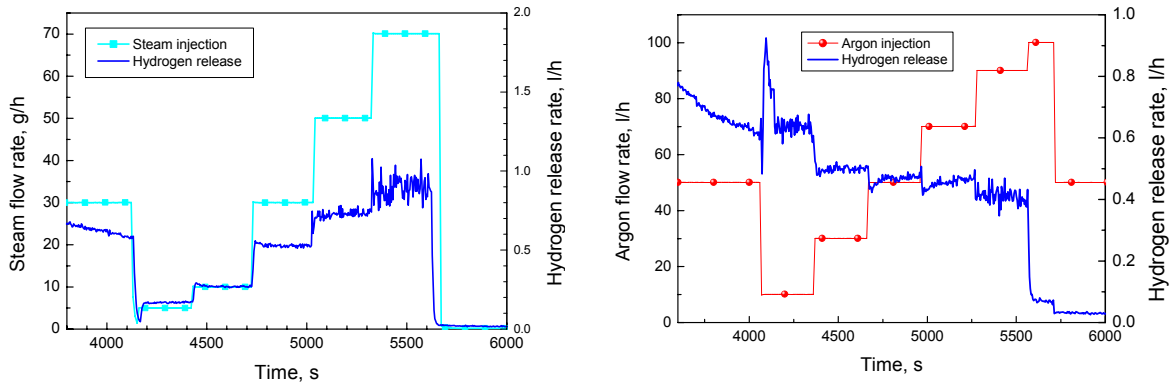

Fig. 19: Influence of steam (left) and argon (right) flow rate on the oxidation kinetics of B_4C at 1200 °C

Figure 19 shows the results of two BOX rig tests with stepwise changing steam and argon atmosphere. The increase of the steam flow rate by one order of magnitude (steam partial pressure 0.11→0.64 bar) enhances the oxidation rate by a factor of five. On the other hand, the increase of the argon flow rate by an order of magnitude (steam partial pressure 0.79→0.27 bar) causes a decrease of the oxidation rate by about 30 %. These results demonstrate that the oxidation rate of boron carbide is strongly influenced by the steam flow rate and by the steam partial pressure of the inlet gas mixture. These two parameters determine the local steam partial pressure at the surface of the specimen and therefore the oxidation rate (Ref.[18]).

The complementary TG tests, with on-line measurement of mass changes of the sample was well suited to understand the complex mechanisms of B_4C oxidation and satisfy modelling needs. This experimental programme enabled to confirm the complex mechanisms of B_4C oxidation mainly determined by the formation and evaporation of a liquid B_2O_3 layer that acts as a diffusion barrier, mainly at a temperature lower than 1400°C (Ref.[19]). The B_2O_3 behaviour is driven by mass transfer and depends on thermal-hydraulic conditions.

Interpretation of IRSN and FZK results on B_4C oxidation (IRSN, FZK)

The B_2O_3 behaviour is driven by the effect of its pressure saturation conditions on mass transfer and depends also on thermal-hydraulic conditions governing the B_2O_3 concentration gradient between the boundary layer and the flow bulk. At higher temperatures (T>1400 °C), the B_2O_3 consumption by evaporation and chemical reaction with steam is very fast, no B_2O_3 exists on the B_4C pellet and the kinetics is linear. At lower temperatures the B_2O_3 layer growth results in initial parabolic oxidation kinetics. A liquid B_2O_3 layer is expected to exist at 1200 °C and is a limiting factor for the B_4C oxidation (Ref.[20]). In the range between 1200 °C – 1400 °C the physical form of the B_2O_3 is more uncertain steam partial pressure and total flow rate were found to influence the oxidation. Surface reaction and gas phase transport phenomena determine the kinetics at temperatures relevant for severe accident conditions (T >1300 °C).

C.1.5 SETs on degradation of B_4C control rod segments and oxidation of B_4C-rich mixtures

Various series of single B_4C-CR segment tests were carried out in BOX as well as in the single rod QUENCH-SR rigs (Ref.[21]). The degradation of B_4C-CR is strongly dependent on the atmosphere. In oxidising atmosphere, the external ZrO_2 oxide scale of the guide tube prevents the control rod from early failure. Consequently, axial melt relocation initially occurs only inside the guide tube and the release of carbon and boron oxidation products is deferred.

The axial cross-section of a 10 cm long B_4C-CR is shown in Figure 20. One can see the B_4C-rich melt generated and its distribution inside the rod as well as the local consumption of the B_4C pellets. More B_4C consumption was found in the upper part near the position of the guide tube failure. The failure temperatures detected by the release of considerable amounts of B_4C oxidation products were found in the range between 1350 and 1500 °C. Rapid oxidation of the internal B_4C (remaining pellets and B_4C-rich melt) was observed after failure of the oxide scale.

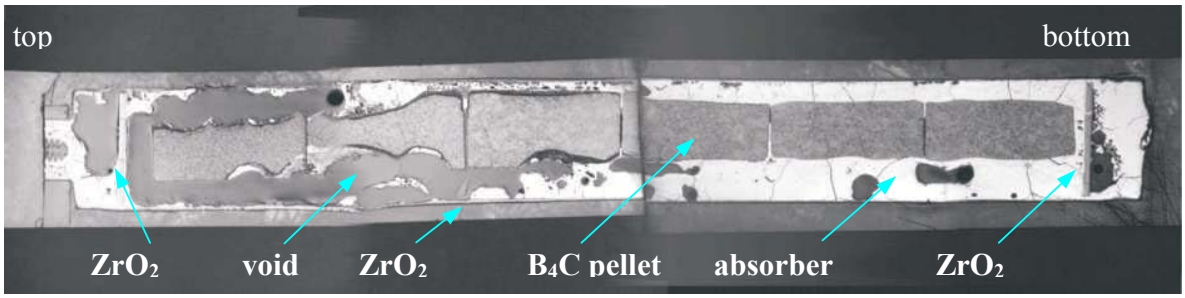

Fig. 20: Vertical cross section of a control rod segment after transient oxidation up to 1580 C in steam (left: top of the vertically tested specimen).

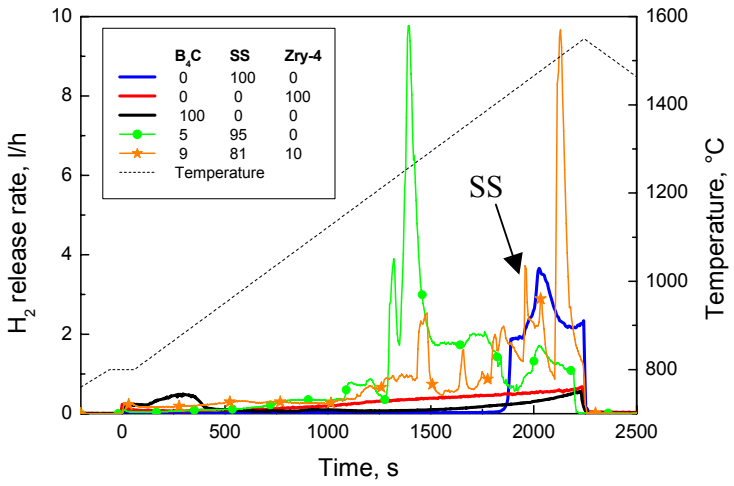

Fig. 21: H_2 release during oxidation of B_4C-rich melts compared with H_2 release from pure components (compositions in wt.%).

Tests on oxidation of B_4C/SS/Zry absorber melts of different composition were also performed in the BOX rig. The oxidation kinetics of these mixtures was significantly higher than that of the pure components and was a stochastic process (Figure 21). The absorber melts were found very corrosive towards the ZrO_2 crucibles under oxidising conditions. These results suggest that a B_4C control rod failure in a fuel rod bundle may cause early failure of surrounding partially oxidized fuel rods. This could impact the early release of fission products, the onset of U-O-Zr relocation and could favour the early degradation of the core.

C.2 Large-scale experiments

Three bundle tests were carried out with a central B_4C-CR, one CODEX-B_4C test with a VVER bundle and two QUENCH-07 and -09 tests with a PWR bundle type. The first two tests being already presented in the special NED issue on FISA-01, this section will mainly focus on B_4C effects and recent Post-Test Examinations (PTE).

C.2.1 CODEX-B_4C: Large scale VVER bundle test with a central B_4C-CR (AEKI)

It is recalled that the CODEX-B_4C test train includes an electrically heated 6-rod VVER bundle arranged on a hexagonal grid with a central B_4C-CR. The test scenario is given in Figure 21 bis. Main particularities are: on-line mass-spectrometry for gas measurements, on-line X-ray radiography of the bundle for degradation evaluation, aerosol particle counters and video recording. Aerosol impactors and gas balloons were used for sampling at selected times.

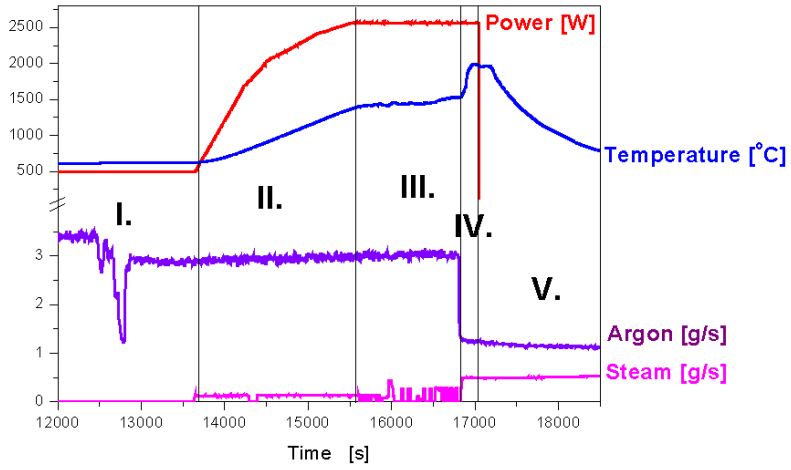

Fig. 21 bis: CODEX-B_4C test scenario.

PTE carried out during the 2nd part of the project include detailed metallographic investigations, radiography, metallography of 13 horizontal cross sections, analysis of the control rod degradation as well as aerosol samples analysis. Figures 22 and 23 respectively illustrate a cross section of the bundle and the axial oxidation profile in the bundle. An electronic experimental database is available for code validation.

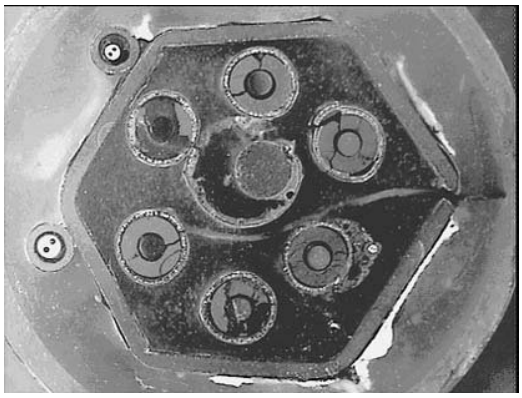

Fig. 22 : CODEX-B_4C bundle cross section at 335 mm elevation.

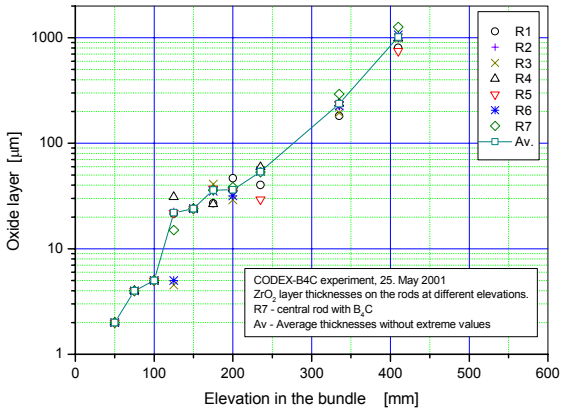

Fig. 23: Clad oxide layer thickness on as versus bundle elevation.

The main objectie of this test was to investigate the impact of a B_4C-CR on the degradation and gas and aerosol production from a VVER-1000 bundle. A significant hydrogen production was observed as a common result of Zr and B_4C oxidation in steam. The peak of hydrogen generation was related to the temperature escalation, the maximum H_2 production being ~40 mg/s and the total H_2 mass ~25 g (Fig. 24).
The methane measurement showed very low values, practically below the detection limit. Both CO and CO_2 production was measured, the maximum production rate was 16 mg/s for CO and 4 mg/s for CO_2 (Fig. 24). The integrated mass of CO and CO_2 showed that ~40% of the original B_4C was oxidized during the test.
The two particle counters indicated high release of aerosols when steam was available in the coolant. The typical concentration of particles in each measured range was close to 10^6 particle/l. The oscillating behavior of the measured values was in direct correlation with the steam supply, which was in manual regulation mode (Fig. 25).

Main outcomes

The CODEX-B_4C experiment provided unique information on the behavior of a VVER-1000 fuel bundle with a central B_4C control rods under severe accident conditions.

- The control rod steel-cladding started to melt and interact with the Zr1%Nb guide tube during phase III. The onset of B_4C oxidation was detected at the end of this period (T~1500 °C).
- No CH_4 was measured during the B_4C oxidation phase. The loss of geometry started with the liquefaction of the steel-cladding of the control rod. B_4C was found to accelerate the fuel rod degradation process.
- The control rod disappeared completely above 335 mm elevation, which means that ~45% of the B_4C was missing. A large fraction of the B_4C was oxidized (~40% of equivalent carbon as was indicated by the release of CO and CO_2). The relocated metallic melt (~3,5 cm^3) in the lower part of the control rod gap contained mainly steel and cladding components.
- The on-line radiography of the bundle indicated that the degradation took place mainly in the high temperature phase (~2000°C), however there was no loss of fuel rod geometry.

- According to metallographic examinations, the Zry cladding and shroud in the upper part of the bundle were completely oxidized (Figure 23). This observation is consistent with the temperature escalation observed during the cool-down phase: the temperature started only to decrease after the complete oxidation escalation in the high temperature zone.
- A very high release of aerosols was observed compared with the previous CODEX tests without control material during the oxidation of core components in steam, the aerosol release being correlated with the steam flow rate. Large amount of blue precipitates was observed on the top of the cooler, containing mainly boron compounds released as a result of B_4C oxidation. Uranium containing particles were also found on impactors activated during the high temperature phase.

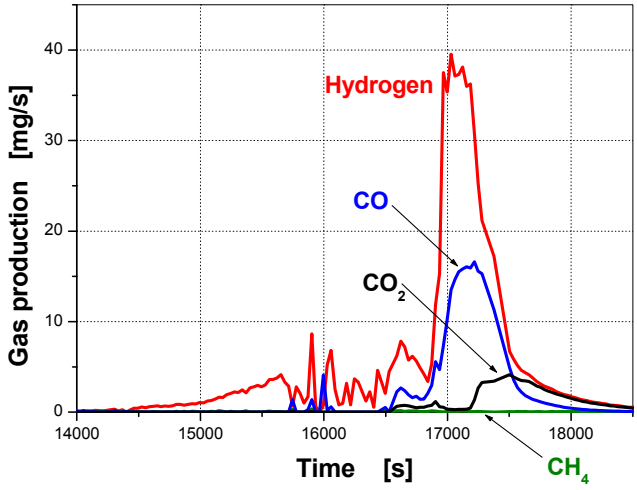

Fig. 24 : Gas flow rates in the CODEX-B_4C test

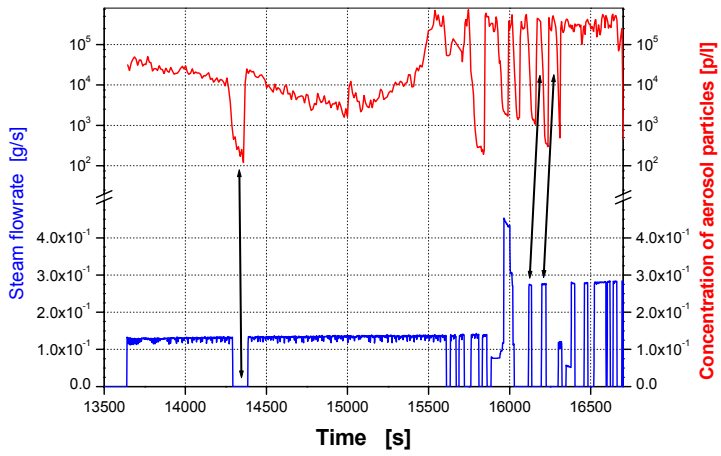

Fig. 25 : Correlation between steam flowrate and aerosol particle concentration

C.2.2 Analytical support to CODEX-B_4C test

Pre-test and post-test calculations were carried out by KI and AEKI with ICARE/CATHARE for the preparation of the test and results were extensively used for the validation of the new B_4C model of the code.

Sensitivity studies carried out by KI on CODEX-B_4C and CORA-W2 tests showed an increase of the total H_2 production from 10% up to 30% due to direct and indirect effects of B_4C i.e. due to B_4C oxidation and to feedbacks on other degradation phenomena (exothermic B_4C oxidation reaction, relocation of hot B_4C-rich mixtures in colder zones,…). The H_2 increase due to B_4C effects is not directly due to the direct B4C oxidation as confirmed by the analysis of the CORA-W2 test (Fig. 25 bis).

Steam starvation conditions were predicted during phase III, 1000s before the B_4C-CR failure (measured at 16600 s in the test). This indicates that the initial phase of the B_4C oxidation could have been limited up to the final steam flow rate increase at ~16900 s.

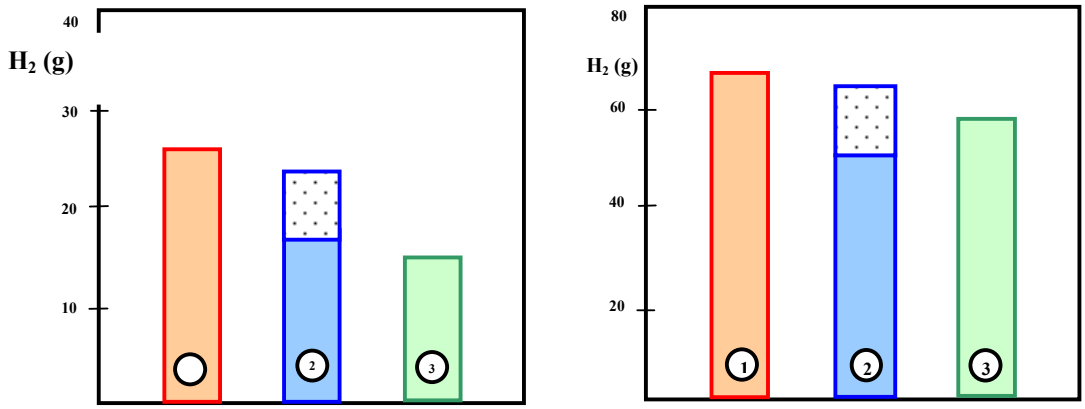

a) CODEX-B_4C test b) CORA-W2 test

Figure 25 bis: Total H_2 generated. (1)-experiment, (2)- calculation with B_4C oxidation (upper rectangle shows H_2 generated from B_4C), (3)- calculation without B_4C oxidation.

An important feature in simulations of the CODEX-B_4C and CORA-W2 tests was connected with the substantial influence of B_4C absorber rod on the transient. This influence was detected experimentally in the two previous CORA-VVER tests and was also evidenced by these calculations as follows:

- B_4C material starts to relocate earlier than the fuel rod cladding (about 50-100 seconds);
- B_4C-rich melts flow down before the bundle temperature escalation and step-by-step preheated the lower part of the bundle up to 1500 K;
- During melt relocation mixtures accumulate in preheated region where the bundle damage is accelerated.

The commissioning test and the preparation of the CODEX-B4C was supported by ICARE/CATHARE carried out by AEKI. The post-test analysis of the CODEX-B_4C test was

performed with the input data set developed for the pre-test calculations. Figure 90 illustrates the top part of the heated section. The early temperature escalation calculated at ~ 15500 s not observed in the test probably due to the overestimation of the Zr oxidation in the transition period during the recrystallization of the cladding material. The final escalation process however was well represented. The overall hydrogen generation was underestimated in the final escalation period (total H_2 measured: 24.5 g, total H_2 calculated: 15.5 g). Strong degradation was predicted in the upper part of the bundle. The control rod pellets disappeared at the upper part. The SS cladding was dissolved in this position with guide tube and the shroud in the upper part was fully oxidized. The overall B_4C effect being underestimated, the current B_4C-modeling remains to be improved.

C.2.2 QUENCH-07 test: Large scale bundle test with a central B_4C-CR (FZK)

The test conduct was broadly similar to previous QUENCH experiments, but with the inclusion of a special temperature plateau to study the B_4C absorber rod degradation and oxidation in steam-rich atmosphere (Ref.[22]). The scenario is recalled in Figure 26. Main results were:

- The B_4C-CR cladding failure occurred at 1320 °C during the first heat-up and was followed by the release of CO and CO_2 shortly afterwards.
- The production rates of CO, CO_2, H_2, CH_4, and boric acids were nearly constant during the temperature plateau. However, the production of CH_4 was small in comparison to other gases. Metaboric and orthoboric acids were also detected by the mass spectrometer.
- The 2nd heat-up in oxidizing conditions was accompanied by a significant increase of H_2, CO, CO_2 but not of CH_4.
- An unexpected temperature escalation occurred during the final cooling with heat-up rates > 40 K/s above the heated zone. Temperatures up to ~2000 °C were reached just after the onset of cool-down. The shroud was severely damaged and partially molten above ~750 mm elevation. The major part relocated below 1000 mm.

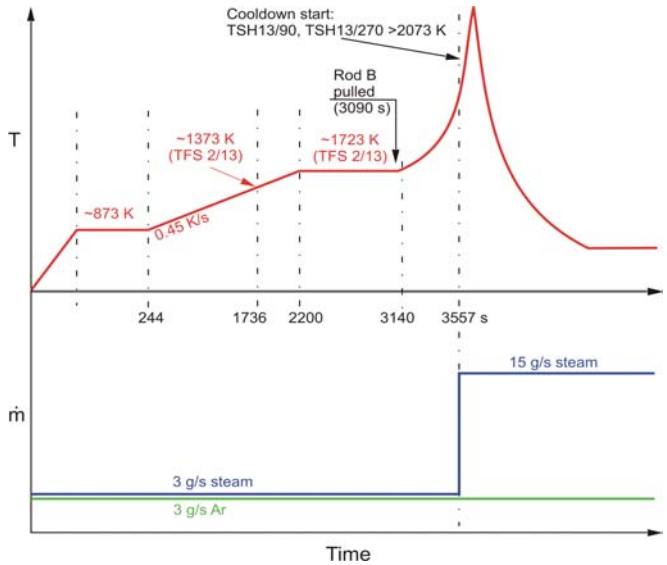

Figure 26: QUENCH-07 scenario.

- During cool-down phase there was a large increase of H_2, CO, CO_2 and boric acids production and a small amount of methane was also detected.

- It was assessed from PTE that 42% of the B_4C was oxidised.

- There is evidence from gas measurements that boron and carbon containing materials were standing in place in the hot zone enabling continuous oxidation of B_4C in the upper part of standing control rods during the 2nd heat-up and cool-down phases. On the lower side of the bundle, the B_4C pellet stack is essentially intact, the pellets being glued together and surrounded by melt. The absorber pellet stack is essentially intact up to ~800 mm elevation. Figure 27 shows the upper part of the degraded B_4C-CR where B_4C oxidation takes place. Thin ceramic structures surrounding the B_4C-CR are identified as guide tube scale.

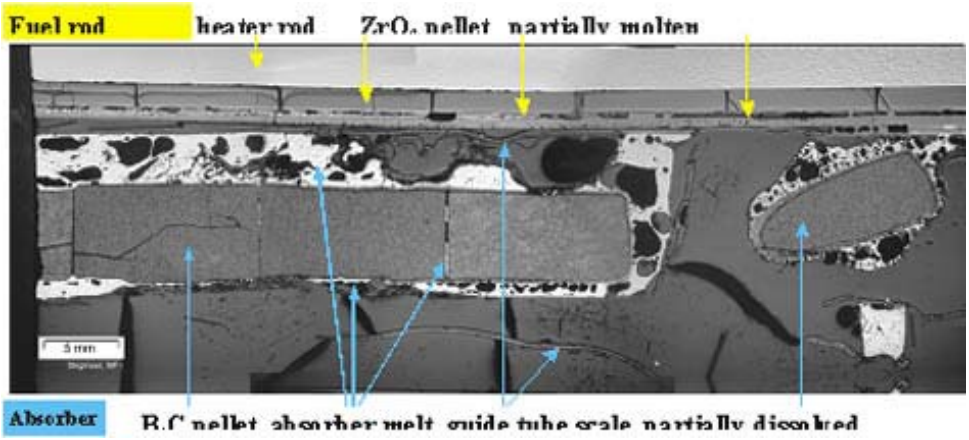

Fig. 27: Axial transition zone in QUENCH-07 test from intact B_4C pellet stack towards absorber rod destruction (760 to ~ 822 mm bundle elevation)

C.2.3 Calculations of QUENCH-07 test (FZK, PSI, UPM, IKE, EDF, ENEA, IRSN)

Extensive QUENCH-07 pre-test calculations carried out with SCDAP/RELAP5, ICARE/CATHARE, MELCOR and ATHLET-CD were necessary to find a test conduct that fulfilled the aims of the test and that guaranteed the integrity of the facility.

Using the initial test protocol recommended, a large sensitivity of the QUENCH facility to changes of experimental parameters such as electrical power or steam mass flow was found. The same codes used for post-test calculations showed difficulties to calculate correct temperature behaviours. Due to the lack of adequate "quench oxidation models", none of the codes could predict the final temperature escalation and associated peak H_2 production observed in the test.

Post-test calculations with SCDAP/R5 (Fig. 28) and ATHLET-CD could not reproduce correctly the temperature plateau. Reasonable results could only be found by using modified boundary conditions.

Post-test calculations with ICARE/CATHARE gave correct temperature and H_2 predictions before the final cool-down phase.

PSI did MELCOR post-test calculations of QUENCH-07 after the adjustement of the input deck on the QUENCH-06 test which was correctly calculated regarding the bundle temperature and the H_2 production using the Leistikov/Prater-Courtright Zry oxidation correlations (Ref.[23]).

- The initial heat-up was in good agreement but the thermal response became increasingly sensitive as the temperatures increased to and beyond 1700 K. The temperature transient was found highly sensitive to the conditions at conditions close to the low-high oxidation transition (~ 1800 K). It appears that the thermal response was driven by the cladding oxidation at these higher temperatures so that small differences in temperature became magnified. Despite these difficulties, the model gave an otherwise good representation of the thermal response, oxidation and degradation up to the initiation of cooldown.
- The offgas composition was calculated with at least acceptable accuracy. In common with the previous SCDAP/R5 analyses, the cooldown excursion was calculated only by artificially enhancing the oxidation kinetics.

Some results are shown in Figure 29.

An additional post-test calculation with MAAP4 was carried out to evaluate the new B_4C model developed by EDF. Among the three B_4C kinetics evaluated, that used by ICARE was found to give acceptable CO, CO_2 and CH_4 production (Table 3).

Table 3: MAAP4 calculations with assessment of hydrogen and non-condensable gases mass at the end of the QUENCH-07 test.

Case	**CO mass (g)**		**CO_2 mass (g)**		**CH_4 mass (g)**	**H_2 mass (g)**	
REFERENCE (no B_4C model)	0,0	-	0,0	-	0,0	152	-23%
ICARE	4,4	-49%	11,7	+1%	$4,0\ 10^{-12}$	189	-4%
MELCOR	10,4	+20%	18,9	+63%	$1,6\ 10^{-9}$	153	-23%
STEINBRÜCK	2,8	-67%	6,4	-45%	$5,2\ 10^{-11}$	106	-46%
EXPERIMENT	8,6		11,6		$2,0\ 10^{-4}$	198	

Sensitivity studies on Zry oxidation laws were carried out by FZK (Ref.[24]), using in particular the FZK recommended correlations of Leistikov/Prater-Courtright (Ref.[35]). Uncertainties on the modelling of electric power and shroud transfer make difficult to conclude on the best Zry oxidation laws. Deficiencies were also stressed regarding oxidation of mixtures.

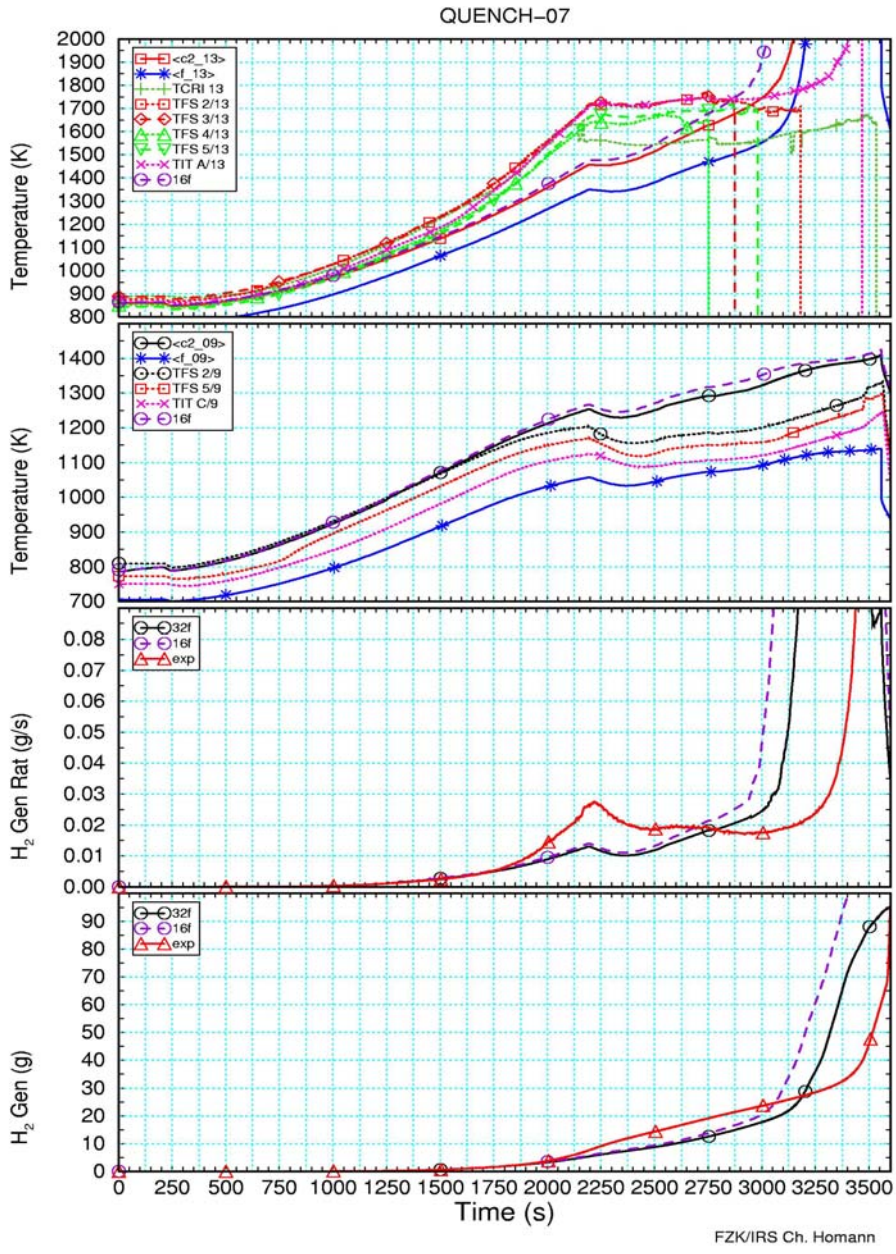

Fig. 28: Post-test calculation of the QUENCH-07 test carried out with SCDAP/R5 by FZK; Comparison of selected measured and calculated variables. From top to bottom: bundle temperatures at axial levels 13 and 9, and measured and calculated H_2 production rate and cumulated H_2 mass.

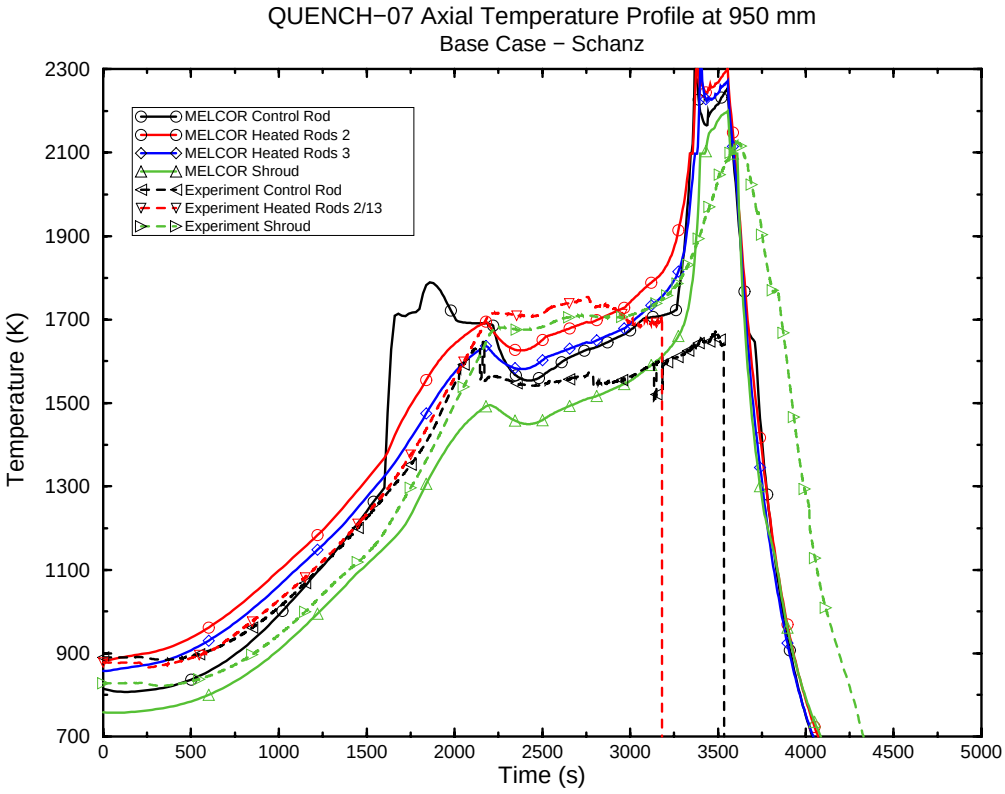

Figure 29: Post-test calculation of QUENCH-07; Comparison of temperatures at elevation 950 mm MELCOR and experimental data, various radial locations.

C.2.4 QUENCH-09 test: Large scale bundle test with a central B_4C-CR (FZK)

The main objective of the QUENCH-09 test was to investigate B_4C effects in steam-starved conditions in order to widen the B_4C database and to provide conditions closer with PHEBUS FPT3 (Ref.[25]). Test conduct was planned to be as for QUENCH-07, but after the temperature plateau steam flow should be reduced to 0.3 g/s to reach steam starvation in the bundle. The final high steam mass flow rate of 50 g/s was aimed at cooling the bundle rapidly to preserve the status of the bundle before cooldown initiation. Figure 20 gives the planned scenario.

Initial degradation of the control rod occurred at ~1550 K during heat-up. Despite the test conduct being identical to QUENCH-07 at this stage, no significant CO, CO_2 or CH_4 generation was observed.

An unexpected temperature escalation occurred at the hottest location (950 mm) when the target temperature of 1770 K was reached. Then a power reduction was initiated as well as a flow rate reduction (from 3 g/s to 0.3 g/s) to limit the oxidation power. This early escalation did not occur in QUENCH-07 test and had not been observed at such temperatures in any previous QUENCH experiment. Despite the lower power, the temperature escalation continued, reaching a peak of ~2280 K. At about the same time the shroud failed. Steam starved conditions were reached with downward evolution of the escalation front (Figure 31). During this period, the

power was progressively increased in order to stabilise bundle temperatures at 2073K. During the steam starved period there was no B_4C-gas production except at the onset of escalation during which small increases of CO and CO_2 were measured (Figure 32). The CH_4 production was negligible.

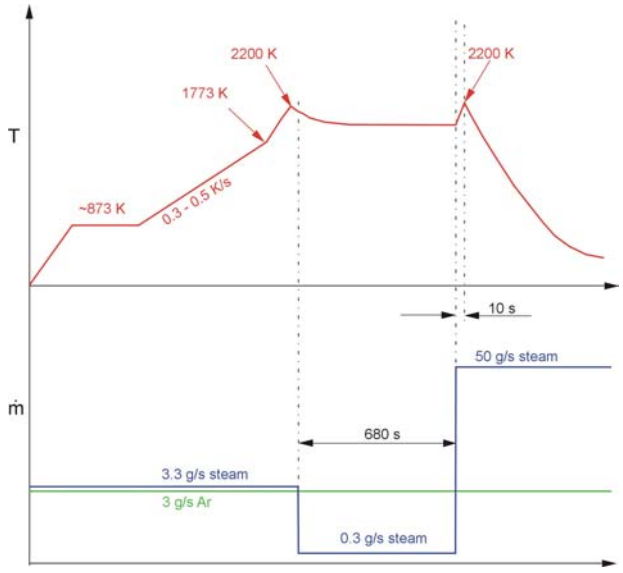

Fig. 30: QUENCH-09 planned scenario

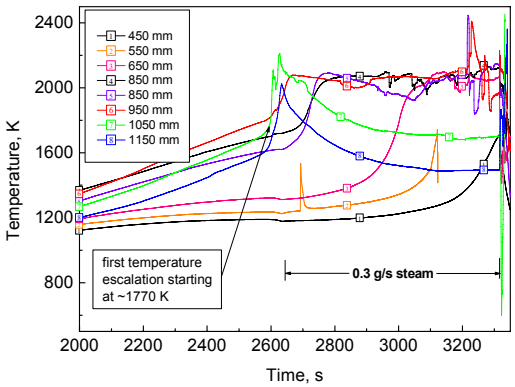

Fig. 31: H_2, CO and CO_2 releases at the onset of the 1st escalation and during steam starvation phase.

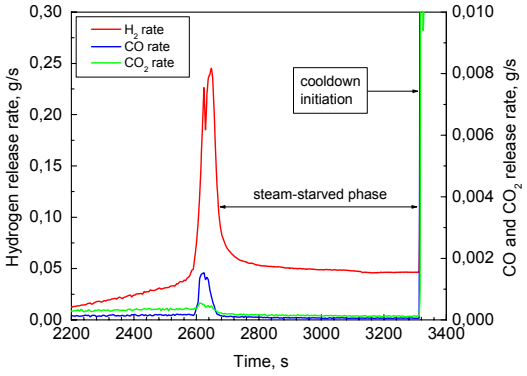

Fig. 32: Fuel rod simulators temperatures during the heat-up and steam-starved phases.

The final cooldown was performed with 50 g/s steam. The temperature escalation that meanwhile had moved into the lower half of the bundle during steam starvation period was immediately terminated at the beginning of the cooldown phase, as shown in Fig. 33. However, several locations above the heated zone which had exhibited stable or even decreasing temperatures prior to the initiation of cooldown experienced a strong temperature escalation (Fig. 34). This led to an increased release of all gaseous species. A large amount of H_2 and significant quantities of CO and CO_2 were produced during the cooldown for a period of about two minutes, i.e. even after electrical power shut down. The detection of boric acids persisted for a further two minutes. Methane production was much smaller and for a shorter period.

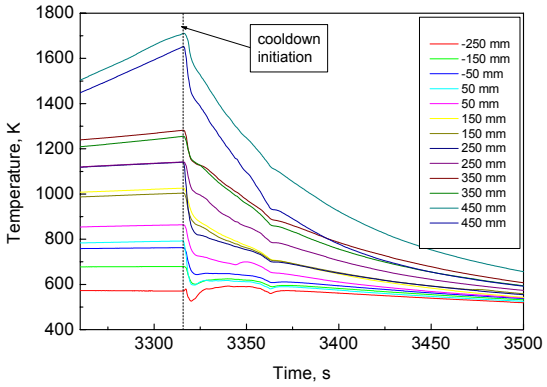

Fig. 33: Fuel rod simulators temperatures at lower elevations during the cooldown phase.

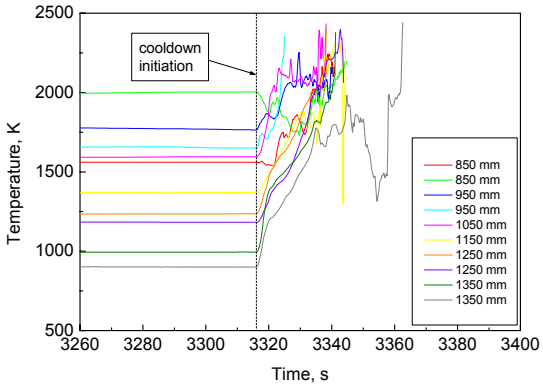

Fig. 34: Fuel rod simulators temperatures at higher elevations during the cooldown phase.

The inner cooling jacket wall failed in the upper part just after cooldown. As a consequence, Ar from the cooling jacket entered the bundle and disturbed the gas measurements by the mass spectrometer calibrated on Ar. Gas species measurements are reliable up to the onset of the final cooling 3315 s. Before cooling, ~60 g of H_2 was produced. Recalibration of the spectrometer gave provisional values of ~400 g of H_2 release during cooldown phase and total amounts of CO and CO_2 of 33 g and 22 g, respectively. Based on CO and CO_2 measurements, the H_2 resulting from the B_4C oxidation was estimated to be ~33 g, i.e. about 7% of the total H_2 produced. The data obtained indicate almost complete oxidation of the Zircaloy of the bundle as well of 50% of the B_4C inventory of the bundle. Additionally, molybdenum and tungsten used as electrodes-heaters could have been oxidized as seen from post-test examination.

During the test, condensate was collected at the sampling point for the mass spectrometer (Fig. 35). A good correlation was found between the boron content in the condensate and release rate of boric acids detected by the mass spectrometer

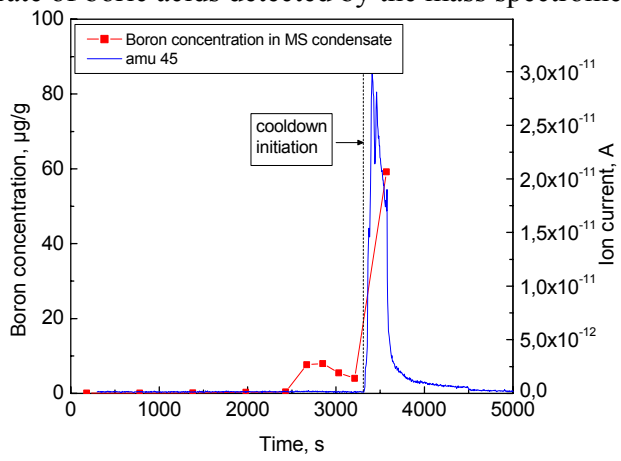

Fig. 35: Boron concentration in the condensate.

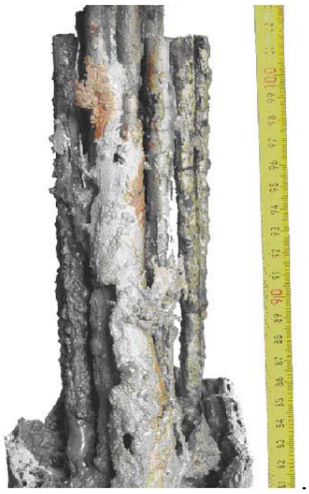

Fig. 36: QUENCH-09 bundle degradation

Test bundle and shroud appear severely damaged above ~500 mm elevation (Fig. 36). In the region between ~520 and 840 mm the shroud and the bundle were partially molten. The major part of the shroud above the heated zone relocated to the region below 800 mm.

C.2.5 Calculations of QUENCH-09 test (FZK, PSI, UPM, IKE, ENEA, IRSN)

Pre-test calculations were carried out by FZK and PSI using SCDAP/RELAP5 and same input models.

Due to the similarity of the first part of the two tests, FZK calculations of QUENCH-09 could be based on post-test analysis of QUENCH-07. The electrical power input was modified with respect to QUENCH-07 to improve the agreement between calculated and measured data up to the start of steam mass flow reduction. The preliminary modelling of the absorber rod did not change results appreciably with respect to former calculations, where an unheated fuel rod was modelled instead of the central B_4C CR. The major difference of axial mesh refinement was only in the upper electrode zone and around the upper end of the heated zone during cool-down. The axial temperature profile became broader with time. The maximum of temperature and oxide layer and, to a larger extent, of hydrogen production shift somewhat to lower elevations during the transient.

Some limited temperature escalation was predicted to occur during steam cool-down, but no difficulties were predicted in the cool-down phase. With the experimental conditions chosen, calculations confirmed that the QUENCH facility would be rather sensitive to changes of experimental parameters as electrical power input and that the facility might even be damaged during the test.

PSI calculations were performed using SCDAP/RELAP5 with the same input model and test conditions as for QUENCH-07 for the phases up to the start of the second heat-up, at which point the steam flow was reduced with the power kept constant. Four cases were run with different reduced flow rates between 0.2 and 1.0 g/s. The results indicated a temperature escalation driven by the oxidation but limited by the steam availability (steam-starvation conditions), so that the escalation was slowest at the low steam flow and fastest at the higher flow.

Post-test calculations were carried out by FZK, PSI, UPM, IKE, ENEA and IRSN. Some results are given bellow.

Preliminary FZK studies showed deviations from experimental data. A parameter study to improve the agreement at the time of the steam mass flow reduction gave no better results in the subsequent test phase. The calculated broadening of the temperature profile was in agreement with experimental data. The recommendations on the choice of Zircaloy oxidation correlations gave some improvement, but this choice remains to be confirmed. Further work is needed to finalise the interpretation taking into account post-test measurements and the analysis of accompanying SET on B_4C oxidation. The sensitivity of the facility, when experimental parameters are changed, and the small safety margin for the given experimental conditions, predicted in the pre-test calculations, was confirmed during the course of the test. Post-test calculations are based on the real test conduct with the same modelling as for the pre-test calculations. Predicted temperatures by FZK are given in Fig. 37 as a function of time using the 16f coarse core model. In the first part of the transient, calculated temperatures are underestimated at the top of the heated zone (axial level 13), and in the plateau phase

temperatures are calculated to increase continuously. Before steam mass flow reduction, hydrogen production is hence underestimated. No significant difference between the coarse and the fine axial discretization of the facility was found except near the bundle exit and furthermore near the upper end of the heated zone during cool-down. This result is in contrast to that for QUENCH-07 (Ref.[24]); it may depend on details of the test conduct; therefore, it cannot be generalized.

Since the axial temperature profile during the second part of the transient was a concern in the preparation of the test, measured and calculated data were analysed in more detail. In Fig. 38, their values are compared at different times; the readings of the questionable thermocouples are not included. As a rough estimate for the bundle behaviour, the shroud thermocouples were also included. At about 2800 s the maximum temperature shifts somewhat to the bundle centre, then the profile becomes flatter, and eventually extends down to elevation 10 (0.65 m). Calculated values overestimate measured ones except in the beginning of the second part of the transient, but the change of the axial profile with time is correctly calculated.

In a sensitivity study, the FZK recommendations for the choice of Zry oxidation kinetics have been applied instead of the standard correlations in S/R5 (Cathcart and Urbanic-Heidrick for low and high temperatures, respectively). Discussions during COLOSS meetings showed that a steam supply limitation in the boundary layer of the cladding is mandatory for the new oxidation model with Prater law for high temperatures. This limitation, already implemented in S/R5, was taken into account. The agreement with experimental data was improved during steam rich periods (Fig. 39, label Schanz) and during cool-down. Preliminary results for QUENCH-07, however, gave with recommended oxidation laws a drastic overestimation of oxidation at high temperatures. Therefore, more work is necessary to apply the new oxidation correlation successfully.

PSI did post-test calculations using the MELCOR code which enabled the modelling of the B_4C control rod. The initial phase of QUENCH-09 was conducted in a similar manner to QUENCH-07 but the temperature ramp was continued slightly further, approaching 1800 K, so the oxidation had an even stronger effect in driving the thermal behaviour. The temperatures during the initial heat-up were underestimated slightly, but sufficiently so that the first oxidation excursion was not calculated with the base model (use of Leistikov-Schanz oxidation correlation). Use of Urbanic-Heidrick instead of the Leistikow/Prater-Courtright model gave more rapid oxidation and overestimated the initial excursion. Thus the two cases bracketed the experimental behaviour during this first heat-up period. Both models correctly calculated the steam starvation following the reduction in steam flow as well as the degradation in the upper part of the bundle. Again, however, the large excursion during cooldown was not calculated so that the extent of degradation and the total B_4C oxidation were underestimated.

A curious difference between the tests was the oxidation of B_4C observed during the main phase of the QUENCH-07, but not in –09. The onset of B_4C oxidation can be controlled by suitable choice of model input parameters, but the difference between the tests cannot be predicted in any MELCOR calculation. The treatment of B_4C oxidation must be considered as somewhat uncertain in MELCOR analyses. Some results are shown in Figures 40 to 44.

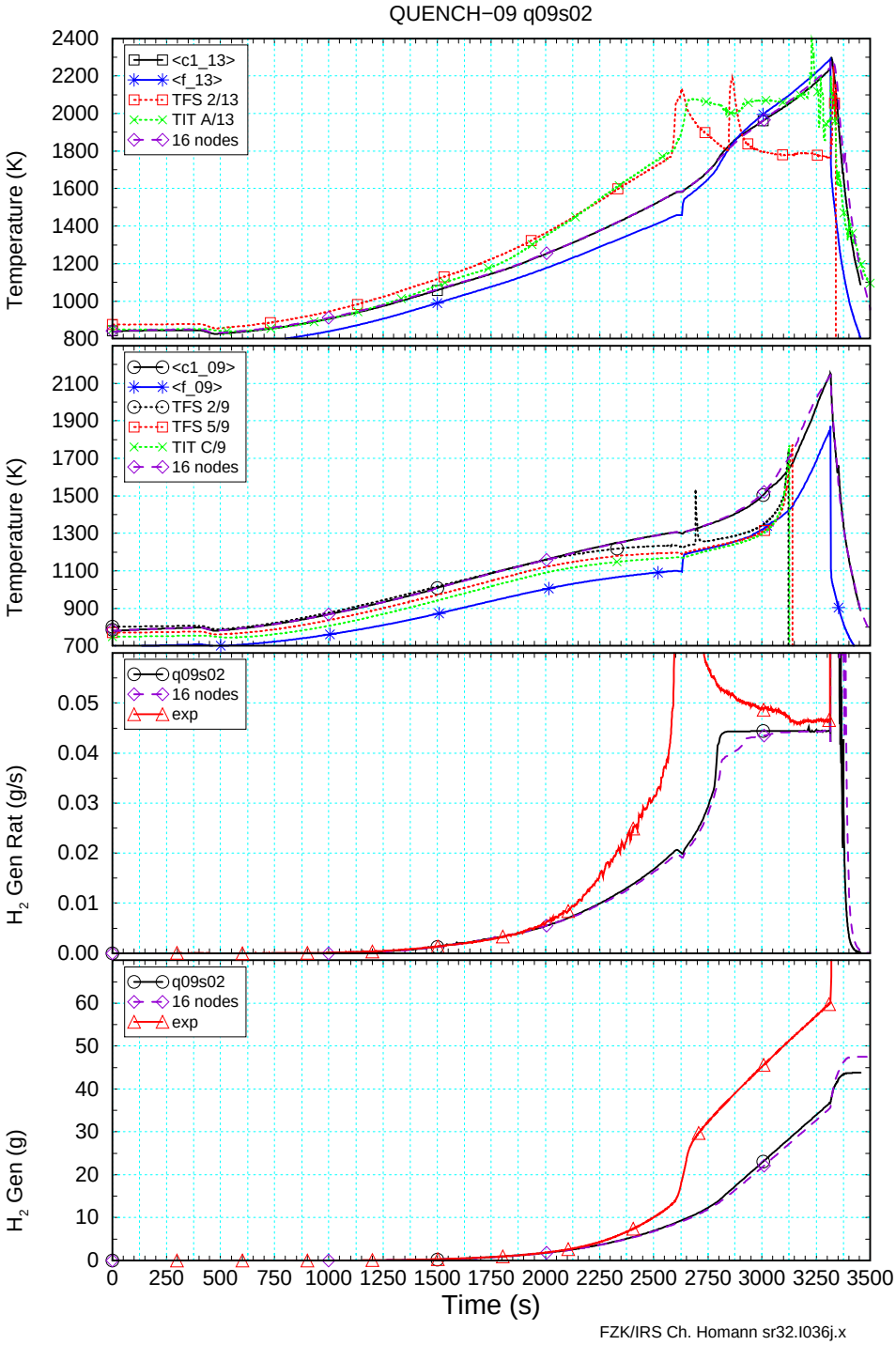

Fig. 37: Post-test calculations with S/R5 using the coarse '16f core model'. From top to bottom calculated and measured values for temperatures at axial levels 13 and 9 (elevations 0.95 and 0.55 m), H_2 production rate, and cumulated H_2 mass for calculated and measured results.

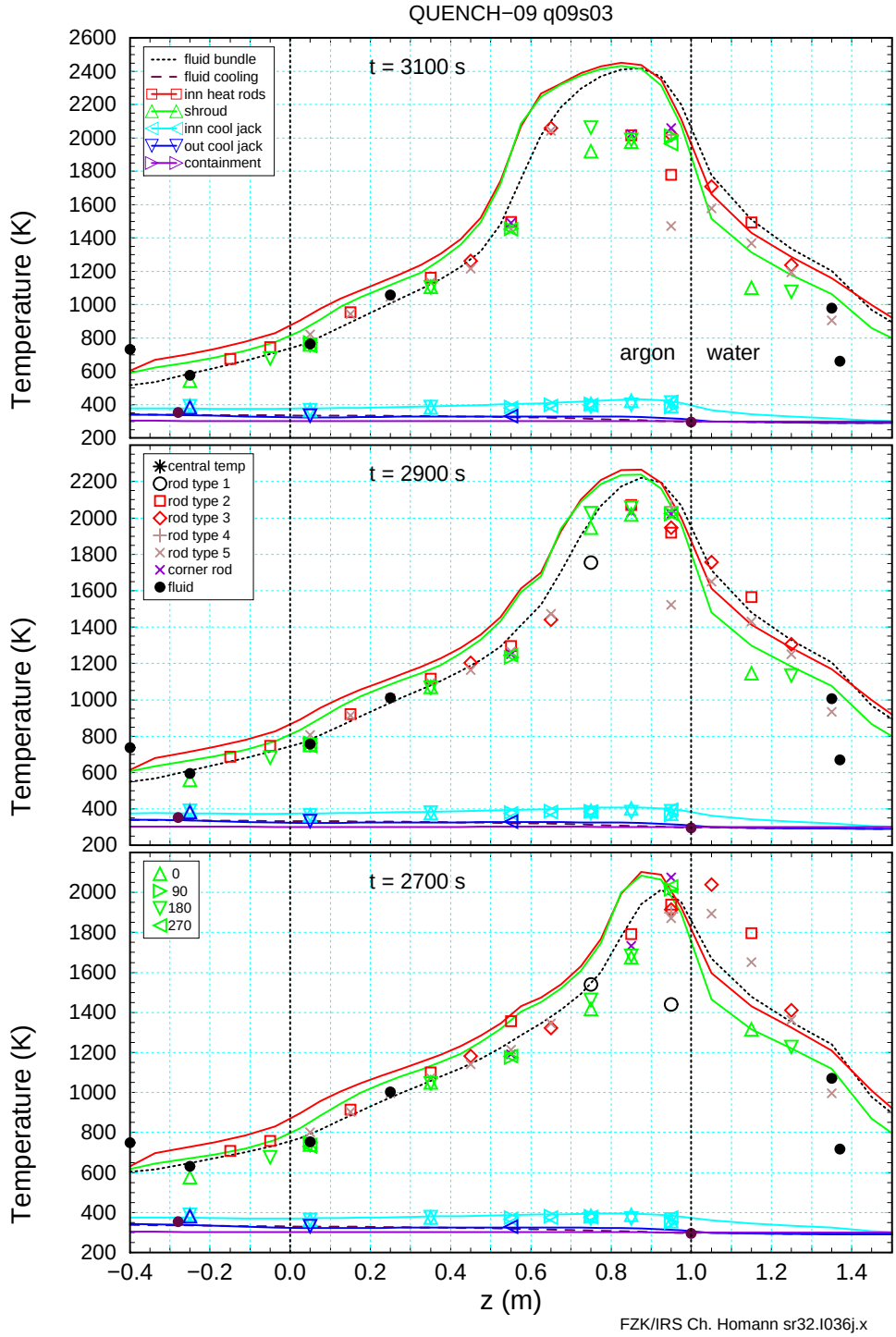

Fig. 38: Axial temperature profiles in the second transient. Calculated and measured temperatures for inner heated rods, the shroud, inner and outer cooling jacket, the containment and for the fluid in bundle and cooling at three times during the second transient. Manufacturer's data for shroud insulation are used in the calculation.

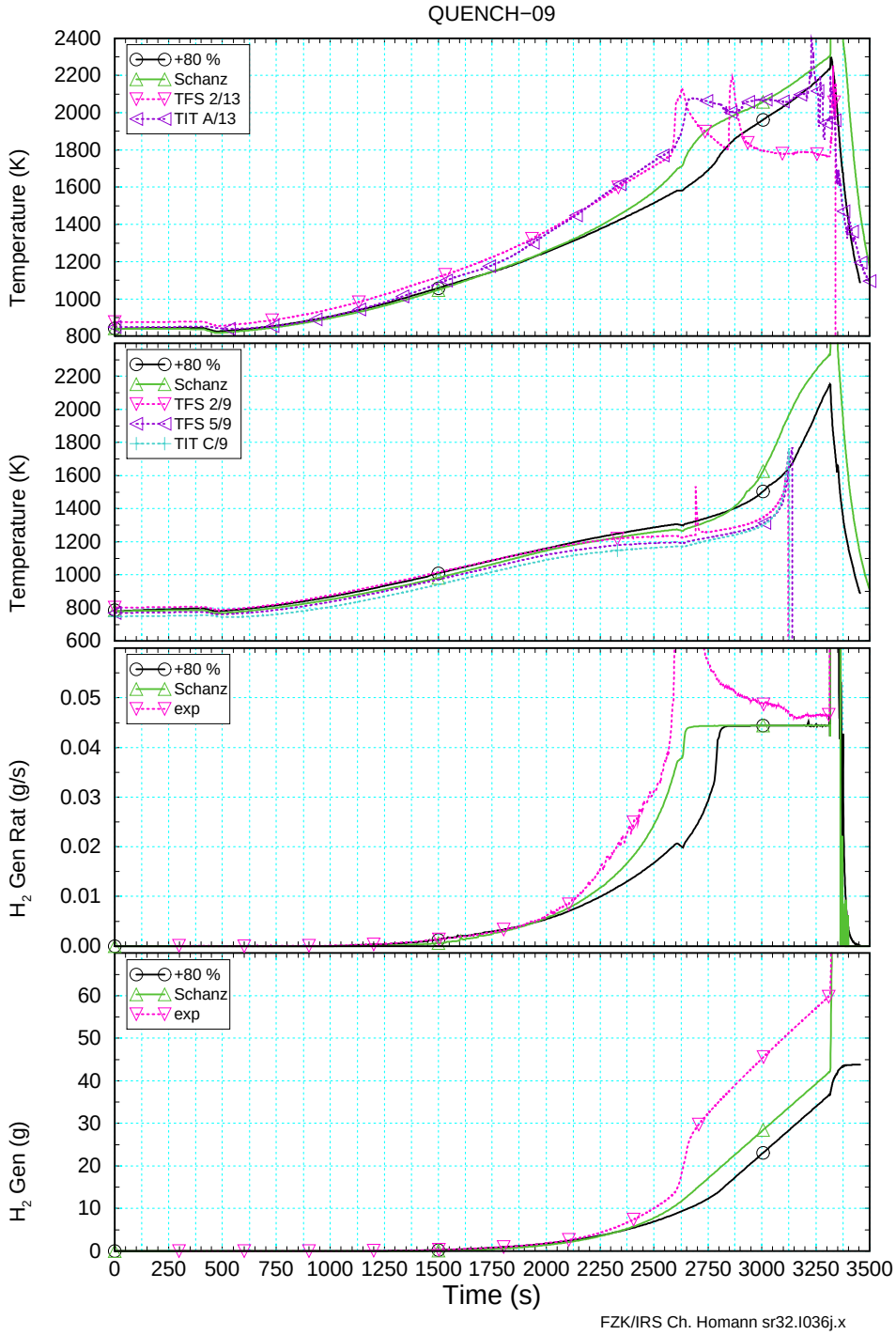

Fig. 39: Sensitivity study to FZK recommended Zry oxidation kinetics. Selected variables as a function of time: From top to bottom calculated and measured temperatures at axial levels 13 and 9 (elevations 0.95 and 0.55 m), H_2 production rate, and cumulated H_2 mass for the standard and the oxidation correlations recommended by FZK.

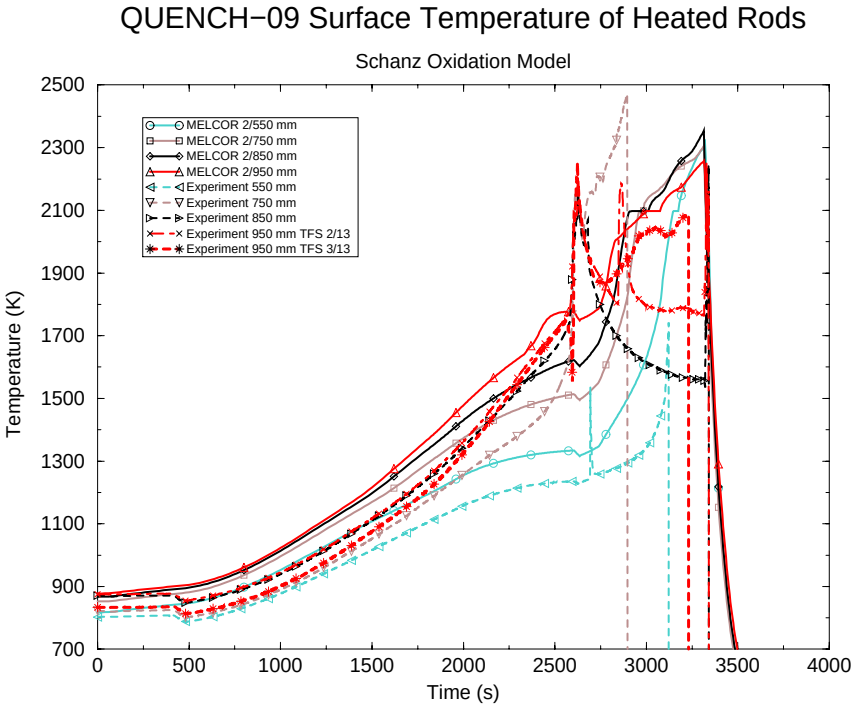

Figure 40: QUENCH-09 test: Comparison of MELCOR calculation using the Schanz oxidation model with measured heated rods surface temperature

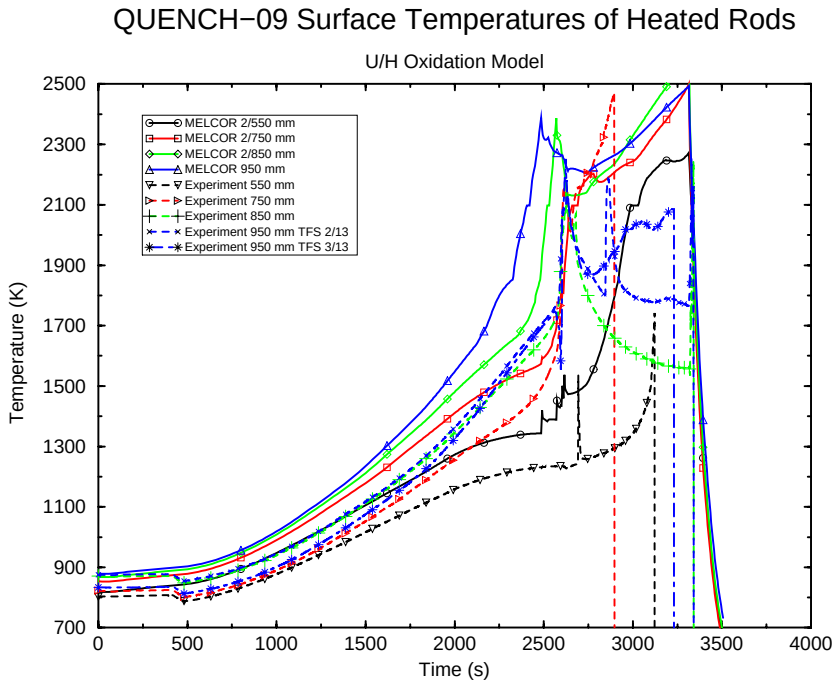

Figure 41: QUENCH-09 test: Comparison of MELCOR calculation using U/H oxidation model with measured heated rods surface temperature

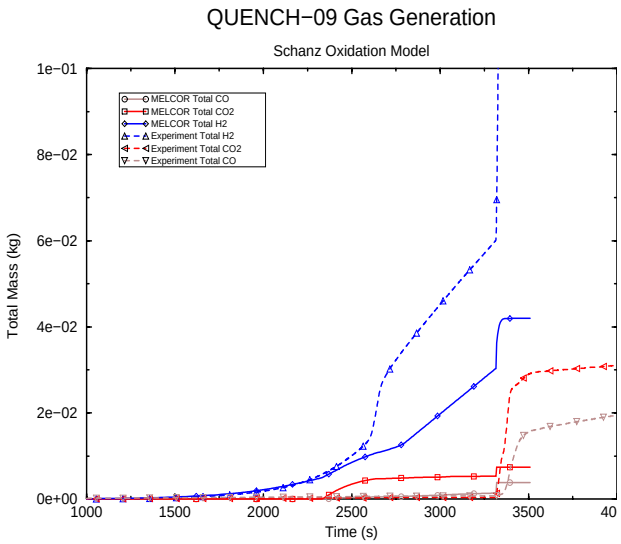

Figure 42: Generation of H_2 using the Schanz oxidation model (MELCOR calculation)

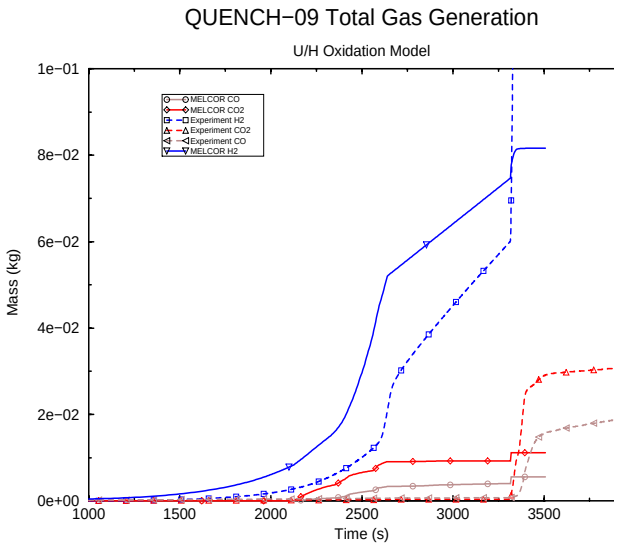

Figure 43: Generation of H_2 using the Urbanic-Heidrick oxidation model (MELCOR calculation)

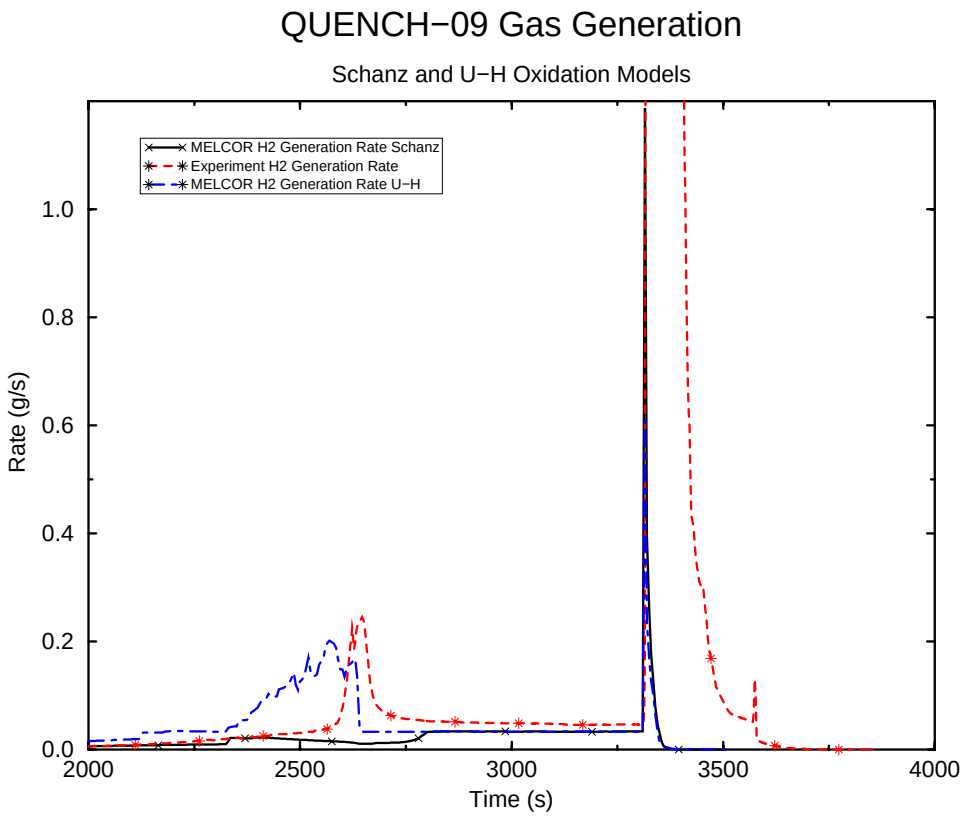

Figure 44: Hydrogen generation rates (MELCOR calculation)

ENEA using ICARE/CATHARE with the new B_4C model did a correct calculation of pre- and post-test calculations of the QUENCH-09 test. The 1st temperature escalation at the top of the bundle (above 0.9 m) was correctly predicted at the end of the heat-up phase. The steam starvation phase in the bundle and the total H_2 generation before cooldown were also correctly calculated. Oxidation escalation during the final cooldown was not predicted.

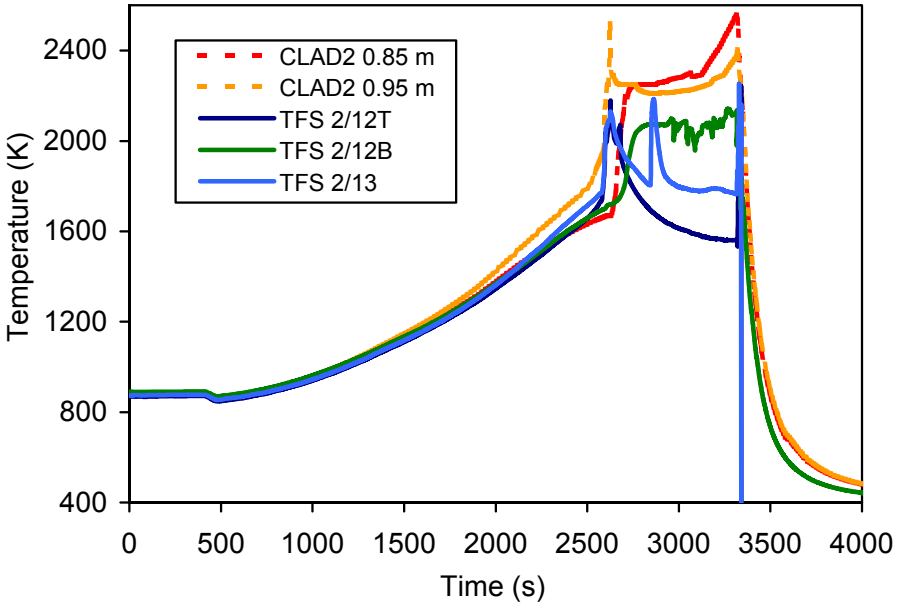

Fig. 45: Clad temperature in the upper part of bundle

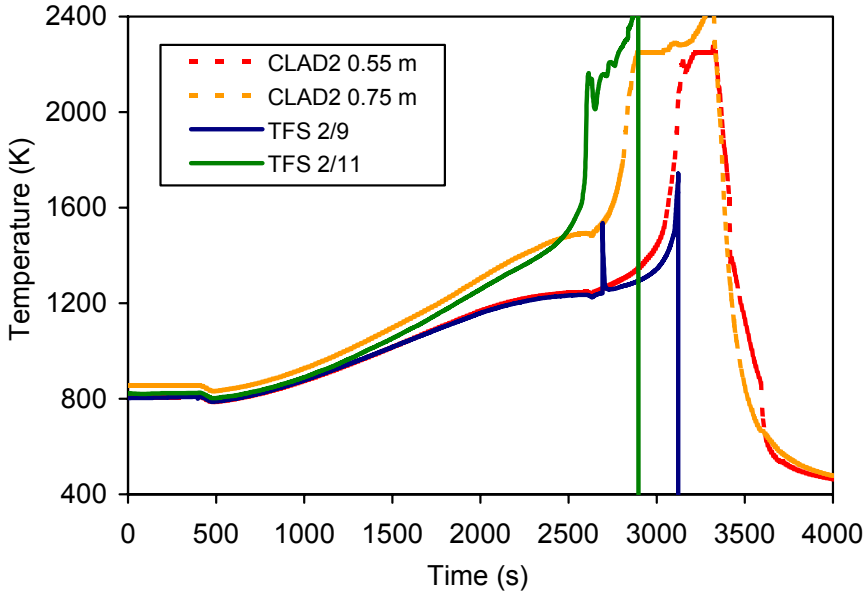

Fig. 46: Clad temperature in the centre of bundle

Clad temperatures are well calculated during the heatup phase. First temperature escalation at the top of the bundle is well predicted at the end of heatup phase (Fig. 45). The large discrepancy in temperature escalation at 0.75 m (Fig. 46) is due to a measurement error (TFS 2/11). The overall clad temperatures behaviour is correct but in general overestimated during the steam starvation phase. As expected, the final temperature escalation during cooldown was not calculated.

The hydrogen release calculated is compared with experimental data in Figs. 47 and 48. The steam starvation conditions and hydrogen generation before cooldown are correctly calculated. The large amount of H_2 released during final cooldown is not predicted due to the lack of a adequate quench model. B_4C oxidation contributes directly by about 7% to the total amount of H_2 release.

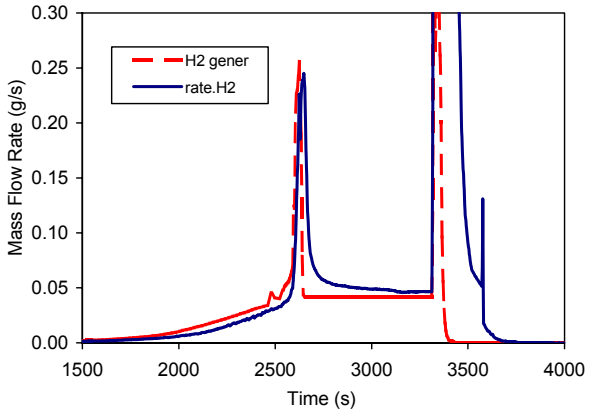

Fig. 47: Hydrogen generation

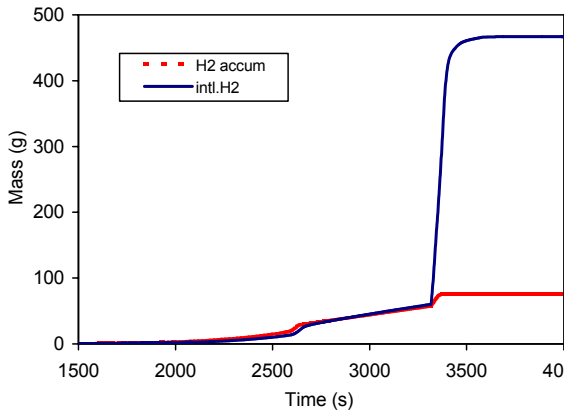

Fig. 48: Total hydrogen release

Bundle degradation calculated at the end of experiment is shown in Fig. 49. The whole bundle is largely degraded in the upper part of heated length and molten material relocated near the middle of the bundle in quite good agreement with experimental observations.

Control rod failure is calculated with some delay, because no chemical interaction between stainless steel absorber cladding and Zr guide tube is taken into account by the code. The control rod failure is observed at 2280s in the test at the temperature of 1580 K; while it is calculated by the code at about 2450s, when the absorber cladding temperature reaches the melting

During cooldown, no bundle degradation was calculated in the upper part of bundle above the heated length as it was observed in the test.

In spite of the difficulties in carrying out the QUENCH-09 experiment according to test specifications, significant data have been obtained regarding core degradation and B_4C effects under steam starved conditions.

- The analysis of the experiment with ICARE/CATHARE has demonstrated the validity of the new model implemented in the code to compute control rod material oxidation and degradation.
- In general the code is able to simulate quite well the experiment up to the final cooldown phase in spite of the difficulty of such a calculation with other codes. The general trend of the thermal behaviour was correctly calculated in pre-test and post-test calculations.
- As already known, large uncertainties still exist in the evaluation of bundle behaviour during cooldown due to the lack of an appropriate oxidation model during quench conditions. In

particular oxidation could have been enhanced during cooldown by a large oxidation of B_4C-SS-Zr mixtures in addition of the oxidation of existing U-O-Zr mixtures and partially oxidised structures.

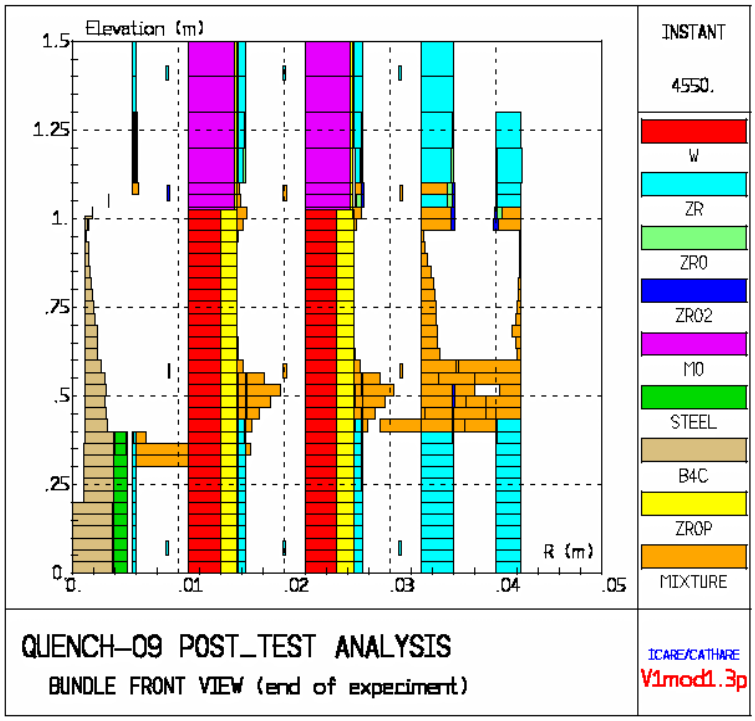

Fig. 49: Bundle degradation at the end of experiment

IRSN did also an in-depth analysis of the QUENCH-09 results. Sensitivity calculations carried out with ICARE/CATHARE showed that the extent of upper temperature escalation was overestimated by measurements due to a TC shunting effect. The very limited oxidation of B_4C before the cooldown was predicted to result from the too limited steam partial pressure. The QUENCH facility was found very sensitive to the inlet gas temperature. The B_4C-CR degradation was correctly calculated. The analysis of the final cooldown phase showed that the H_2, CO and CO_2 measured were overestimated (large spectrometer uncertainty in this test after the failure of the cooling jacket). A possible oxidation of molybdenium electrodes was suspected.

Figures 50 and 51 exhibit a good agreement between the temperature evolution measured and calculated, taken into account the shroud temperature evolution at the elevation 750 and 850 mm. This feature indicates that the modelling of the zircaloy oxidation, using the *Prater* correlation and considering that the Zr-rich mixture is able to flow down only once the outer zirconia layer began to melt, permitted to predict fairly well the thermal behaviour up to the cool down phase.

The guide tube, the claddings and the shroud failure were rather well predicted also. As in the test, the failure of the shroud and of the rod claddings occurs at the hot spot of the bundle (at 950 mm high) around 2600 seconds. Furthermore, the control rod failure is observed at 2280 s in the test, whereas it is calculated at 2350 s. The corresponding temperature of the rod is 1580 K in the calculation, against 1560 K in the experiment.

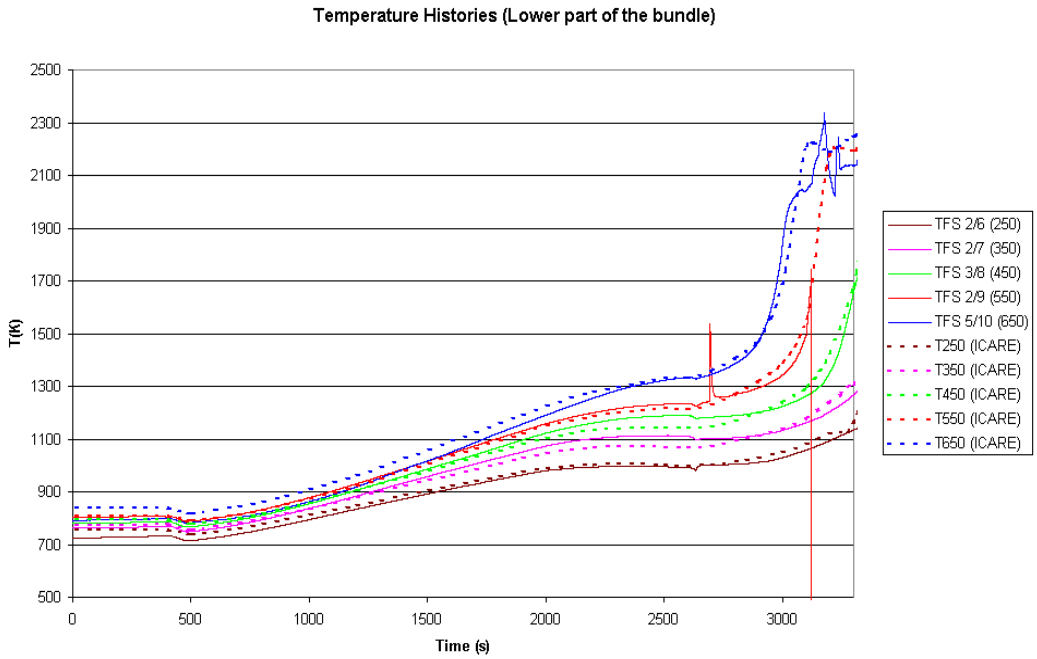

Figure 50: Bottom temperature evolution calculated and measured up to the cool down

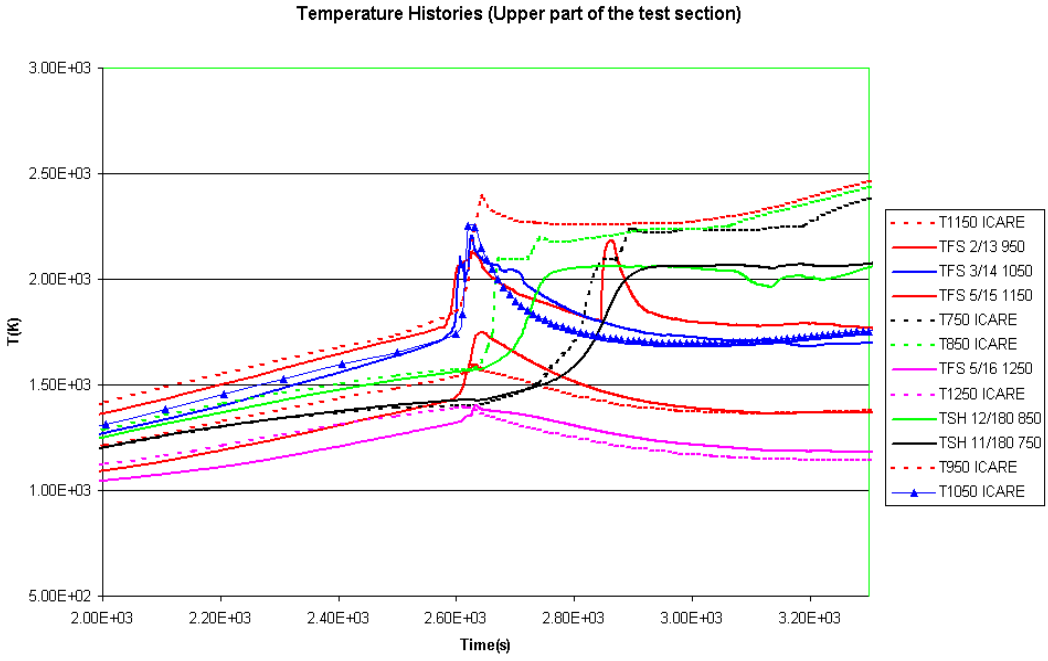

Figure 51: Top temperature evolution calculated and measured up to the cool down

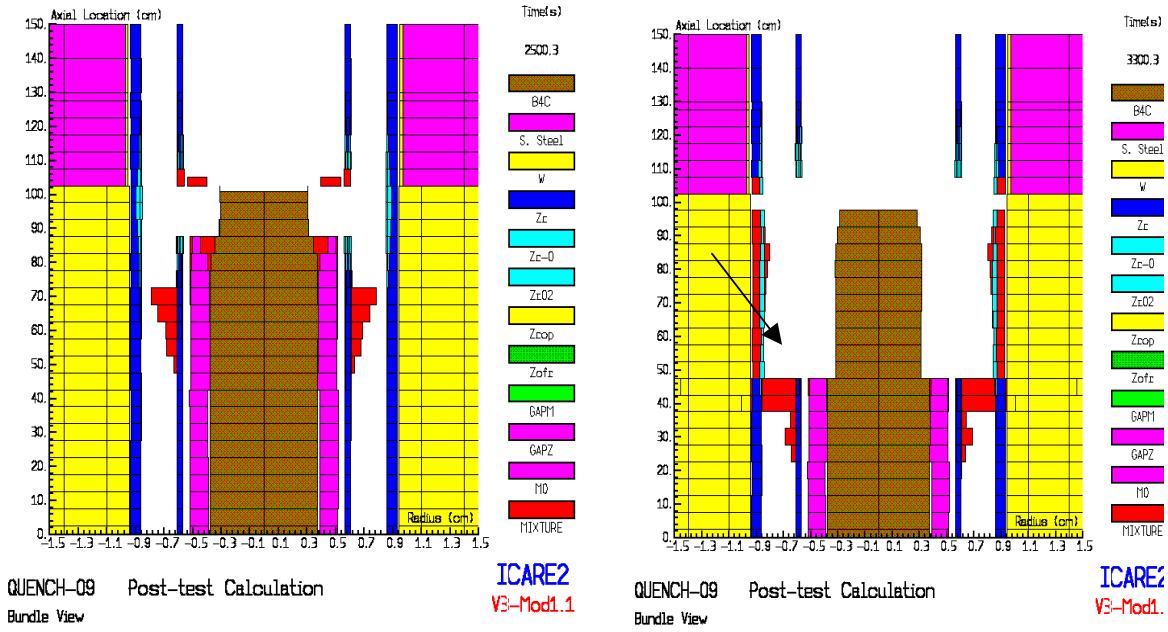

Figure 52: Views of the control rod at the end of the heat-up and during the steam starvation just before the cool down

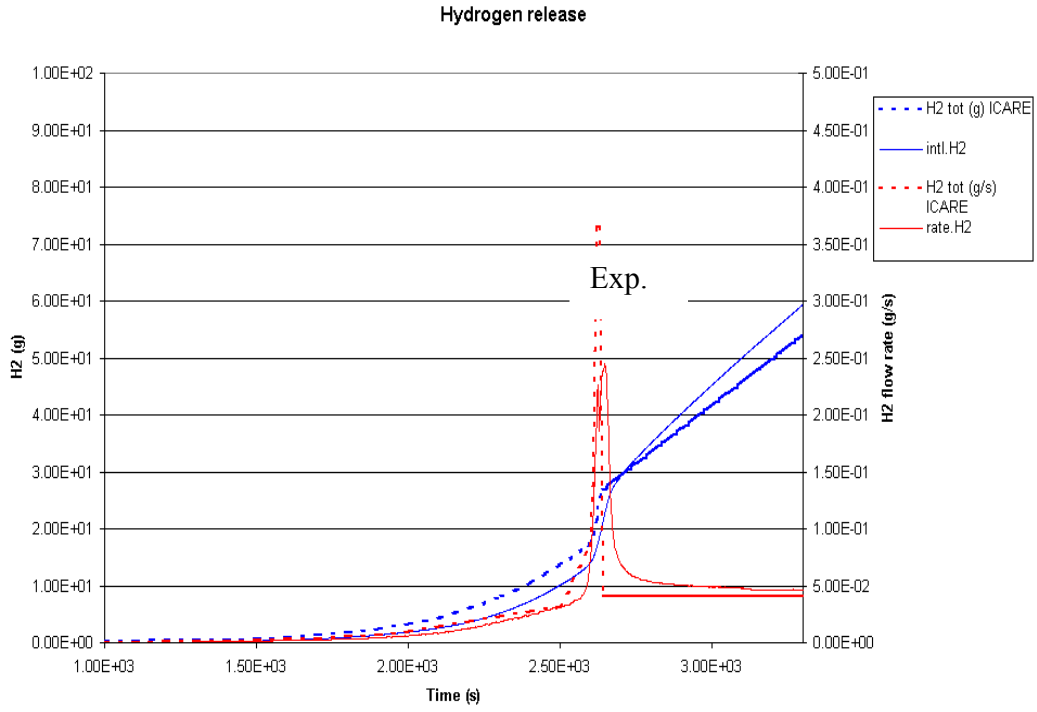

Figure 53: Instantaneous and total hydrogen release

Finally, the control rod degradation is rather well predicted up to the cool down phase during which the experimental evidences regarding this point are not quite clear. However, the early phase of this QUENCH-09 calculation provided a good validation exercise for the B_4C oxidation model of the ICARE2 code. In particular, the influence of the steam partial pressure on the oxidation process is correctly taken into account by ICARE2. Consequently, though the guide tube failed 150s before the starvation phase, the B_4C has been slightly oxidized during this short period in a limited small zone in the upper part of the bundle as illustrated on the Figure 52 (left side).

During the following steam starvation period, the steam was mainly consumed by Zr oxidation as shown by the temporal shift of the successive temperature escalations. Due to the too low steam partial pressure provided after the flow rate reduction (near 2600 seconds), the control rod was almost no more oxidized up to 3300 seconds but dissolved by its cladding and partly relocated (right side of Figure 52).

According to the experimental result, the B_4C seems to have been oxidized, even when the control rod is not yet broken. This behaviour is not reproduced by the code modelling, since it is assumed that the B_4C oxidation begins only after the failure of the control rod cladding and of the guide tube. Despite this discrepancy, the order of magnitude of the B_4C oxidized at the end of the cool down (based on gas measurements) is correctly predicted by the ICARE2 calculation.

This ICARE2 calculation illustrates the ability of the code modelling, to take correctly into account, the effect of the partial pressure on the B_4C oxidation process as well as the coupling of this process with the Zircaloy oxidation and with the thermal-hydraulics phenomena.

The hydrogen release up to the onset of the final cool down is represented on the Figure 53. The agreement between the calculated and measured H_2 release is fairly good, even though in the calculation the steam starvation is obtained just before the steam flow reduction, which is not the case in the test. At the end of the starvation phase there is a slight under-prediction of the H_2 release.

The temperature recorded during the test showed that during the cool down phase, the lower part of the test section did not experience oxidation after the onset of the cooling. Conversely, the upper part of the test section experienced a very violent oxidation runaway which destroyed the major part of the thermocouples. The so-called best-estimate calculation permitted to reproduce correctly the thermal behaviour observed up to 650 mm (Fig. 54). Above this elevation, the comparison to the experiment is very difficult because the major part of the thermocouples failed at the beginning of the cool down. During cool-down, a massive oxidation was calculated due to an efficient convective energy transfer from the lower part to the upper part of the test section (Fig. 55). Nevertheless, the H_2 generation calculated during the final cooling phase is significantly lower: 250 g calculated instead of 468 g measured for the whole transient (Fig. 56). The H_2 mass flow rate in the experiment at the onset of the cool-down indicated that the steam starvation was reached. In this condition, the steam flow rate injected in the bundle (50 g/s) induces a 5,5 g/s of H_2 mass flow rate and a very large oxidation power (around 800 kW). These conditions have not been obtained in the base case calculation (Fig. 56).

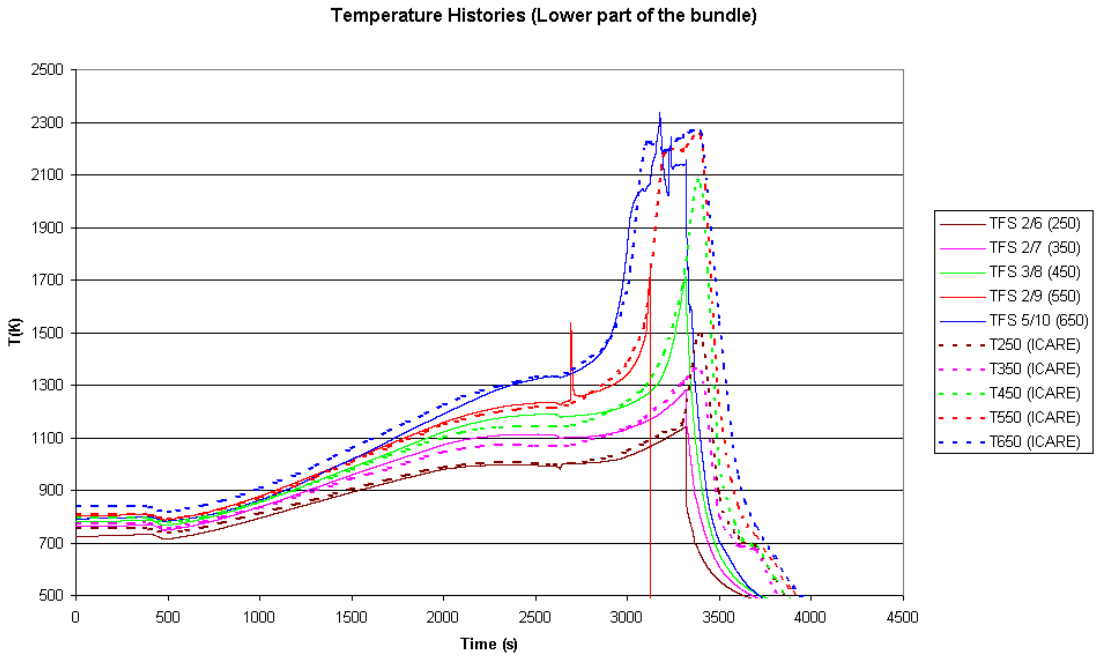

Figure 54: Comparison between the temperature measured and calculated

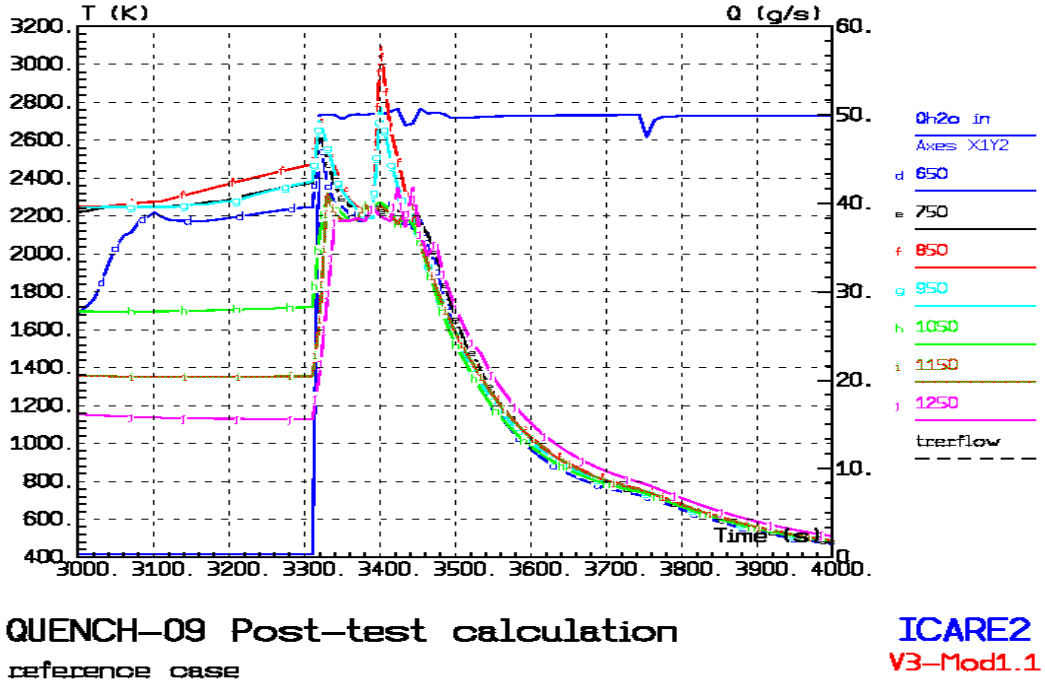

Figure 55: Temperature evolution calculated in the upper zone of the bundle

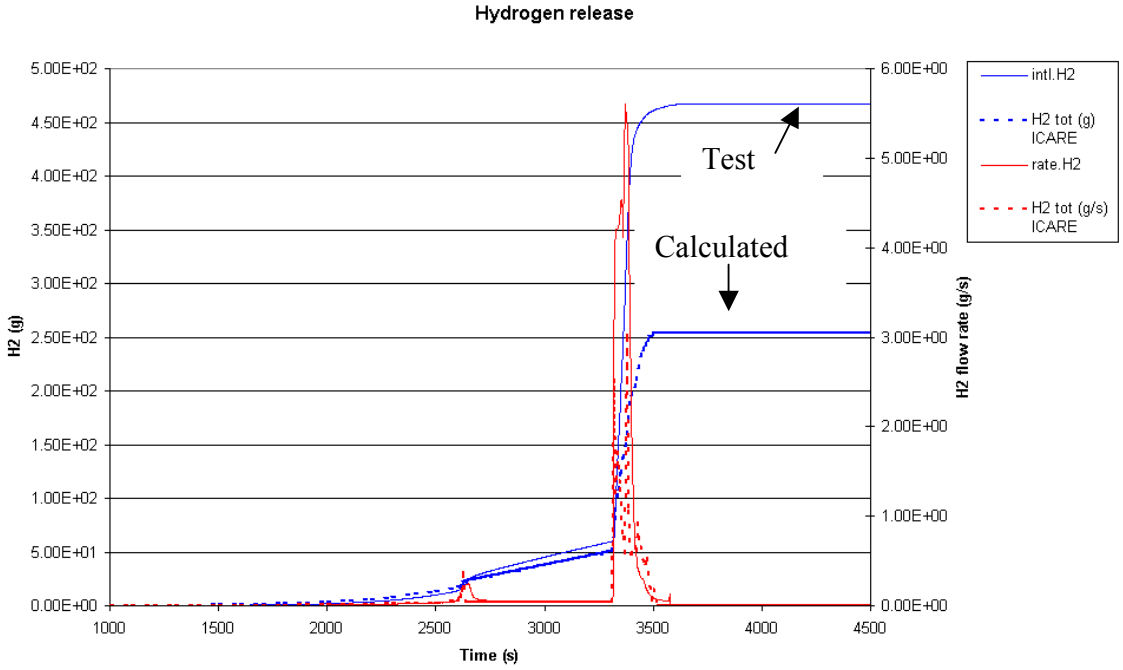

Figure 56: Hydrogen release measured and calculated

Nevertheless, the huge hydrogen release measured during the cool down is not consistent with the absence of oxidation in the lower part of the test section (as observed according to the thermocouple). The experimentalists confirmed that the hydrogen release by the spectrometer during the cool down might be over-measured and needs to be re-evaluate by means of the carbon balance

During the quench phase, the Ar flow rate (Ar is used as the reference spectrometer gas) firstly decreased near to zero (during the first 30 seconds), then increased due to the injection of argon from the failed cooling jacket. Thus, even if the ratios CO/H_2 and CO_2/H_2 remain well defined, uncertainties on the released gas flow rates are very high, and the overall released quantities are probably overestimated. More investigations are required to quantify the uncertainty on the H_2 release during the quench phase.

A second hypothesis to explain the discrepancy on the amount of hydrogen released could be the oxidation of other materials than claddings such as the molybdenium of the upper part of the electrodes for instance. This hypothesis was confirmed by post-test examinations.

C.2.5 European added value from large scale QUENCH and CODEX tests

Bundle tests provided an extensive database for the model development and code verification. For the first time B_4C oxidation effects with related gas production and degradation of the B_4C control rods was quantitatively assessed in integral experiments.

These tests carried out in different conditions are regarded as a significant support for the preparation of PHEBUS FPT3 (information related with control rod failure, gas release, core degradation etc.) during the early phase of the bundle degradation.

Combined progress meetings were held with QUENCH workshops (Ref.[26, 27]) and PHEBUS meetings (Ref.[28]) providing a forum where the results could be widely discussed and analysed. (Ref.[29]).

C.3 Modelling tasks

The objective of this activity was to improve SA codes used in the EU considering the experimental database on B_4C oxidation, fuel dissolution and oxidation of U-O-Zr mixtures. In addition, best estimate laws for Zry oxidation kinetics have been selected by FZK and recommended for the plant calculations carried out in the project.

C.3.1 B_4C-CR degradation and oxidation models (IRSN, ENEA, IKE and EDF)

ICARE/CATHARE: The existing B_4C model, which takes into account the B_4C-Stainless Steel (SS) interaction and the Zry guide tube rupture was extended to B_4C oxidation by steam. The IRSN model was described in the special NED issue of FISA-01 and recently presented (Ref.[20]). Due to limitations of the thermal-hydraulic model only the H_2 production is taken into account. In SA conditions, the B_4C oxidation occurs at temperatures greater than 1500 K (B_4C exposure to steam after the control rod rupture). In these conditions, the resulting B_2O_3 is supposed totally consumed by vaporisation and/or reaction with steam. This configuration corresponds to a linear kinetics behavior. A simple Arrhenius law combined with additional terms to take into account the steam partial pressure and the total pressure effects observed in VERDI, TG and BOX rig tests has been chosen. This law has been validated on several tests carried out in the project. The coupling between thermal-hydraulics and chemical processes is correctly taken into account via the temperature, the steam pressure and the total pressure. A similar model has also been introduced in ATHLET-CD and ASTEC codes.

MAAP4: A recent model has been developed by EDF covering the B_4C-SS interaction, the Zry guide tube rupture and the B_4C oxidation. It takes into account chemical reactions responsible of H_2, CO, CO_2 and CH_4 production (Ref.[30]). Chemical constants have been derived from a thermodynamic equilibrium calculation. Various reaction kinetics have been introduced including the oxidation kinetics used in the ICARE/CATHARE code.

FZK model: The BORCA model was developed in order to explore the whole potential of TG and the BOX rig tests and evaluate reaction kinetics parameters. The B_4C oxidation model assumed two competing processes: a parabolic B_2O_3 scale formation and a linear B_2O_3 evaporation. Kinetics parameters were derived from BOX and TG oxidation tests carried out with dense B_4C. With this approach a reasonable simulation of SETs was performed. A preliminary version has been introduced in the FZK version of SCDAP/RELAP5.

C.3.2 U-O-Zr oxidation models (IRSN, ALIAZ CZ, JRC/IE, IBRAE and RUB)

The objective was the development of models that can simulate the oxidation of U-Zr-O and Zr-O mixtures suspected to be the main cause of temperature escalation and large H_2 release during the quenching of degraded cores. This effort involved modelling of solid and liquid U-O-

Zr mixtures, the former being representative of relocated and frozen mixtures in the lower part of a core.

Solid mixtures: ALIAS CZ analysed the experimental data produced by ÚJP-PRAHA on oxidation of solid U-Zr-O alloys by steam. The existing database at the beginning of the project was very limited. Regarding U-Zr-O alloys, it was only found data for the 66U-30Zr-4O wt.% alloy measured at PNL (Ref.[15]) in the temperature range 1415-2140 °C. The PNL and ÚJP data were found consistent at 1400 °C, but at low-temperature the ÚJP data showed much higher oxidation than those of PNL extrapolated below 1400 °C. Both datasets obey parabolic law above 900 °C, but quite linear kinetics was observed by ÚJP between 450-900 °C.

The mixture oxidation model of ICARE2 (ZROX) was upgraded keeping the modelling as simple as possible. The parabolic approach was preserved, the Arrhenius-type parabolic correlations being replaced by parabolic rate constants K_P tabulated over two parameters: temperature (T>400 °C) and U-content in the U-Zr-O mixture (0-60 wt.%). The ÚJP database being not sufficient, the tabulated K_P rates could not be dependent on the oxygen content in the mixture. In this preliminary model, intermediate values are interpolated linearly as a function of temperature and U-content in the mixture (Figure 57).

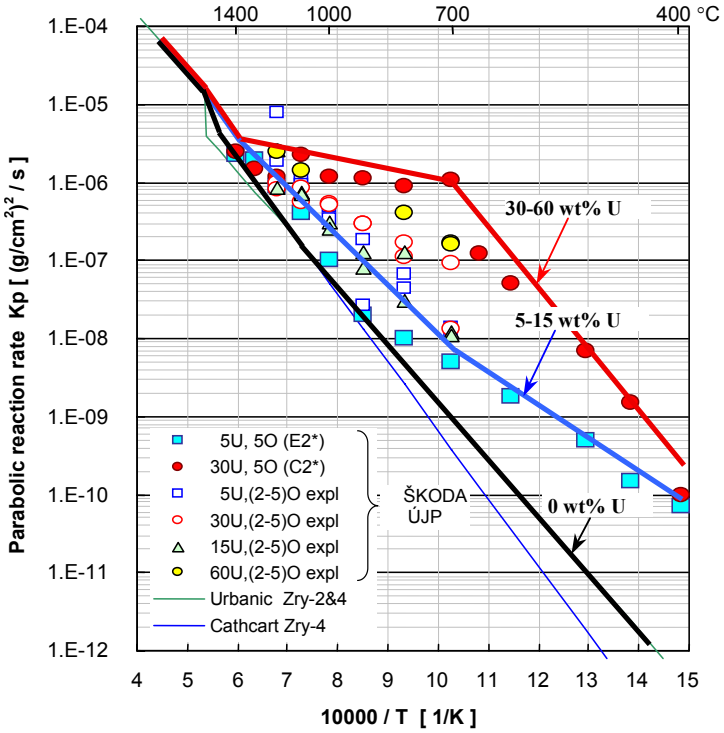

Fig. 57: Improved ZROX model; Schematically indicated reaction rates K_P as a function of temperature and U-content in the mixture.

The validation was performed against integral bundle experiments CORA-5, CORA-13, PBF 1-4 and FLHT-5 carried out under different oxidizing conditions. The new model improved both the timing and the total value of the hydrogen generation observed in these bundle tests.

The H_2 release, previously underestimated, was significantly improved. Nevertheless, the model was not sufficient to simulate the H_2 peak observed during quenching. For this, it is suspected that the model should be completed by an oxide ZrO_2 shattering effect that would expose, as observed in the CORA programme, a 'limited amount' of the underlying Zry metallic surfaces to steam.

Liquid mixtures: In order to model the oxidation of Zr-O and U-Zr-O melts, available FZK data from post-test examinations of molten materials oxidation in the CORA and QUENCH bundle tests, as well as new FZK SETs on ZrO_2 crucible dissolution by molten Zry (described in § C.1.3) were taken into account by IBRAE (Ref.[31]). Crucible tests were specially designed for the investigation of long-term behaviour representative of the melt oxidation stage.

Detailed analysis of post-test images of re-solidified Zr-O melts in the QUENCH-02 and 03 tests was performed. A close similarity was found with the melt appearance in the ZrO_2 crucible dissolution tests where oxide layer growth was accompanied by precipitation of ceramic particles in the corrosion (oxidation) stage. The model proposed explains the emergence of the ceramic precipitates under non-equilibrium conditions induced by the temperature difference between the crucible wall and the melt, and predicts continuous oxidation/precipitation process after attainment of the saturated state of the melt (as well as the 'late dissolution' phase observed in the new FZK crucible tests). The model predicts a close to linear time law for the rate of the $(U,Zr)O_2$ ceramic phase (oxide layer + precipitates) growth during U-Zr-O melt oxidation that corresponds to a much faster kinetics of melt oxidation and H_2 generation in comparison with the standard parabolic rates used for pure Zry (Ref.[32]).

Calculations with the model allowed quantitative interpretation of the vigorous melt oxidation and ZrO_2 or $(U,Zr)O_2$ phase precipitation observed in the QUENCH and CORA tests respectively characterized by Zr-O and U-Zr-O melts. It was demonstrated that complete solidification of the melts could occur rather quickly owing to formation of ceramic precipitates in the melt during its oxidation. This explains the significant underestimation usually found using standard oxidation models on hydrogen production in these integral tests characterised by large amount of melts.

On the basis of the analysis performed for the binary Zr-O system behaviour (i.e. solid ZrO_2 and Zr-O melt), it is anticipated that similarities exist with the dissolution of UO_2 fuel by the U-Zr-O melt suspected to be also strongly influenced by the temperature difference between heated fuel pellets and melt. This was the case in the FZK past experiments where the UO_2 dissolution was surprisingly no longer restricted by the melt saturation limit and proceed actively in the over-saturated melt (Ref.[3])

IRSN developed also the so-called "MAGMA oxidation model" derived from the IBRAE modelling work. The MAGMA oxidation model was implemented in ICARE/CATHARE and is specific to the so-called "MAGMA components" representative of molten mixtures.

The RUB contribution was focussed on the synthesis of high temperature oxidation results. In addition, the stand-alone RELOS code dealing with transport processes that govern key melt oxidation processes through the liquid-gas interface enabled exploratory calculations for the preparation of the experimental programmes of the project and sensitivity studies showing uncertainties in the melt oxidation process.

C.3.3 Dissolution of fuel rod by molten Zry (IBRAE, JRC/IE and IRSN)

The activity on fuel rod dissolution was aimed at reducing existing uncertainties in the prediction of the simultaneous UO_2 and ZrO_2 dissolution by molten Zry for fresh fuel in the rod geometry and on the prediction of the burn-up effect on fuel dissolution by molten Zry. On the latter aspect, existing data on the burn-up effect on UO_2 behaviour from PHEBUS FP, VERCORS and the CIT project (4^{th} FP) indicate significant differences between fresh and irradiated fuel with enhanced liquefaction due to burn-up.

Simultaneous dissolution of UO_2 and ZrO_2 by molten Zry (IBRAE, JRC/IE)
Separate models of UO_2 dissolution and ZrO_2 dissolution were developed by IBRAE in the previous CIT project while in this project, an upgraded model for simultaneous dissolution of these materials was developed for the mechanistic code SVECHA. This model considers interactions of solid materials with the convectively stirred melt during the two saturation and precipitation stages of interaction, and self-consistently describes either dissolution (erosion) or growth (corrosion) of ZrO_2 layer during these interactions. The system of equations includes mass balances for three components (U, Zr, O) as well as flux matches (solid diffusion and melt convection) at two solid/melt interfaces (Ref.[33, 34]).

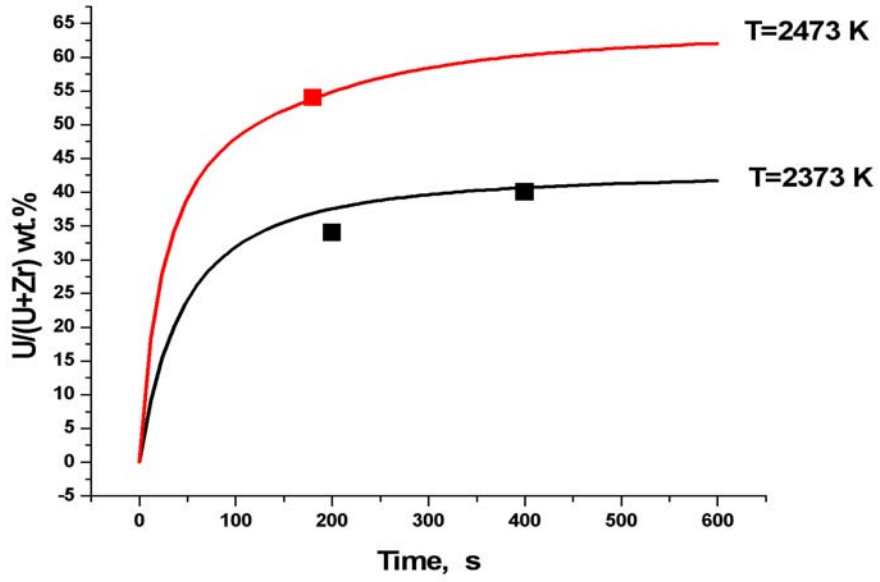

Fig. 58: Comparison of calculated and measured uranium weight content in the melt in the 2^{nd} series of RIAR tests performed at 2100 and 2200°C.

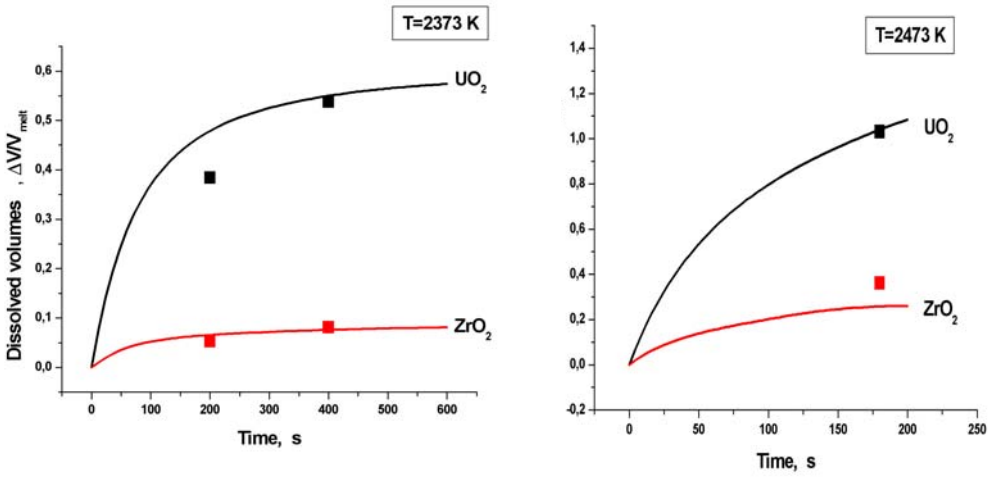

Fig. 59: Code-to-data comparison of dissolved volumes of UO_2 and ZrO_2 in the melt

The model was thoroughly improved and validated against RIAR crucible dissolution tests (described in § C.1.1.1) and demonstrated satisfactory agreement with the test measurements (Ref.[14]). (Figures 58 and 59). It predicts that the mass transfer mechanisms in the liquid phase is affected by the natural convection in the melt and, for this reason, the two problems of the UO_2 and ZrO_2 dissolution by the same melt cannot be described by separate dissolution models. It is also anticipated that dissolution of UO_2 fuel by the U-Zr-O melt is also strongly influenced by the temperature difference between heated fuel pellets and melt. This process was recently confirmed by the FZK tests on dissolution of ZrO_2 crucibles by molten Zry. This was also the case in past experiments carried out with UO_2 crucibles where dissolution was no longer restricted by the melt saturation limit due to precipitation of ceramic phase in the over-saturated melt. Such behaviour is also possible in the bundle tests during the early fuel liquefaction for which a relatively quick transformation of the UO_2 phase into the mixed $(U,Zr)O_2$ ceramic phase of the U-O-Zr mixture can be predicted. This trend is consistent with the early loss of rod geometry observed in the PHÉBUS FP tests.

C.3.4 Burn-up effect on fuel dissolution (ALIAS CZ, IRSN)

Current fuel dissolution models in severe accident codes were developed from fresh fuel data. JRC/ITU showed in experiments performed within both CIT and COLOSS projects that the burn-up effect enhances the kinetics dissolution. In addition, extended apparent dissolution results from the simultaneous fuel decohesion.

The fuel dissolution model of ICARE/CATHARE (UZRL) for fresh fuel was extended to take into account the enhanced effect of the burn-up using a parametric approach. The faster kinetics for irradiated fuel were simulated by a higher "effective" temperature of interaction. The temperature shift (T-shift) between this effective temperature and the actual one depends on type of fuel, temperature, burn-up and was deduced from JRC/ITU dissolution tests with fresh and irradiated fuel. The T-shift is the largest near the melting point of Zry (T-shift =340) but

decreases with temperature up to zero at ~2500 °C. T-shift is assumed to increase with burn-up but not enough data is available to quantify this assumption. While the dissolution between fresh MOX and fresh UO_2 was assumed the same, the T-shift table for MOX was assumed ~ 50 K smaller than for irradiated UO_2.
A limited amount of additional experiments with irradiated fuel is needed to complete the provisional T-shift tables. Data are especially needed for short reaction times (20 to 200 s) and temperatures between 1750 and 2200 °C and for burn-ups in the range 32-62 GWd/t. The preliminary model on the burn-up effect of fuel dissolution has to be confirmed and validated.

C.3.5 Best estimate Zry oxidation kinetics laws (FZK)

In order to reduce the user effect in plant calculations carried out in the project, recommendations were produced by FZK (Ref.[35]) regarding the choice of correlations for Zircaloy oxidation kinetics and on the transition between the low temperature and the high temperature correlations. Correlations of Leistikov and Prater-Courtright were recommended for low temperature (T <1800 K) and high temperature (T >1900 K) domains respectively to carry out final plants calculations of the project. Additional investigations were launched out of the project to provide more input on Zry oxidation modelling in SA codes (Ref.[36, 37, 38]).

C.4 Plant calculations

The large work-package WP8 was devoted to the applications of results to the calculation of selected SA sequences characterized by large core degradation. This activity has been reported in the "Part 2 of the final report" (Ref.[12]).
Eleven partners of the project were involved in this activity and formed the Plant Analysis Group (PAG) led by IRSN and Framatome-ANP SAS.
The specific objectives were:
- to assess the ability of SA codes to calculate the core degradation and the related gas production, in particular those resulting from the degradation of B_4C-CR's,
- to identify improvement needs and give recommendations for future code developments,
- to evaluate implications of new results.

Main European plants involving B_4C material were investigated, focussing on the impact of B_4C on selected SA sequences. IRSN, EDF and ENEA were also involved in the calculation of the TMI-2 accident. Mainly the core and, to a lesser extent, the primary circuit were considered in these calculations. Key SA codes such as the integral codes ASTEC, MAAP4 and MELCOR and the detailed codes ICARE/CATHARE and SCDAP/RELAP5 were used.

The work plan involved three stages:

- At the beginning of the project, a 1st set of calculations was performed for key SA sequences selected on various plant designs (Table 4). At this stage, the input decks were harmonised in order to facilitate code assessment and comparisons between calculations run with different codes.
- Afterwards, codes were upgraded and partially validated using experimental results of the bundle tests QUENCH-07, QUENCH -09 and CODEX-B_4C carried out in the project.

- At the end of the project, improved codes were run again to provide a 2nd set of calculations and assess the effect of new models and SA code improvements carried out during the project.

Table 4: Plant calculation activity in COLOSS.

Plant designs	SA codes	Partners	SA sequences
PWR 1300	ASTEC-MAAP4	IRSN/EDF	"H2 sequence" (*)
PWR 900	ASTEC	IRSN	Same "H2 sequence"
BWR	MELCOR	PSI	Station Blackout (SBO)
VVER-1000	ICARE/CATHARE	KI/LTKK	Large break / SBO
EPR	MAAP4-MELCOR-SCDAP/R5	FRA-SAS/GmbH/FZK	SBO
TMI-2	ASTEC-SCDAP/R5-ICARE/CATHARE-MAAP4	IRSN/ENEA/ENEA/EDF	

(*) Total loss of feedwater to the steam generator without safety injections.

Table 4 describes the SA calculations carried out during the project. For the 1st set of calculations run during the 1st year, code versions used were not able to take into account B_4C effects except MELCOR which had a parametric B_4C model for BWRs.

The 1st set of calculations produced useful results on code capabilities. Recommendations have been made on model improvements underway in the project and associated experimental needs to help reduce code uncertainties in B_4C and fuel rod dissolution modelling. Sensitivity studied on some user parameters known to affect the core degradation such as the Zry and B_4C oxidation laws, ZrO_2 clad failure, fuel rod collapse criteria and some B_4C modelling parameters were recommended for the final set of plant calculations. Benchmarks between calculations of the project were extended to plant calculations carried out in EVITA project (Ref.[39]).

The 2nd set of plant calculations was performed with upgraded codes. Accompanying sensitivity studies and code-to-code benchmarks enabled a general assessment of codes to calculate core degradation, more particularly core oxidation and H_2 production (both the rate and the total production), B_4C effects, and corium formation resulting from fuel dissolution and burn-up effects.

Based on these calculations, needs for short-term developments were also identified as well as implications of new results for safety.

C.4.1 Summary of the plant calculations

C.4.1.1 Sequence "H2" on French 1300 PWR

- The preparation of the French PWR-1300 calculation required the development of an input deck for MAAP4 and ASTEC V0 codes. This work was carried out in close co-operation between the French Utility EDF and IRSN in order to use consistent data in both decks. A "total loss of feedwater without safety injection" (named "H2 sequence" in Table 4) was calculated. This sequence promotes large core degradation.

MAAP4 calculations (EDF)

- Very detailed modelling was needed to cope with the core-uncovering phase. The timing of the H_2 production was very sensitive to the level of water in the core.
- The 2nd calculation was carried out with the B_4C oxidation model developed by EDF in MAAP4.
  - Sensitivity studies were carried out on the choice of Zry oxidation correlations and on the B_4C oxidation kinetics (Tables 5 and 6).
  - Main results regarding the B_4C effect are an extra production of about 50 kg of hydrogen on the H2 scenario (Table 6) and about the same quantity in CO and CO_2, a negligible amount of CH_4 is produced in the core during this oxidation. The possible production in the primary circuit from CO and CO_2 has to be investigated in the future due to the importance of CH_4 on volatile FP chemistry. Parametric calculations showed that no more than 100 kg of extra hydrogen can be produced from the B_4C oxidation while the total H_2 production is ~600 kg (Table 5).

Table 5: Mass of hydrogen in the different calculations

	Ref (no B4C)	Urbanic+ Melcor (with B4C)	Urbanic+ Steinbruck (with B4C)	Urbanic+ Icare (with B4C)
Total Mass of Hydrogen produced at Vessel failure	548 Kg	632 Kg	527 Kg	597 Kg

Table 6: Masses of non-condensable gases in the different calculations

	1300 MWe (URBANIC+ MELCOR)	1300 MWe (URBANIC+ICARE + COACH)	1300 MWe (URBANIC+ STEINBRUCK+ MELCOR)
Total Mass of CO2	47 Kg	51 Kg	50 kg
Total Mass of CO	58 Kg	44 Kg	23 kg
Total Mass of CH4	0.03 Kg	0.0001 Kg	0.00001 kg

ASTEC calculations of a PWR 1300

- In the 1st calculations with ASTEC V0, initial conditions at the end of Phase 1 as well as the pressuriser valves opening and the accumulator injection as calculated by MAAP4 have been imposed in order to facilitate comparisons of the two calculations. The significant differences observed in the H_2 release are due to the choice of different oxidation models and to the calculation of different core dry-out behaviours.

- The 2nd calculation was carried out with the new ASTEC V1 code using new thermal hydraulics and core degradation modules, the latter being derived from ICARE/CATHARE. ASTEC V1 has to be considered has a new code compared with ASTEC V0 (Ref.[40]). First plant calculations using this young code could be carried out with success, nevertheless these calculations done with and without the new B_4C model developed by IRSN have to be considered as preliminary. The case without B_4C run up to the vessel failure, ~7 h after the onset of the transient. The total mass of hydrogen at the end of calculation is equal to 846 kg, which corresponds to 418 kg during early phase from fuel rods and 428 kg during late phase after relocation in the lower head. The transition early/late phase was defined here by the 1st corium slumping into the lower head. The very high H_2 production in the late-phase could come from enhanced oxidation of standing rods due to steam spike generated by the corium slump into the lower head. The maximal rate of H_2 production reached about 0.3 kg/s. The case with the B_4C model failed near the onset of corium slump into the lower head.

- The comparison between MAAP4 and ASTECV1 showed thermal-hydraulic conditions significantly different in spite of the use of the same sequence scenario. Main differences occured after the core uncovery, with more than 1 hour delay in ASTEC V1 with respect to MAAP4. An additional difficulty was connected with the late accumulator injection when the primary pressure reached 42 bars. When this pressure threshold was reached, large differences were found on the water level in the core explaining large differences on the H_2 production in the two calculations.

C.4.1.2 Sequence H2 on a PWR 900

A «H2 sequence» on PWR 900 has been simulated with ASTEC V1 code focussing on the core degradation phase of the accident (~3 h transient). Two exploratory calculations have been carried out, one refers to 100% silver indium cadmium (SIC) control rods (existing case), the other to 100% B_4C. The latter does not correspond to any PWR 900 core but is a comparative study to investigate what could be the B_4C influence on the FP chemistry in the primary circuit, this being of interest for a PWR 1300 which could not be directly calculated during the project due to the lack of operational input deck.

Main conclusions are:

- Different control rods materials lead globally to the same speciation for iodine and different speciation for cesium in the primary circuit;
- Iodine is largely in vapour phase at the break: CsI, RbI and HI (gas) dominate in both cases.
- CH_3I formation is observed in the primary circuit, in reducing and low temperature conditions (T<1100 K), corresponding to favourable conditions for CH_4 formation in the circuit (Fig.60). The formation of CH_3I has been predicted, nevertheless the amount seems low compared to the production of CH_3I by heterogeneous reactions in the containment building itself.

- Major part of Cs is in aerosols phase: Cs_2MoO_4 in SIC case, Cs_2MoO_4 and Cs BO_2 in B_4C case. CsOH constitutes the main part of the vapor phase in SIC case. It has been converted in Cs BO_2 in the B_4C case. More than 50% of Cs at the break is associated with B (Fig.61).

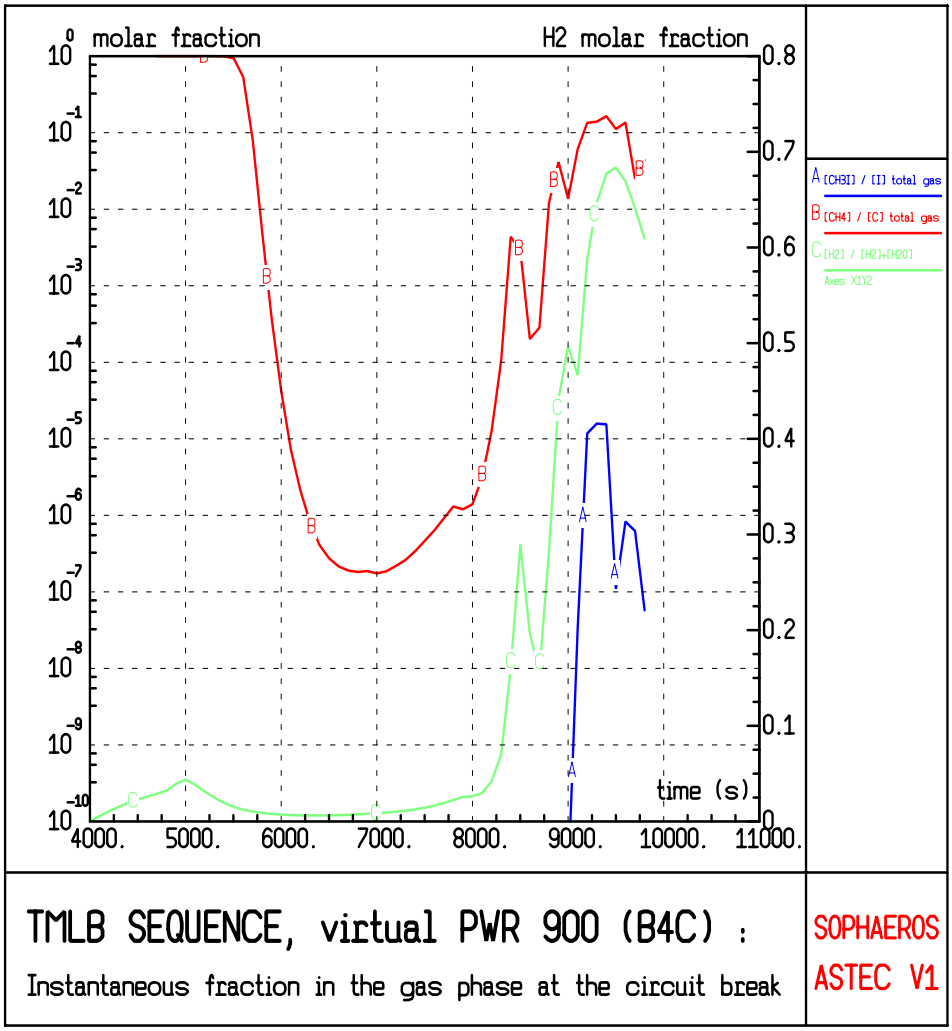

Figure 60: Relative concentrations of CH_4 / (total C in gas) [B], H_2/ (H_2+H_2O) [C] and CH_3I/(total gaseous I) [A] at break

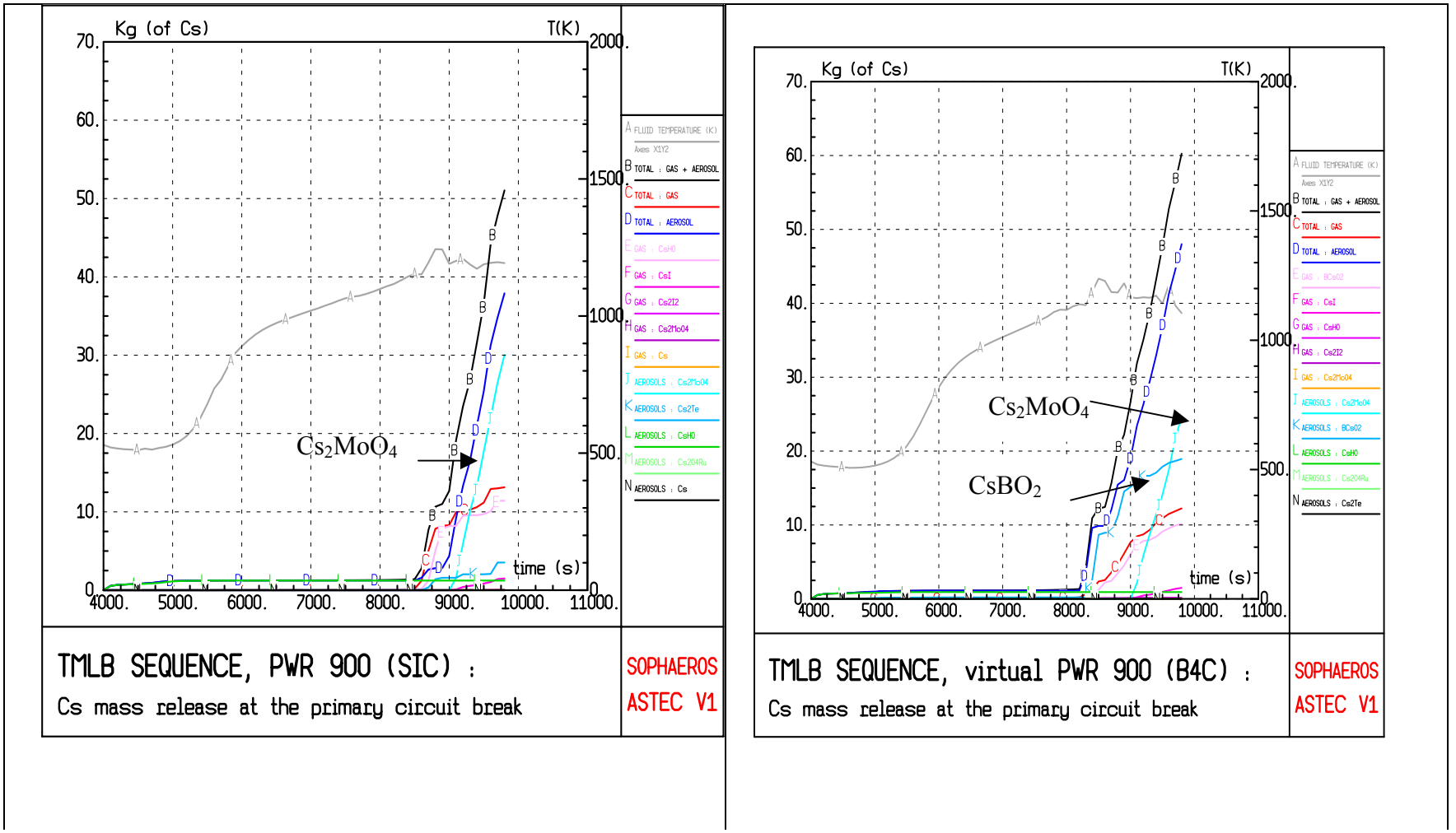

Figure 61 : Cs speciation evolution at the primary circuit break (SIC and B_4C cases)

C.4.1.3 EPR SBO sequence (loss of offsite power)

1st set of calculations

- Results of the EPR SBO sequence (loss of offsite power) have been produced by Framatome-ANP GmbH using MELCOR. Three calculations were carried out during the 1st series of calculations assuming silver indium cadmium (SIC) and B_4C CRs, the later case using different B_4C modelling parameters**.** MELCOR calculations were carried out using B_4C models developed for BWRs (simple and more detailed B_4C models). Main results are:

  - B_4C CR instead of SIC CR does not affect the core degradation significantly,
  - The CH_4 production (less than 28kg) is limited and strongly depends on user-specified B_4C parameters.

- The 1st calculations were also carried out by Framatome-ANP SAS and FZK using MAAP4 and SCDAP/RELAP5 respectively. In both cases, no B_4C models were available at the beginning of the project. Severe core degradation was predicted by MAAP4 with a H_2 production of 595 kg and a vessel rupture 7h after the reactor scram. The SCDAP/RELAP5 calculations predicted 460 kg of H_2 at 5h 19 min after the reactor scram.

2nd set of calculations

- The 2nd calculations were carried out using harmonized timing of the depressurisation of the reactor cooling system in order to facilitate code-to-code benchmarks. Simplified B_4C models developed by Framatome-ANP SAS and FZK were developed in MAAP4 and SCDAP/RELAP5. The previous B_4C model was unchanged in MELCOR.

- The 2nd set of SCDAP/RELAP5 calculations could not be carried out using the B_4C model developed by FZK, this model being not operational at the end of the project. Efforts were focussed on sensitivity studies to the choice Zry oxidation kinetics. The base case was run with Cathcart correlation for temperature lower than 1853 K and Urbanic and Heidrick correlation at higher temperature. The sensitivity case was run using the FZK recommendations: Lezistikov (in the low temperature range) and Prater-Courtright correlations above 1853 K. In the latter case 574 kg of H_2 was predicted instead of 460 kg before the core slumping into the lower plenum.

- The MAAP4 calculation with a preliminary B_4C model showed an increase of the H_2 production by ~ 7% compared to the case with SIC control rods and negligible amount of CH_4. A sensitivity study on the choice of Zry oxidation correlations (default and FZK recommended correlations) showed limited effects on H_2 production, the SBO sequence being characterized by steam starvation conditions.

- With MELCOR, the impact of B_4C was found limited regarding core degradation, CH_4 production (less than 5kg) and FP chemistry at the outlet of the core. CH_4 production was found to depend on modelling parameters of the B_4C models. The lack of gas and FP chemistry in the circuit do not enable to evaluate the real impact of B_4C on the source term. Sensitivity calculations were done with MELCOR.

- Between two calculations carried out with SIC and B_4C CRs, there is a difference on the total H_2 production of ~ 50 K (Fig. 62).

- Similar H_2 production was found between the Urbanic and Heidrick correlation used in the lower and at higher temperature range and the FZK recommended correlations (Fig. 63).

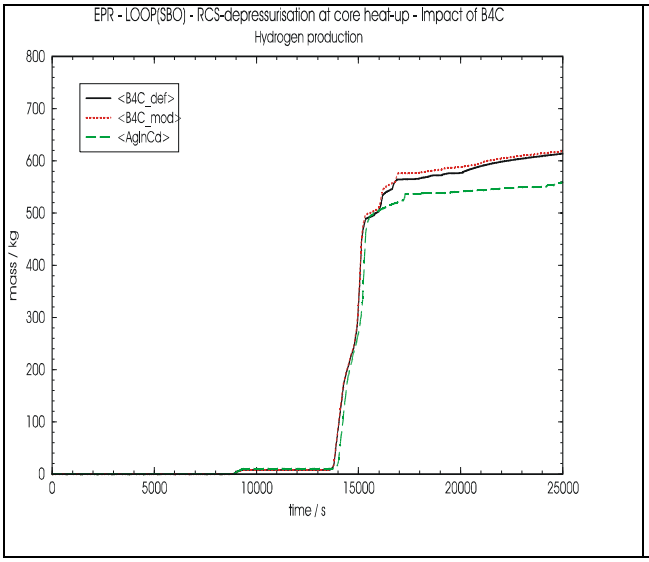

Fig. 62 : H_2 production for B_4C and SIC-CRs

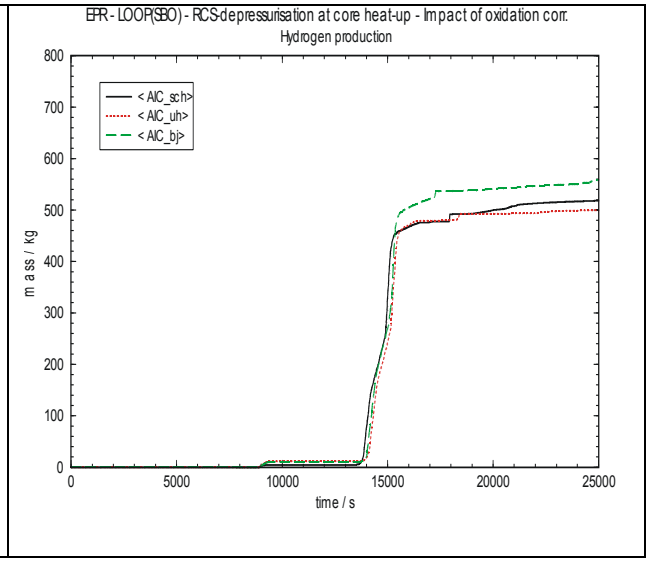

Fig. 63 : Hydrogen production for different Zircaloy oxidation correlations

- The benchmark between MAAP4, MELCOR and SCDAP/R5 indicated different effects of the choice of Zry oxidation correlations using FZK recommended correlations instead of default options.

  - In the first two cases the effect was limited probably due to steam starvation conditions at high temperature in the SBO sequences.
  - The difference with SCDAP/R5 could be due to large differences with the other cases on the prediction of clad failure and melt relocation and on the thermal hydraulic conditions in the core.

Table 7 and Figure 64 illustrate the code-to-code differences on H_2 production using default correlations (Urbanic-Heidrick correlations) as well as the B_4C effects on total H_2 production with MAAP4 and MELCOR.

Table 7: Benchmark on H2 production between MAAP4, MELCOR and SCDAP/R5.

	MAAP4 (with AIC)	**MELCOR (with AIC)**	**SCDAP/R5 (with AIC)**
Max. H_2 rate (kg/s)	0.95 kg/s		0.48 kg/s
Total H_2 (kg) before relocation to lower head	595	624	460
Corresponding oxidized part of core Zr	35.7%		29%

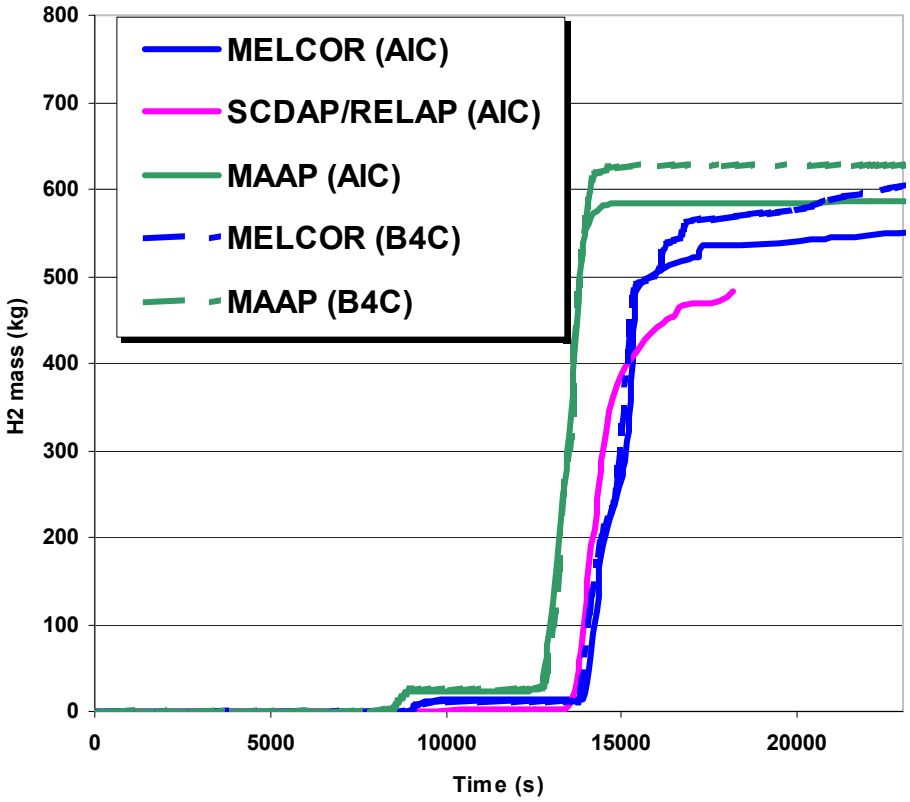

Figure 64: H_2 production according to MAAP4, MELCOR and SCDAP/R5 on a SBO sequence occurring on the EPR. Impact of B_4C on total H_2 (compared with cases with AIC).

C.4.1.4 Large break LOCA with a cold leg double-ended rupture in a VVER-1000

The LOCA sequence calculated with ICARE/CATHARE V1 Mod1 by KI considered also a simultaneous loss of external electrical supply. Calculations have been run up to the onset of corium relocation to the lower head. The 2nd calculations were carried out using an upgraded version of ICARE/CATHARE involving in particular a revised B_4C model and a new MAGMA model (2D corium relocation) instead of the 1D candling model available at the beginning of the project. Various sensitivity studies were carried out on B_4C oxidation, ZrO_2 clad failure and fuel rod collapse criteria.

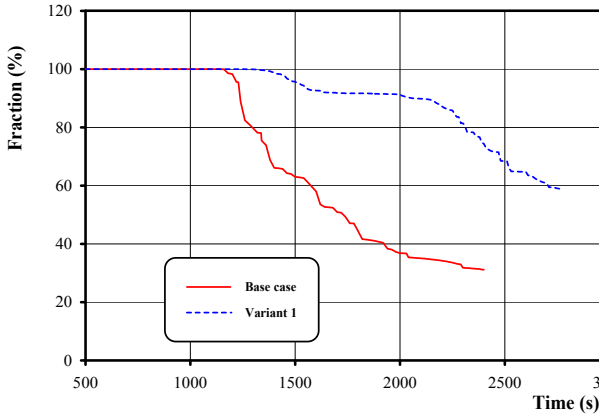

Fig. 65: Fraction of UO_2 remaining in place

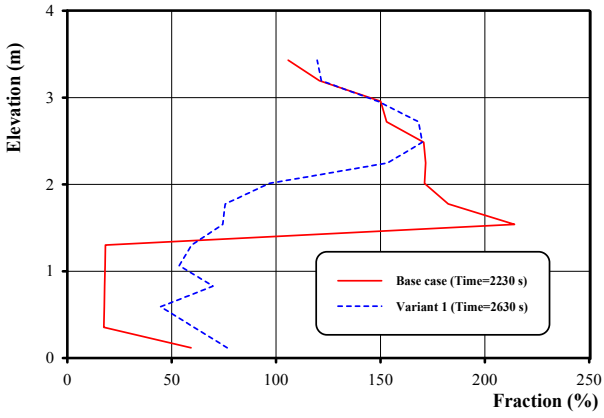

Fig. 66: Axial profile of flow area

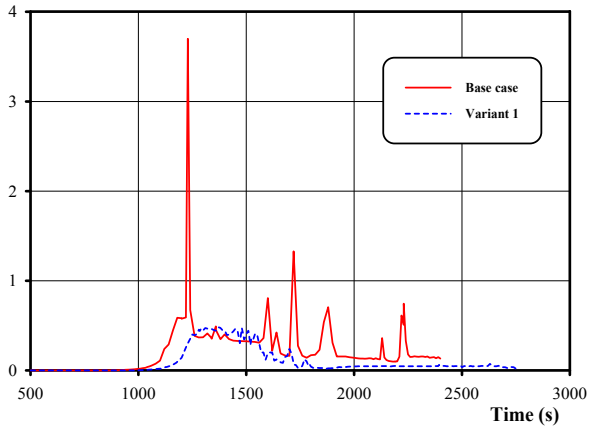

Fig. 67: Hydrogen Production Rate In-Vessel.

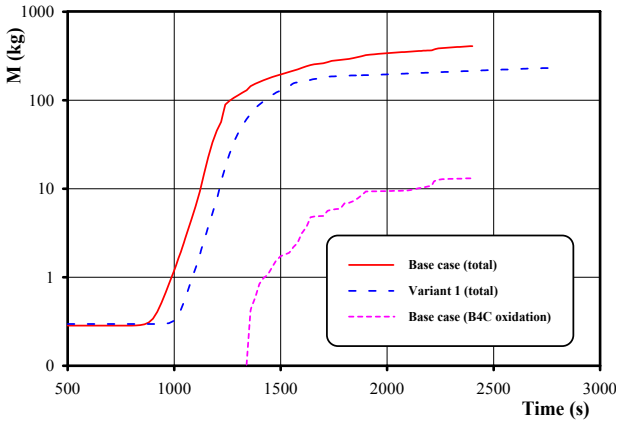

Fig. 68 : Mass of Hydrogen Generated In-Vessel.

Figures 65 and 66 show comparisons between the first calculation (Variant 1) and the base case of the 2nd set of calculation carried out with the upgraded code. Earlier and more important core liquefaction were found in the 2nd calculation. This large difference is mainly resulting from the replacement of fuel rod collapse criterion from 3100 K in the Variant 1 calculation by the value of 2550 K used in the Base Case calculation (value recommended by IRSN from Phébus FP results). Up to 68 % of the fuel is found "dislocated" in the Base Case (this means liquefied both by fuel dissolution by molten Zry and fuel melting) instead of ~ 28% in Variant 1 at the same time (case with UO_2 dissolution only).

Figures 67 and 68 illustrate H_2 production rate and total mass of H_2 generated in the accident. In the Base Case, the peaks on the H_2 production rate and the increase of total amount of H_2 generated from 230 kg up to 380 kg are resulting of the modelling of a 2D relocation model linked with the modelling of the oxidation of relocating U-Zr-O mixtures characterized by a limited protective effect of the ZrO_2 resulting from the melt oxidation.

The fraction of H_2 generated due to B_4C material oxidation is negligible in comparison with H_2 generated due to Zr oxidation and does not exceed 5% of the total amount of H_2 production (Figure 68). This small value is linked with the lack oxidation of B_4C-rich mixtures and to steam starved conditions predicted in the core during the high temperature period. The B_4C effect on the core degradation was found limited.

The state of the reactor in the Base Case calculation near the end of the calculation is presented in the Figure 69

A severe accident station blackout scenario for a VVER-1000 reactor was calculated by LTKK with ICARE/CATHARE using the same code versions as KI at the beginning and at the end of the project. The final calculations run up to the severe degradation of the core at 15000s (Fig. 70). Once more the B_4C effect on H_2 production was found limited (8% of total H_2 production) due to the same reasons than in the KI calculations: lack of oxidation of B_4C-rich mixtures and steam starvation conditions in the core.

C.4.1.5 Large break LOCA and station blackout in a Swiss BWR-6

In the 1st set of calculations, numerous MELCOR calculations were performed by PSI for a large break LOCA and station blackout in a Swiss BWR-6 (KK Leibstadt design). The

conditions under which the B_4C reacts are wider than expected, most often under steam-starvation conditions.

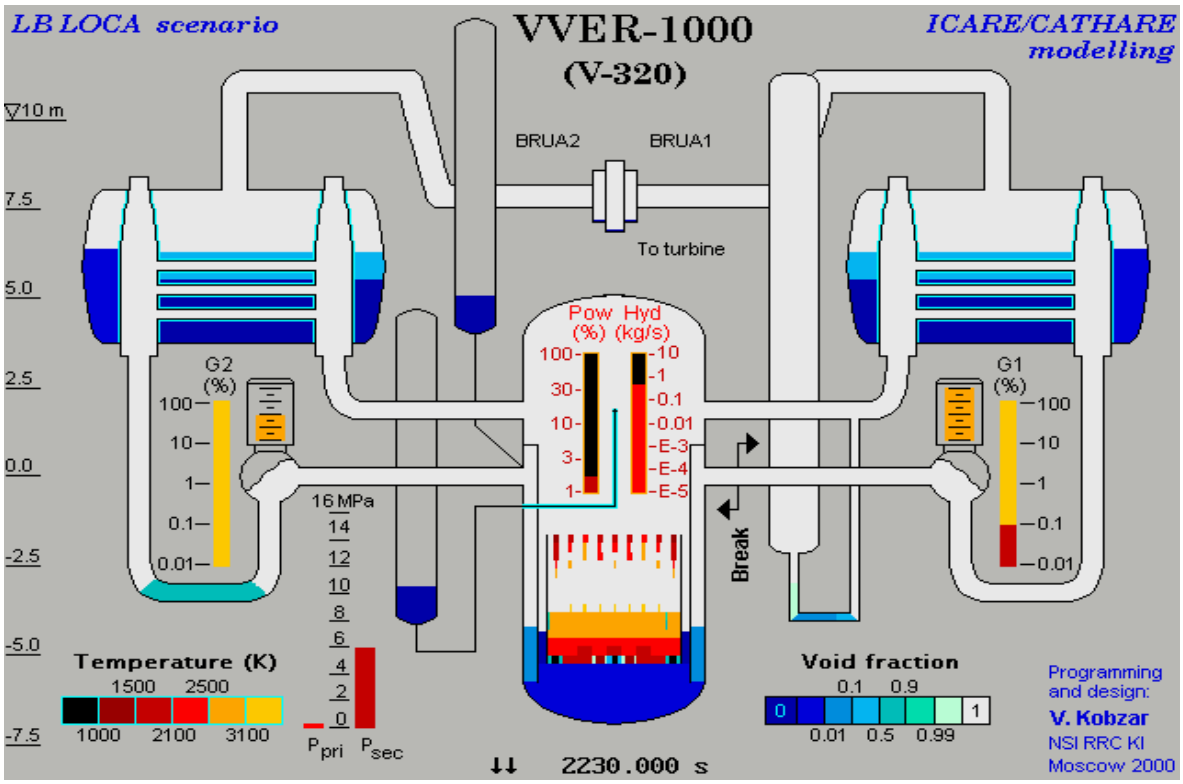

Fig. 69: State of the Reactor Facility Just After the Melt Reached the Core Bottom (Base Case).

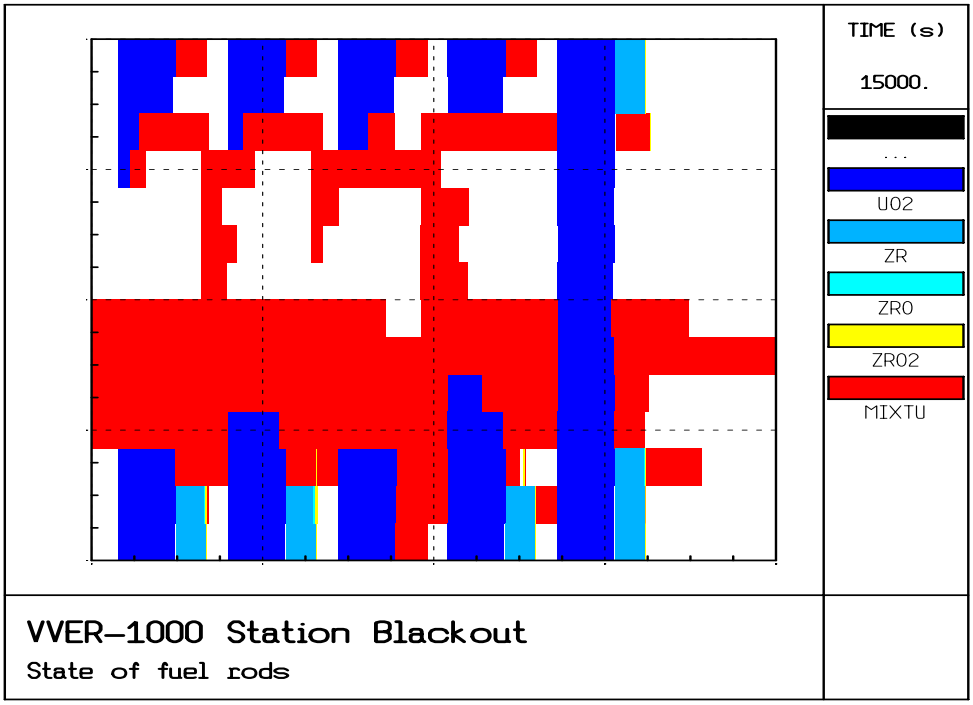

Fig. 70: SBO sequence calculated by ICARE/CATHARE. Final state of fuel rods in the first simulation

A large number of sensitivity studies were performed to investigate the impact of various assumptions concerning B_4C-SS control blade behaviour on degradation and oxidation, including B_4C reaction off-gas chemistry. Since the B_4C oxidation is strongly influenced by the steam flow and temperature, there is wide variation in amount of B_4C reacted and in off-gas composition which is dictated by the relative timings of core degradation events. The extent of B_4C oxidation is in the range 4-18 % in the station blackout, depending on the assumptions for initiation of B_4C oxidation. Rather less oxidation of B_4C, up to 7 %, occurs in the LOCA sequence, due to its shorter duration. Calculations indicate production of up to 1kg of CH_4, a quantity sufficient, potentially, to convert a substantial fraction of the iodine to volatile CH_3I species. The results exhibit strong spatial and temporal variations, and demonstrate the role of integral effects as phenomena occurring in different regions that interact with each other. Improvements of B_4C models were identified and discussed with the MELCOR code authors.

Between the 1st and 2nd set of calculations, no modelling improvements could be done by PSI not involved in MELCOR developments. Only code developments from MELCOR developers in Sandia were available for the 2nd set of calculations.

The 2nd set of calculations was accompanied by several sensitivity studies: B_4C model parameters (oxidation kinetics reduced by factor of 1000, with-without B_4C/steel interaction), Zr oxidation with Leistikow-Prater/Courtright recommended by FZK instead of the Urbanic-Heidrick correlation (default in MELCOR) and revised degradation criteria.

The pressure history is shown in Figure 71, while the cladding temperatures in the core innermost and outmost rings are shown in Figure 72. Heat-up of the cladding accelerates as the core is progressively uncovered and when Zircaloy oxidation begins at 2660 s. Oxidation of B_4C begins at 2890 s after some of the steel has melted and moved away due to the eutectic interaction.

The first canister failure occurs at 3570 s. Hydrogen generation continues and accumulates in the containment. The deflagration condition is reached at 3600 s, initiating the first of several burns that occur. The pressure temporarily increases in the containment following each burn, perturbing the pressure distribution in the vessel and provoking flow transients in the core (Fig. 71). The high temperatures result in a succession of degradation events: metallic melting, fuel dissolution, oxide scale failure, relocation of liquefied (U, Zr)O, collapse of the fuel rods to debris, and accumulation on the support plate.

A major change occurs when the central part of the core support fails at 4506 s. A large quantity of fuel rod and core structures drops into the lower head and is quenched by the residual water, causing a large pressure spike and flow of steam through the core which quenches before heating up again after 5000 s. Oxidation of metallic structures and B_4C in the core recommences, but the bulk of the hydrogen is now generated in the lower head. The remainder of the core continues to degrade and relocates in piecemeal manner to the lower head, such that all of the core and support is finally transferred at 18850 s. At the same time the debris in the lower head transfers heat to the vessel shell, which ablates and eventually fails at 21684 s, having almost completely melted through at the bottom.

The core hydraulic conditions vary widely during the transient, with long periods of low flow and steam starvation, punctuated by surges of steam associated with relocation events and hydrogen burns.

In the base case, a total of nearly 1400 kg of hydrogen is generated, just over half of which is in the core (726 kg). About 8% of the B_4C is oxidised or decomposed, resulting in 12 kg of

H_2, 21 kg of CO and 1.2 kg of CH_4. Thus the B_4C contributes only slightly to the oxidation heat and H_2 release.

Sensitivity studies show unexpected effect on the H_2 production, which was lower using FZK correlations due to unexpected reverse feedback effects between different phenomena. Reverse effects were also found on the total H_2 production with the degradation criteria. B_4C effects were limited, only 1-2% more H_2 but the impact of CH_4 on iodine speciation cannot be ruled out. In summary, during the early stage of degradation sensitivity studies had limited effects. During the later period of core degradation, the core oxidation depends on the degradation sequence - the movement of materials within the core and to the lower head - such that the total generation no longer bears any clear relation to model choice. These calculations enabled the identification of modelling weaknesses, in particular for the B_4C.

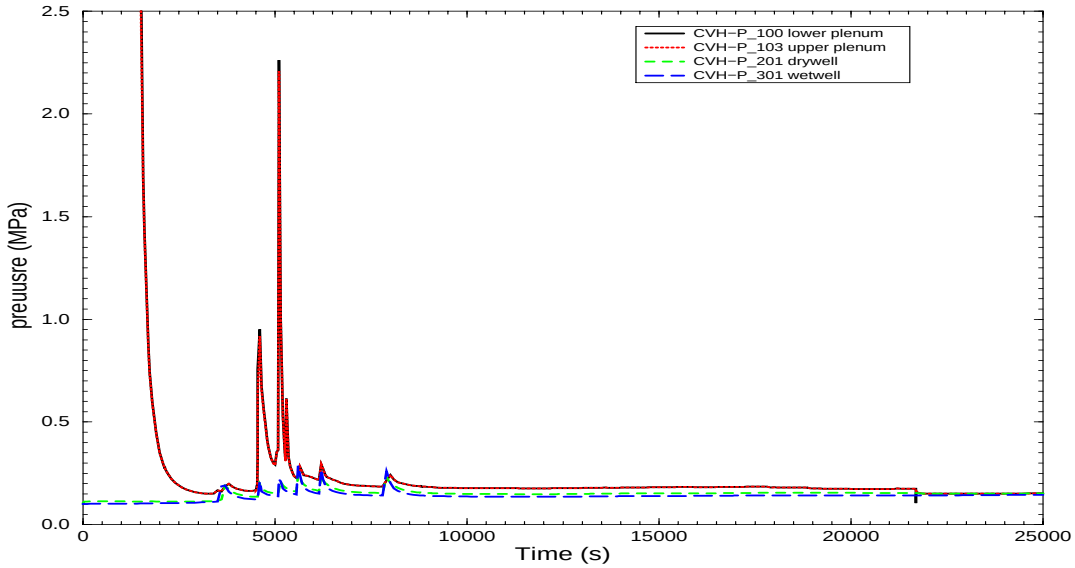

Figure 71: Base Case system pressures

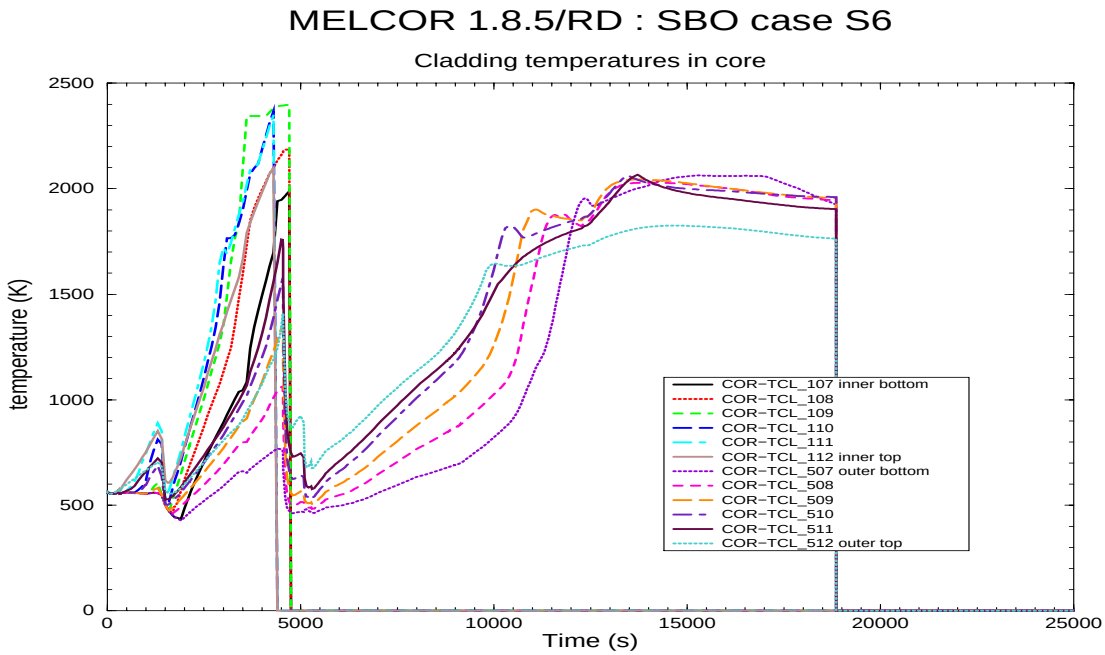

Figure 72: Cladding temperatures in central and outer core regions (Base Case RD)

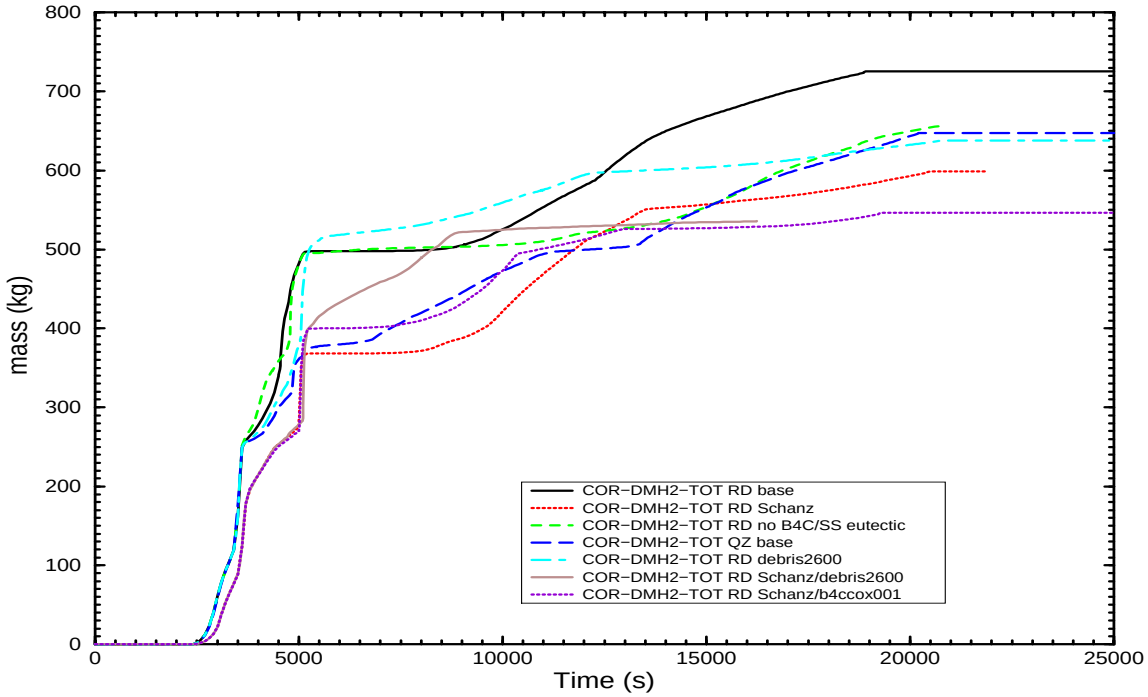

Figure 73: H_2 generation rate (all cases)

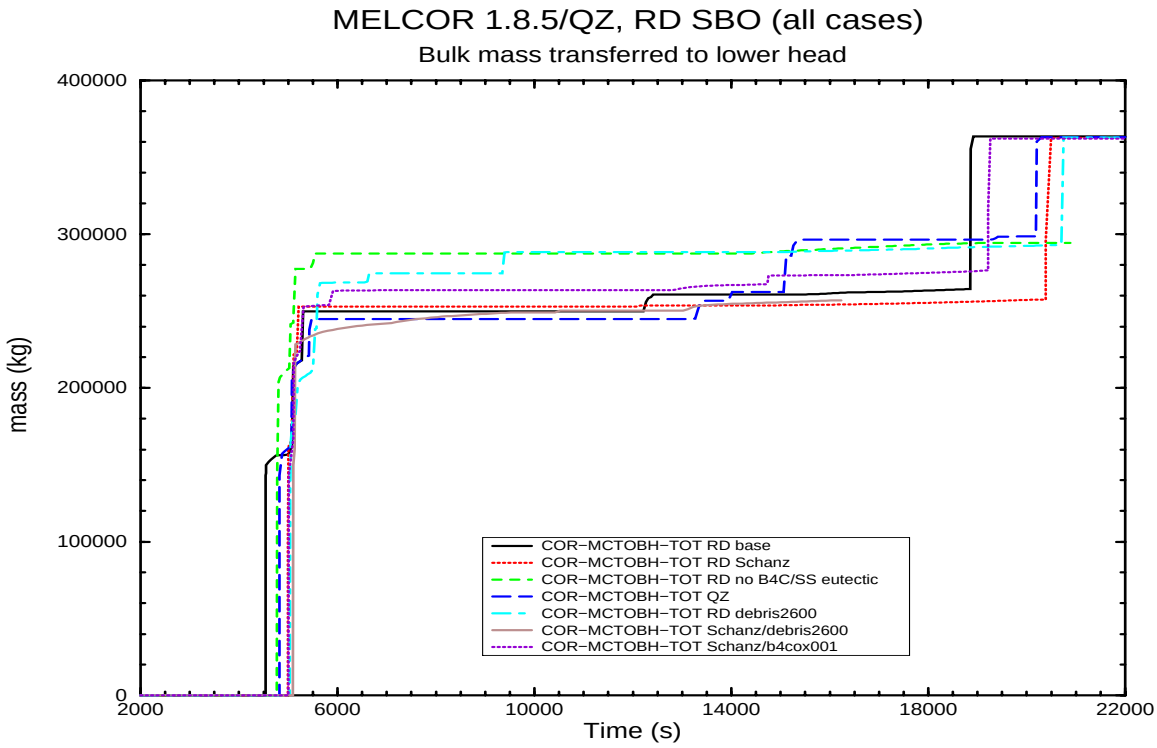

Figure 74: Bulk mass transferred to lower head (all cases)

C.4.1.6 TMI-2 calculations

Three calculations have been performed by ENEA and IRSN using respectively SCDAP/RELAP5, ICARE/CATHARE and ASTEC V0. The main objective was to evaluate code uncertainties regarding the H_2 production and melt formation. A significant effort of standardization was undertaken by ENEA with SCDAP/RELAP5 Mod3.2, ACTEC and

ICARE/CATHARE V1 Mod1 in order to facilitate comparisons. Additional calculations were provided by EDF using MAAP4.

ICARE/CATHARE and SCDAP/RELAP5 calculations

ENEA carried out preliminary comparisons between ICARE/CATHARE and SCDAP/RELAP5 calculations performed respectively up to the onset of core reflood and the core material slumping to the lower head.

- The two calculations are consistent with the TMI-2 core behaviour when core uncovery is reasonably well predicted by the codes and suitable core degradation parameters are used to describe core melt progression. Differences in melt progression are mainly due to the use of different models (i.e. UO_2 and mainly ZrO_2 dissolution kinetics and solubility limits). Nevertheless, the core degradation calculated by the codes at the end of Phase 2 is similar (Figures 75 and 76) and in substantial agreement with the expected one inTMI-2.

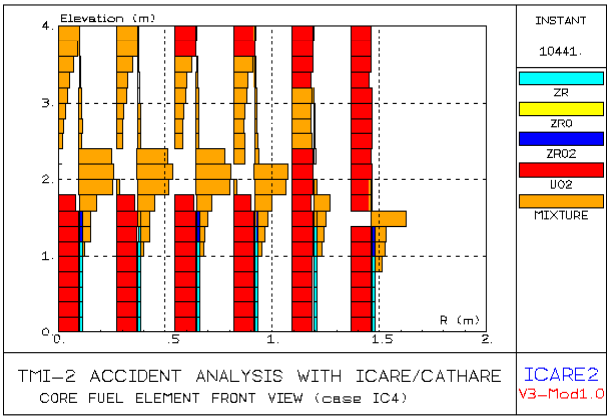

Fig. 75: Core degradation computed by I/C code at end of Phase 2

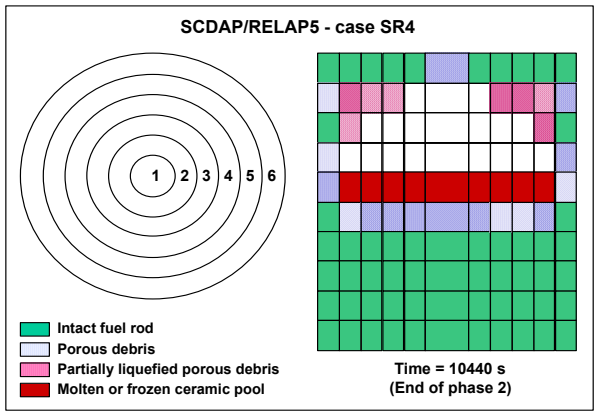

Fig. 76: Core degradation computed by S/R5 at the end of Phase 2

After reflood, SCDAP/RELAP5 calculates correct spreading of the molten pool at the core periphery and slumping of corium into the lower head is correctly estimated. After crust failure, the massive slumping of 100% molten pool material (28200 kg) into the lower head of is in good agreement with TMI-2 estimations (~ 29000 kg at 224 min) but there is no more corium staying in the core in the calculation while ~30000 kg were found in the TMI-2 core.

The total H_2 releases calculated are compared with TMI-2 data in Fig. 77 and Table 8.

- ICARE/CATHARE slightly underpredicts the hydrogen release in TMI-2 at the end of Phase 2 while SCDAP/RELAP5 overestimates it.
- SCDAP/RELAP5 also computes high hydrogen release during core reflood by a simplified oxide scale shattering model. The H_2 peak produced during quenching is underestimated (~70 kg instead of ~160 kg in TMI-2). Nevertheless, the total amount of hydrogen computed at the end of the reflood phase (463 kg) is very close to TMI-2 data (460 kg).

Table 8: H_2 production in TMI-2

Calculation & TMI-2	H_2 released before reflood	H_2 at the end of TMI-2
SCDAP/RELAP5	394 kg	463 kg
ICARE/CATHARE	277 kg	-
TMI-2	~ 300 kg	~ 460 kg

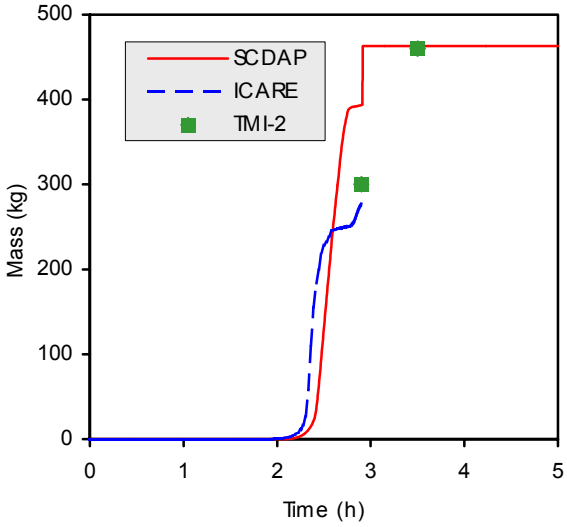

Fig. 77: Total H_2 production

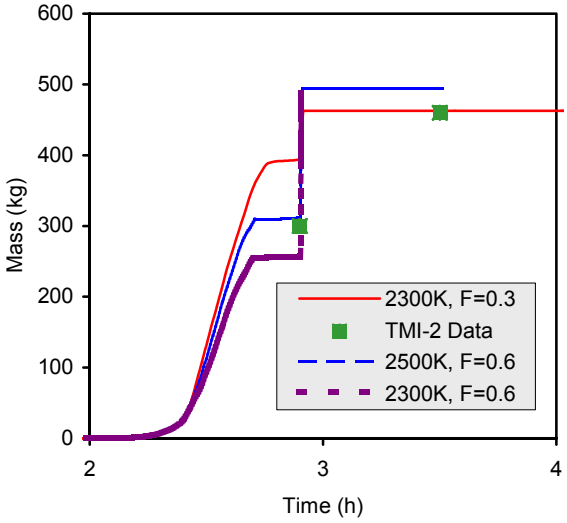

Fig. 78: Sensitivity on H_2 production (kg) with SCDAP/R5

- Sensitivity studies have been also carried out during the 1st set of calculations varying several fuel rod degradation parameters. Results enable the uncertainties on the H_2 production and the amount of melts formed to be evaluated, in particular:

- The impact of the clad failure criteria on the timing of H_2 release was found significant with SCDAP/RELAP5 (Fig. 78) but limited with ICARE/CATHARE due to differences in core heat-up and fuel rod dissolution models. Considering all calculations, the H_2 predictions before reflood is between 220 and 394kg (300kg evaluated in TMI-2). Nevertheless the impact on the final H production at the end of the calculation was limited.

- The fuel rod "collapse temperature" was found to significantly affect the core fraction melted. The influence of fuel rod collapse temperature on core degradation has been evaluated with ICARE/CATHARE, by reducing slightly the rod collapse temperature from 2830 K to 2730 K. The total amount of fuel melted was increased from 15000kg to 22000 kg. The latter value is still underestimated compared with TMI-2 evaluation. A second study carried out in different conditions (2nd set of calculations) showed also larger fuel liquefaction 33000 kg instead of 24000 kg when the fuel rod collapse parameter is reduced from 2830 K to 2550 K.

- The choice of FZK recommended Zry oxidation correlations such as Cathcart below 1800 K, Prater above 1900 K (SC1 case) instead of the Urbanic-Heidrick correlations in the base case (RC case) induced a decrease of the total H_2 production at the end of Phase 2 (from 285 kg to ~245 kg). This evolution is not consistent with TMI-2 results (~300 kg).

- The 2nd set of calculations was carried out using ICARE/CATHARE and ASTEC V1 (the latter code instead of SCDAP/R5). The upgraded I/C version V1 mod1.3p developed during the project was used using the revised dissolution model with the burn-up effect and the provisional model for oxidation of solid U-O-Zr mixtures.

- The calculation done with the burn-up effect on the fuel dissolution model was as an exploratory test to check the effect on fuel liquefaction (the TMI-2 fuel had a low burn-up). More significant UO_2 dissolution was found at the end of oxidation phase (Fig. 79) compared

with initial calculations. The fuel dissolution was limited by the clad failure temperature criterium (2300 K) as the oxide scale was not thick enough to hold in place the molten mixture due to the overestimation of the ZrO_2 dissolution.

- The fuel rod degradation at the end of Phase 2 is shown in Fig. 80. Referring to the first calculation, the total amount of fuel dissolved and melted is increased, 24000 kg instead of 15000 kg.

- The total H_2 release at the end of Phase 2 (285 kg) is not significantly affected by the new oxidation model for relocated solid mixtures. In spite of the large amount of materials relocated during the early degradation phase, metallic material relocates and solidifies near the water level (Fig. 81), where the temperature is too low to have significant mixture oxidation. In fact, a large amount of unoxidized Zry is still present at the end of Phase 2 in relocated mixture around 1.2 m level above the core bottom. This calculation does not take into account oxidation of "relocating" mixtures, but only that of "relocated" mixtures.

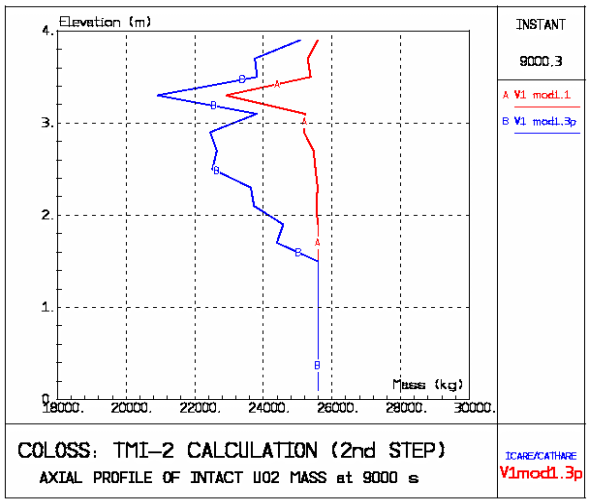

Fig. 79: UO_2 dissolution by molten Zry at 9000 s.

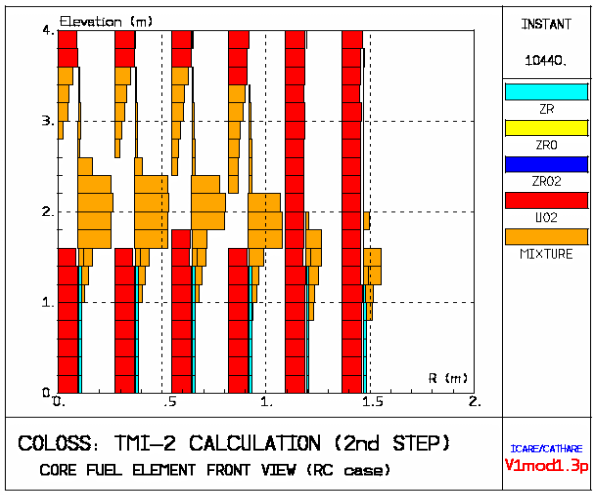

Fig. 80: Fuel rod degradation at the end of Phase 2.

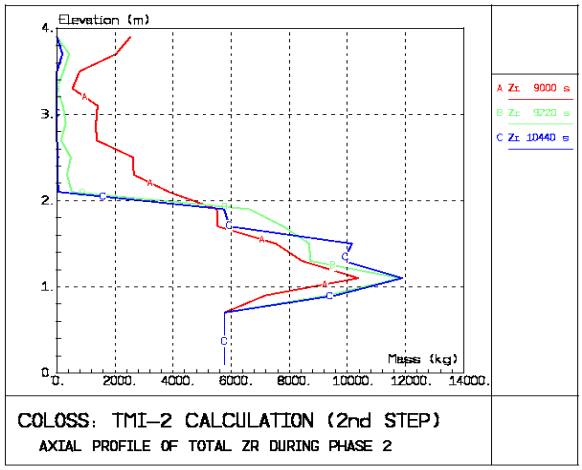

Fig. 81: Axial profile of total metallic Zry mass during Phase 2 (I/C calculations).

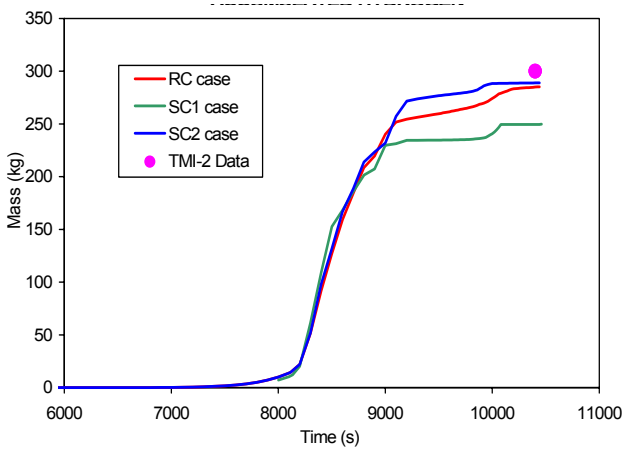

Fig. 82: Impact of the ZrO_2 clad failure criteria on the total hydrogen release (I/C calculations).

- Sensitivity studies on the ZrO_2 clad failure and on fuel collapse criteria. A small effect was found on total H_2 production (Fig. 82) as in the 1st calculations. The influence of the **fuel collapse temperature** recommended by IRSN was important as in the 1st calculations on axial fuel distribution and liquefaction as shown in Figures 83 and 84 giving the axial distribution of intact and total UO_2 masses at the end of Phase 2. The total amount of fuel melted increases by about 40% compared to the one in reference case. A molten pool is formed just above the metallic melt blockage that developed during the early degradation phase. This new evolution seems more consistent with the TMI-2 understanding.

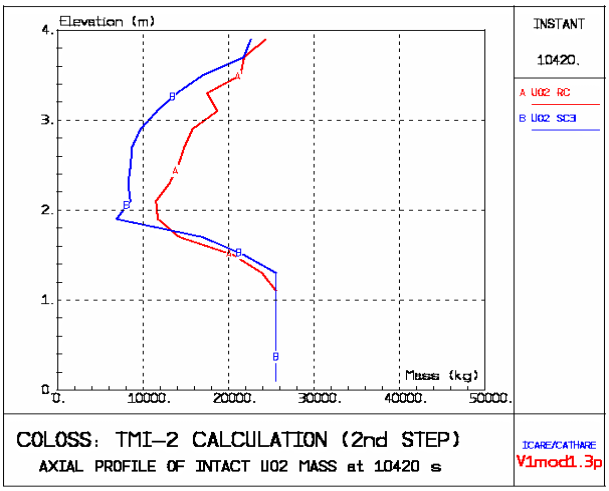

Fig. 83: Effect of fuel collapse at 2550K: Intact UO_2 mass at the end of Phase 2

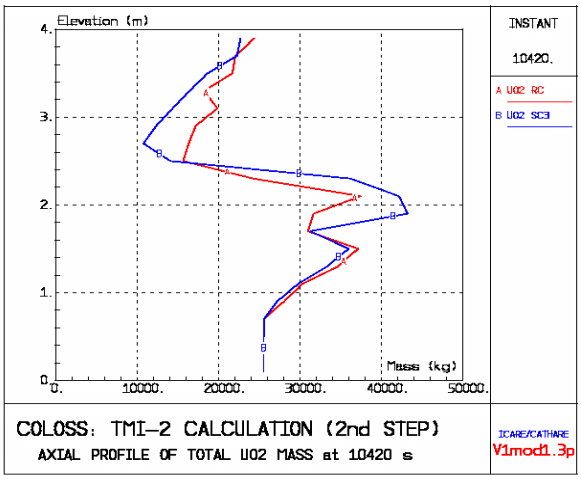

Fig. 84: Effect of fuel collapse at 2550K: Total UO_2 mass formed end of Phase 2

ASTEC V1 calculation

The new code ASTEC V1, totally different compared with ASTEC V0 regarding the modelling of the thermal-hydraulics in the primary circuit (CESAR module) and regarding the modelling of core degradation (DIVA module) was user for a TMI-2 calculation, the first reactor case calculated with this young code. This work has been carried out in close co-operation between IRSN and ENEA. The ASTEC V1 calculation was limited at the 1st half of Phase 2 due to numerical convergence problems. It was compared with the ICARE/CATHARE calculation carried out using same conditions and user-specified options.

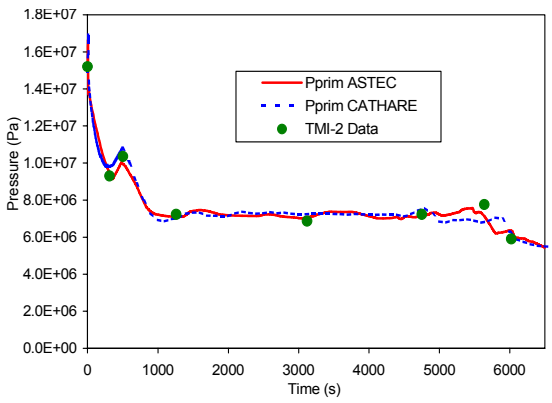

Fig. 85: Primary system pressure

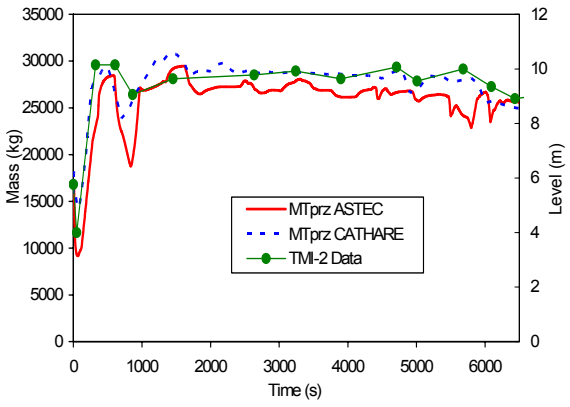

Fig. 86: Pressurizer coolant mass

- The thermal-hydraulics in the primary system calculated by ASTEC V1 is in agreement with ICARE/CATHARE. Figures 85 and 86 show the primary system pressure and the pressurizer behaviour calculated by the ASTEC V1 and I/C codes and TMI-2 data.

- The coolant inventory depletion in the primary system (Fig. 87) is computed by ASTEC V1 in good agreement with ICARE/CATHARE. The Fig. 88 shows the history of coolant mass in the core. Code result difference is enhanced at primary B-pump shutdown at 74 min.

- The core water level calculated by ASTEC V1 during Phase 2 is underestimated with respect to ICARE/CATHARE. In spite of difference the core heat-up starts some hundreds of seconds later in ASTEC V1 calculation. Clad burst is computed around 8000 s, about 300 s later than ICARE/CATHARE, in agreement with TMI-2 data. The reason for the difference in core heatup could be mainly related to the enhanced 2D gas natural circulation in the core calculated by ASTEC V1 during the first part of Phase 2.

- Calculated fuel rod degradation at 8500 s is shown in Figures 89 and 90. ASTEC V1 predicts a less important core degradation at the periphery of the core and relocation of molten material at lower elevation with respect to ICARE/CATHARE. This is consistent with the lower core water level predicted by ASTEC V1.

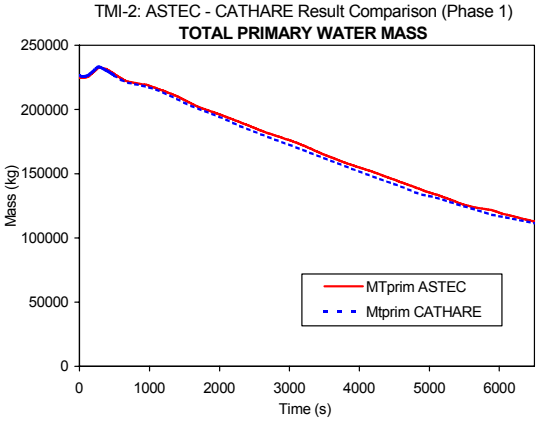

Fig. 87: Coolant inventory in the primary system

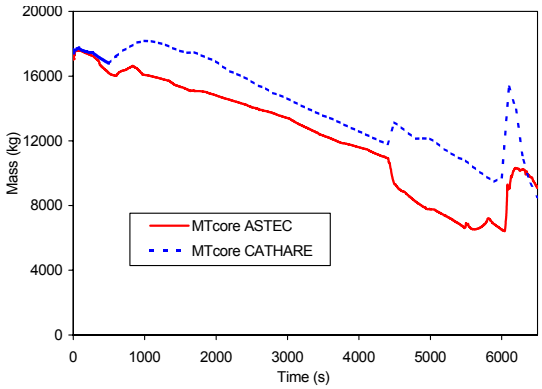

Fig. 88: Coolant mass in the core

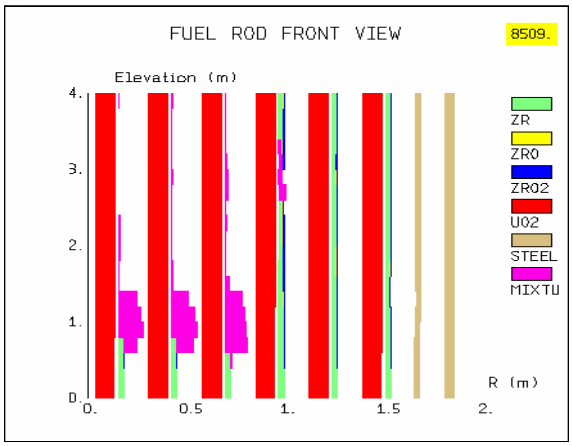

Fig. 89: Fuel rod degradation by ASTEC V1

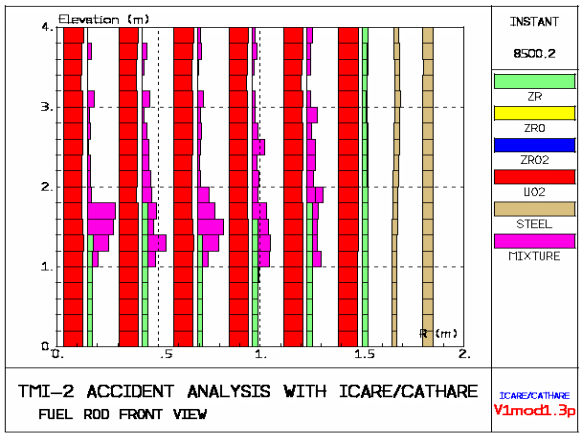

Fig. 90: Fuel rod degradation by ICARE/CATHARE

MAA4 calculation

The MAAP4.0.2 calculation carried out by EDF focussed on the end-state configuration of the core. The full sequence was calculated for benchmarking purpose with SCDAP/R5 and ICARE/CATHARE codes. The calculated mass of corium transferred to lower head was found too low (~20000 kg instead of ~30000 kg in TMI-2). It was suspected to be due to an incorrect liquidus temperature of the U-Zr-O mixtures. Regarding H_2 production, it is believed that 300 kg of hydrogen were produced in TMI-2 before the quenching of the core and an extra production of about 160 kg during the quench. In this field, MAAP4 gave a good evaluation of the total H_2 production as in TMI-2 while the rapid production of 160 kg during quenching was not calculated and the H_2 produced end Phase-2 was overestimated (376 kg instead of 300 kg in TMI-2).

C.4.2 Assessment of SA codes on H_2 production, B_4C effects and corium formation

In the plant calculation activity, the analysis of code-benchmarks and sensitivity studies on key parameters of the core degradation enabled the identification of abilities and deficiencies of codes and needs for improvements, in particular for the following topics:

H_2 production: Sensitivity studies on early degradation models showed more significant effects on *H_2 rate* during early core heat-up or during quenching than on *total* production for which the scattering of results was found to be in the 20-35% range depending on the SA sequence. The following table summarises the H_2 dispersion between various sensitivity studied performed with various SA codes.

SA sequence	H_2 prediction range
BWR-SBO with MELCOR	550 - 720 kg
PWR 1300 “H2 sequence” with MAAP4	527 - 632 kg
EPR-SBO with MELCOR	400 - 545 kg
TMI-2 Phase 2 benchmark I/C and S/R5	277 - 394 kg
EPR-SBO benchmark MAAP4, MELCOR & SCDAP/R5	480 - 630 kg

The H_2 rate is certainly underestimated during melt relocation due to missing or incorrect melt oxidation models. Regarding the best choice of Zry oxidation kinetics, the Prater-Courtright correlation was recommended above ~1900 K. Above 2100 K, this law gives higher kinetics than the Urbanic-Heidrick one often used in SA codes. Sensitivity studies carried out on different SA sequences using different codes did not showed a clear trend. Various effects were found on H_2 production depending on thermal-hydraulic conditions and on the core degradation modelling. More investigations are needed to conclude on the best Zr oxidation correlations, in particular there is a need at high temperature of modeling improvements regarding the steam supply limitation before recommending Zry oxidation correlations for plant calculations.

Oxidation of mixtures: Based on sensitivity studies, the melt oxidation during melt progression is significant but difficult to assess, except globally on TMI-2. Large uncertainties are suspected on the oxidation of relocating/relocated mixtures while H_2 coming

from mixtures can represent a large fraction of total H_2 production (> 30%). This topicis a key weakness of SA codes resulting in the underestimation of the H_2 production during the early melt progression and, more important, during the quenching of a degraded core. In general, the modelling of the oxidation of mixtures is either missing or inadequate while experiments on oxidation of U-O-Zr and B_4C-rich mixtures showed larger kinetics than for pure Zry and B_4C materials. A correct modelling of the oxidation of mixtures requires not only a specific mixture oxidation kinetic but also a 2D corium progression and thermal-hydraulic description in the core to take into account reasonably the corium-coolant surface interaction and the steam supply. These bi-dimensional aspects were missing in SA code versions available in the project.

B_4C oxidation: Effects on core degradation were calculated as limited, nevertheless the modelling of the degradation induced by B_4C is in general limited in present SA codes (B_4C-Zr and B_4C-ZrO_2 interactions are not taken into account). Regarding gases produced, H_2 induced by B_4C oxidation was often less than 10% of total H_2 and very little CH_4 was produced. As already mentioned, more important for FP chemistry in the circuit are the CO, CO_2 and B-compounds productions. The rapid oxidation of B_4C-melts is not yet modelled in spite of the large impact suspected on H_2 production during core quenching. In general, SA codes do not calculate the *gas chemistry* in the core (except MELCOR) and, more important, downstream the core (except ASTEC V1) where the FP chemistry, in particular iodine and cesium speciation, can be affected by B_4C-gas production as evidenced in an exploratory ASTEC calculations.

UO_2 dissolution by molten Zry and burn-up effect: Large uncertainties on the prediction of corium formation were evidenced by large differences observed between SA codes on the modelling of fresh fuel dissolution. Main modelling differences concern the solubility limit of fuel in Zr-rich mixtures, the simultaneous dissolution of ZrO_2 more often neglected and finally the ZrO_2 clad failure criteria which limit the rod dissolution and drive the onset of U-O-Zr melt relocation. All these phenomena are closely coupled while the coupling in SA codes is not sufficient. There is some experimental evidence that the solubility of UO_2 in the U-O-Zr melt is not limited by the melt saturation as supposed in the majority of SA codes. This finding favours the early formation of U-O-Zr melts during core degradation. In addition, the burn-up effect known to enhance significantly UO_2 and MOX liquefaction and suspected to favour early rod collapse and volatile FP release was not modelled in the majority of SA codes. When existing, such as in ICARE/CATHARE, the burn-up effect model is preliminary and needs consolidation for plant applications.

Loss of rod geometry: The user-effect linked with the **choice of the ZrO_2 clad failure** conditions, user-specified in SA codes, was found to be modelling dependent and also core-condition dependent. In particular sensitive effects on hydrogen release rate were mainly found under steam-rich atmosphere during heat-up. Effects were also found on fuel dissolution and on early corium behaviour. The **choice of a fuel rod collapse criterion,** also user-specified in codes, was found to be an overwhelming parameter for the corium progression (see the following table). Fuel rod collapse conditions driving the transition from rod like geometry to molten pool need to be more clearly identified in order to reduce large uncertainties induced on the further corium progression.

SA sequence	Sensitivity on fuel rod collapse temperature	Effect on core degradation

TMI-2 end Phase-2 with I/C	2830 K→ 2550 K	+40% of corium
VVER 1000 LOCA with I/C	3100 K→ 2550 K	70% of fuel relocated (instead of 30%)

Corium behaviour: Large discrepancies were found between calculations on the amount and timing of corium produced, on its composition and on the distribution between core, core by-pass and lower head. The corium behaviour is affected by the different assumptions made in the early core degradation models. Nevertheless the corium behaviour was found to be more dependent on the late melt progression modelling than on that of the early degradation. In particular the modelling of the corium progression is over-simplified regarding material properties or its 1D description. The *fuel rod collapse criterion*, which controls the early formation of large quantities of corium was found to affects significantly the late corium behaviour, in particular its amount and metal-oxide composition.

Synthesis within the 5th FWP

SA code weaknesses identified on safety relevant phenomena have been transmitted to the thematic network EURSAFE (Ref.[41], Ref.[42]) devoted to a PIRT focused on safety ranking priorities on SA phenomena. A synthesis was also carried out with the thematic networks THENPHEBISP devoted on the ISP 46 based on the PHEBUS FPT1 test (Ref.[43], Ref.[44]). In particular, a final meeting was made between THENPHEBISP (Ref.[45]), COLOSS, EVITA (Ref.[46]) and ENTHALPY (Ref.[47]) projects where main outcomes and conclusions on core degradation, corium aspects and other SA topics such as Source Term were derived (Ref.[48]).

C.4.3 Needs for short-term SA code improvements

Short-term code improvements were recommended in the continuation of the modelling effort carried out in the project in order to take full account of findings from experimental programmes of the project and from the ongoing QUENCH, PHEBUS and ISTC programmes. Main short-term needs on modelling improvements concern:

- B_4C oxidation considering "all main gases" and B-compounds resulting from the B_4C oxidation, the oxidation of "B_4C-rich mixtures" and the implementation of a gas chemistry modelling *in and beyond* the core for the calculation of the gas and FP chemistry,
- fuel rod dissolution, including the burn-up effect taking into account results produced in the CIT and COLOSS projects and complementary ones expected in the ISTC project and in the 6th FWP SARNET network (Ref.[49]),
- ZrO_2 clad failure criteria and fuel rod collapse conditions considering a wider set of loss of core geometry conditions,
- oxidation of solid and molten U-O-Zr mixtures taking into account results produced in the project and improved coupling between 2D thermal-hydraulic and melt progression behaviours,
- adaptation of the mixture oxidation models and validation on conditions representative of core reflooding.

C.4.4 Safety implications of results

The *H_2 rate* during early core heat-up or during quenching is at least as important as the *total H_2 production* regarding the explosion risk and the efficiency of H_2 mitigation measures in the containment. This rate is suspected to be underestimated due to code weaknesses on the oxidation of mixtures. Indeed, experiments on oxidation of U-O-Zr and metallic B_4C-rich mixtures showed faster kinetics than for pure Zry and B_4C and indicate that mixtures can be a key source of H_2, in particular during core reflooding.

The main risk with *B_4C oxidation* comes from the production of CO and CO_2 gases that can be converted into CH_4 in the cooler zones of the primary circuit during H_2-rich phases. The formation of CH_3I has been predicted in a demonstrative plant calculation, nevertheless the amount seems low compared to the production of CH_3I by heterogeneous reactions in the containment building itself. Significant effects of B-compounds were also found on Cs chemistry. The additional H_2 production from B_4C oxidation is limited to about 10% of the total H_2 production during core degradation (not taking into account oxidation of B_4C-rich metallic mixtures) but has to be taken into account correctly being produced during the largest H_2 production phase during the early core oxidation escalation.

In-vessel corium behaviour is affected by large uncertainties in the timing and amount of corium formation and in its oxidation which drive the metallic-oxidic composition and the final corium distribution between the core, the core by-pass and the lower head. Corium oxidation is a key factor affecting the late H_2 release, the corium metal-oxide composition in the lower-head and the final vessel failure mode in case of unavailability of water safety injection.

D. MAIN ACHIEVEMENTS AND PERSPECTIVES

Production of a very fruitful experimental database on B_4C effects, fuel dissolution and oxidation of mixtures:

- Main B_4C oxidation issues have been covered thanks to several SETs carried out in different conditions with B_4C material representative of different plant designs. The large database produced showed that B_4C oxidation kinetics is dependent on material properties and strongly dependent on thermal-hydraulic conditions such as steam partial pressure and flow rate which control the mass transfer with the oxidizing phase. Significant production of gases such as H_2, CO, CO_2, very low CH_4 and large amounts of aerosol were measured in SA conditions.
- Small scale B_4C control rod tests enabled the identification of main degradation processes such as B_4C/steel and Zr/steel eutectic interactions, crucible effect of the external ZrO_2 layer of the guide tube, failure conditions and final oxidation of the remaining B_4C fragments (un-dissolved part of the B_4C pellets) and metallic B_4C-rich mixtures. Complementary tests with longer B_4C-CR are needed for modeling improvements and validation purposes.
- Preliminary data obtained on the oxidation of B_4C-rich metallic mixtures representative of the early degradation of B_4C-CRs showed much more rapid kinetics than the oxidation of pure B_4C material. This could enhance the H_2 peak production generated during quenching of degraded cores with B_4C material. The modelling of the oxidation of such a melt will require additional data.

- Three key large-scale bundle experiments characterized by a central B_4C-CR have been carried out in the QUENCH and CODEX facilities with bundles representative of PWR (2 tests) and VVER designs respectively. The B_4C was found to be a contributor to the core degradation but its specific effect could not be quantified. No significant differences could be observed between PWR and VVER designs. For the first time, the gas production from B_4C oxidation was measured during the core degradation phase. Significant quantities of CO, CO_2 and B-compounds (as aerosols) were produced while CH_4 release was very low. The behaviour of B_4C gas production was found to be dependent on the oxidizing thermal-hydraulic conditions in the bundle. These bundle tests are of particular interest for code validation and for the future PHEBUS FPT3 test planned also with a central B_4C-CR.
- Data from the oxidation of U-O-Zr solid and molten mixtures showed faster kinetics than for pure Zry. This confirms that Zr-rich metallic mixtures can be a significant source of rapid H_2 production during core degradation and, mainly, during core reflooding. This is a key insight for modeling. The oxidation of mixtures being in general absent or inadequate in codes, this could explain why the H_2-peak production during core reflooding is usually underestimated.
- Data on dissolution of high burn-up UO_2 (65 and 90 GWd/tU) and MOX fuel (~45 GWd/tU) could be obtained for the first time. Compared with fresh fuel, enhanced kinetics and greater apparent dissolution and fuel decohesion were observed due to fuel cracking and gaseous fission products release and bubbling in the liquefied fuel. Burn-up is confirmed as a key factor of early fuel rod collapse. Whether UO_2 or MOX fuel of similar burn-up dissolves faster could not be concluded from these experiments, since the burn-ups of the two fuels were too different. These preliminary results require additional experiments covering a wider range of experimental conditions, in particular medium burn-up UO_2 fuel.
- New data were produced on simultaneous dissolution of UO_2 and ZrO_2 by molten Zry. This interaction was investigated in a crucible geometry and in the fuel rod configuration. Different configurations and test conditions enabled progress in the understanding of the mechanisms of this double interaction, in particular regarding the continuation of the interaction after the melt saturation.

Modelling and transfer of knowledge in SA codes:

- Each experimental task was accompanied by a significant analytical activity enabling the production of models on B_4C oxidation, fuel dissolution and oxidation of solid and molten mixtures.
- Models produced were implemented in ASTEC, ATHLET-CD, ICARE/CATHARE and SVECHA codes. The improved versions of the first three codes were used to carry out the final set of severe accident plant calculations.
- Models developed on B_4C, fuel dissolution and oxidation of mixture were applied in the calculation of the global tests QUENCH-07, QUENCH-09 and CODEX-B_4C for validation purposes. This effort was continued after the project to take full account of the experimental results produced near the end of the project.
- Preliminary versions of SA codes need to be consolidated and validated with complementary experimental results expected from ongoing PHEBUS FP, QUENCH and EC-ISTC programmes before applications for safety studies.
- Large user-effects were found in calculations regarding the choice of fuel rod degradation criteria (ZrO_2 clad failure and fuel rod collapse) and, to a less extent, the choice of oxidation kinetics law. Based on an in-deph analysis of existing data, recommendations were given by FZK for the oxidation laws and by IRSN for the degradation criteria on the choice of these user-specified models in SA codes. The latter were based on PHEBUS PF results. For the Zry

oxidation, the use of Leistikow (or Cathcart) correlation at low temperature (T <1800K) and Prater-Courtright correlation at high temperature (T >1900K) were recommended in the calculations of the project. More investigations are needed to conclude on the best Zry oxidation correlations, in particular there is a need at high temperature of modeling improvements regarding the steam supply limitation before recommending Zry oxidation correlations for plant calculations. Additional investigations were launched out of the project.

Application of results in plant calculations:

- Two large series of severe accident sequences involving different plants design and the TMI-2 accident were calculated using three integral codes ASTEC, MELCOR and MAAP4 and two mechanistic codes ICARE/CATHARE and SCDAP/RELAP5. The final calculations were run with improved codes and knowledge acquired during the project.
- Each series of plant calculations was enriched by sensitivity studies on key parameters of the core degradation.
- The implications for safety were identified as well as strengths and weaknesses of SA codes regarding core degradation.
- The project enabled code-benchmark exercises on severe accident plant calculations. Valuable results on code capabilities and uncertainties were obtained. Recommendations to optimise future benchmarks could be given regarding the harmonization of input decks, the choice of SA scenario and how to limit user-effects.

Perspectives:

Remaining uncertainties and SA code weaknesses in safety-relevant phenomena of core degradation have been transmitted to the PIRT review on severe accidents carried out in the EURSAFE thematic network (5^{th} FWP) to be addressed in the SARNET network of excellence (6^{th} FWP). In particular results on dissolution of irradiated fuel and oxidation of metal-rich mixtures during core degradation and reflooding should be consolidated. The follow-up of the COLOSS activity on plant calculations with sensitivity studies and benchmarking exercises has also been recommended, the priority being put in SARNET on the European ASTEC code.

Acknowledgements

The partners of the COLOSS project warmly thank EC DGXII for their financial support under the 5th Framework programme on Nuclear Fission Safety, contract number FIKS-CT-1999-00002, and, in particular Dr Alejandro Zurita, for his deep interest and contribution as EC project manager.

References

[1] B. Adroguer, et al., Corium Interactions and Thermochemistry. CIT project, FISA-99 Symposium, EUR 19532 EN, Lux., Nov. 1999.

[2] I. Shepherd et al., Investigation of Core Degradation, COBE project. FISA-99 Symposium, EUR 19532 EN, Lux, Nov.1999.

[3] B. Adroguer et al., 2000. Status Report on Dissolution of Fuel Rods and Related Effects, CIT project, INV-CIT(99)-D004, July 2000.

[4] M. Firnhaber et al., OECD/NEA CSNI International Standard Problem N° 31: CORA-13 Experiment on Severe Fuel Damage. Comparison Report, NEA/CSNI/R(93°17, July 1993.

[5] W. Hering et al., OECD/NEA CSNI International Standard Problem N° 45: QUENCH-06, Comparison and Interpretation Report, FZKA 6722, April 2002.

[6] L. Belovsky et al., Chemical Interaction in B_4C-filled Control Rod Segments above 1000°C under transient conditions, ICONE5, Nice, May 1997.

[7] B. Adroguer et al., Core Loss During a Severe Accident (COLOSS), FISA-01 Symposium, Lux., 12-14 Nov. 2001.

[8] B. Adroguer et al., Core Loss During a Severe Accident (COLOSS), FISA-03 Symposium, Lux., 10-13 Nov. 2003.

[9] Adroguer, B. et al., "Core Loss during a Severe Accident" COLOSS project", Nucl. Eng. and Design, 221, 55-76, 2003.

[10] Adroguer, B. et al., "Core Loss during a Severe Accident" COLOSS project", Nucl. Eng. and Design, to be published, 2004.

[11] Adroguer, B. et al., COLOSS Final Extended Report: Part 1 ; Experimental and analytical activities, SAM-COLOSS-P079, IRSN/DPAM/Dir-2004-0279, April 2003.

[12] Adroguer, B. et al., COLOSS Final Extended Report: Part 2 ; Synthesis on plant calculations, SAM-COLOSS-P080, IRSN/DRS/SEMAR 03/30, June 2003.

[13] Hayward, P.J, et al., 1999. UO_2 Dissolution by Molten Zry. New Experimental Results and Modelling. Report FZKA 6379, INV-CIT(99)-P029, Karlsruhe, Germany.

[14] Müller, K., Goryachev, A.V., Smirnov, V.P., Svyatkin, A.M., Stuckert, J., Veshchunov, M.S, Berdyshev, .A.V., 2004. Simultaneous Dissolution of UO_2 and ZrO_2 by Molten Zircaloy. New Experiments and Modelling, Report FZKA 6947, SAM-COLOSS-P074, Karlsruhe, Germany, January 2004.

[15] Prater, J.T., and Courtright, E.L., 1987. Oxidation of Zircaloy-4 in Steam at 1300^o C to 2400^o C, Zirconium in the Nuclear Industry, 7th International Symposium, ASTM STP 939, R.B. Adamson and L.F.P Van Swan, Eds., American Society for Testing and Materials, Philadelphia, pp. 489-503, 1987.

[16] P. Hofmann, J. Stuckert, A. Miassoedov, M. S. Veshchunov, A. V. Berdyshev, A. V. Boldyrev, 1999. ZrO_2 Dissolution by Molten Zr and Cladding Oxide Shell Failure. New Experimental Results and Modelling, FZKA 6383, Forschungszentrum Karlsruhe, 1999.

[17] M.S.Veshchunov, J.Stuckert, A.V.Berdyshev, Modelling of Zr-O and U-Zr-O Melts Oxidation and New Crucible tests. Report FZKA 6792, SAM-COLOSS-P040, Karlsruhe, Germany, December 2002.

[18] M. Steinbrück, W. Krauss, G. Schanz, H. Steiner, M. S. Veshchunov, A. V. Berdyshev. FZK Separate-effects Tests on B_4C Oxidation; Final Analysis Report, SAM-COLOSS-P054, FZK/NUKLEAR 3385, Apr. 2003.

[19] W. Krauss, G. Schanz, H. Steiner, TG-rig tests (thermal balance) on the oxidation of B_4C. Basic experiments, modelling and evaluation approach, Report FZKA 6883, Forschungszentrum Karlsruhe, 2003.

[20] Bertrand, F., Marchand, O., Repetto, G., 2003. B_4C control rod oxidation during a severe accident in a PWR power plant, separate-effects and integral tests analysis for modeling purpose with the ICARE/CATHARE code, NURETH-10, Seoul, Korea, Oct.5-9, 2003.
[21] Steinbrück, M., Meier, A., Nold, E., Stegmaier, U., 2004. Degradation and oxidation of B_4C control rod segments at high temperatures, Report FZKA 6980, Forschungszentrum Karlsruhe, May 2004.
[22] Miassoedov, A. et al., 2000. Results of the QUENCH-07 Experiment, 10th International Conference on Nuclear Engineering, ICONE10-22137, Arlington, VA, April 2000.
[23] J. Birchley. "Analysis of Quench-06, -07, and 09 Experiments using MELCOR 1.8.5. Preliminary Post-test Calculation using SCDAP/RELAP Mod3.2", SAM-COLOSS-P015, PSI report, 2002.
[24] Homann, Ch., Hering, W., Birchley, J., Fernandez Benitez, J. A., Ortega Bernardo, M.: Analytical Support for B_4C Control Rod Test QUENCH-07, FZKA 6822, April 2003.
[25] Clément, B., and Repetto, G., 2000. Survey of FPT3 objectives and pre-test analyses, 4th Technical Seminar on the Phébus FP Programme, Marseille, 20-22 March 2000.
[26] Miassoedov, A., "Minutes of the COLOSS Topical Meeting on QUENCH-09 and CODEX-B_4C Experiments", SAM COLOSS-M009, Karlsruhe, 22 and 23 Oct. 2002.
[27] Steinbrück M. and Granosa M. (Editors), "8th International QUENCH Workshop", Karlsruhe, Oct.29-31, 2002.
[28] A. Miassoedov et al., "Main Results of the Large-Scale Experiments QUENCH-07 and QUENCH-09 with B_4C Control Rods", PHEBUS FP Information Meeting, JRC Petten, 26 March 2003.
[29] B. Clément and T. Haste, Minutes of the Application Workshop, Aix-en-Provence, 23rd June 2003.
[30] Lamy, J.S., Marguet, S., 2002. First MAAP4 Calculation of QUENCH-07, 6th International Quench Worshop, Kalrsruhe, October 29-31, 2002.
[31] M.S. Veshchunov, A.V. Berdyshev, "Final Report on U-O-Zr Melt Oxidation Model", JRC Technical Note N° P.02.84, SAM-COLOSS-P039, Petten, August 2002.
[32] Veshchunov, M.S., Stuckert, J., Berdyshev, A.V, 2002. Modelling of Zr-O and U-Zr-O Melts Oxidation and New Crucible tests. Report FZKA 6792, SAM-COLOSS-P040, Karlsruhe, Germany, December 2002.
[33] M.S. Veshchunov, A.V. Berdyshev, "Development of a model for the simultaneous dissolution of UO_2 and ZrO_2 by molten Zr", JRC/COLOSS-IBRAE, JRC Technical Note, N° P.03.78, SAM-COLOSS-P047, March 3003.
[34] K. Müller, A.V. Goryachev, V.P. Smirnov, A.M. Svyatkin, J. Stuckert, M.S. Veshchunov, A.V. Berdyshev, "Simultaneous Dissolution of UO_2 and ZrO_2 by Molten Zircaloy. New Experiments and Modelling", Report FZKA 6947, SAM-COLOSS-P074, Karlsruhe, Germany, January 2004.
[35] Schanz, G., 2003. Recommendations and Supporting Information on the Choice of Zirconium Oxidation Models in Severe Accident Codes, FZKA 6827, SAM-COLOSS-P043, March 2003.
[36] G. Schanz, B. Adroguer, A. Volchek, "Advanced Treatment of Zircaloy Cladding High-Temperature Oxidation in Severe Accident Code Calculations, PART I. Experimental database and basic modeling", To be published in Nucl. Eng. and Design.
[37] A. Volchek, G. Schanz, Yu. Zvonarev, "Advanced Treatment of Zircaloy Cladding High-Temperature Oxidation in Severe Accident Code Calculations, PART II. Best-fitted parabolic correlations", To be published in Nucl. Eng. and Design.

[38] F. Fichot, B. Adroguer, A. Volcheck and Yu. Zvonarev, " Advanced treatment of Zircaloy cladding, High-Temperature Oxidation in Severe Accidents Code Calculations, PART III. ", To be published in Nucl. Eng. and Design.
[39] Allelein, H.J. et al., 2001. European validation of the integral code ASTEC (EVITA), FISA 01, Lux., Nov. 2001.
[40] J.P. Van Dorsselaere, F. Jacq, H.J. Allelein, B. Schwinges, "ASTEC status and applications", CSARP 2003, Bethesda (USA).
[41] D. Magallon et al., " "European Expert Network for the Reduction of Uncertainties in Severe Accident Safety Issues", EURSAFE, FISA-03, Luxembourg, 10-13 Nov. 2003.
[42] A. Mailliat et al., « EUROSAFE Project : The Status of the European Severe Accident PIRTs", EUROSAFE Seminar, Berlin, 4-5 Nov. 2002.
[43] T. Haste and B. Clément, Synthesis meeting between THENPHEBISP, COLOSS, ENTHALPY and EVITA, CR DRS/SEMAR 2003/037, June 2003.
[44] B. Clément et al., "Thematic network for a PHEBUS FPT-1 International Standard Problem (THENPHEBISP)", FISA 2003, Luxembourg 10-13 novembre 2003.
[45] B. Clément et al., "Thematic network for a PHEBUS FPT-1 International Standard Problem (THENPHEBISP)", FISA 2003, Luxembourg 10-13 novembre 2003.
[46] Allelein H.J. et al., European validation of the integral code ASTEC (EVITA), FISA 01, Lux., Nov. 2001.
[47] A. De Bremaecker et al., "European nuclear thermodynamic database for in- and ex-vessel applications (ENTHALPY)", FISA 01, Lux., Nov. 2001.
[48] B. Clément and T. Haste, Minutes of the Application Workshop, Aix-en-Provence, 23rd June 2003.
[49] Micaelli, J.C., et al., 2003. SARNET : Sustainable Integration of EU Research on Severe Accident Phenomenology and Management, FISA-03, Luxembourg, 10-13 Nov. 2003.